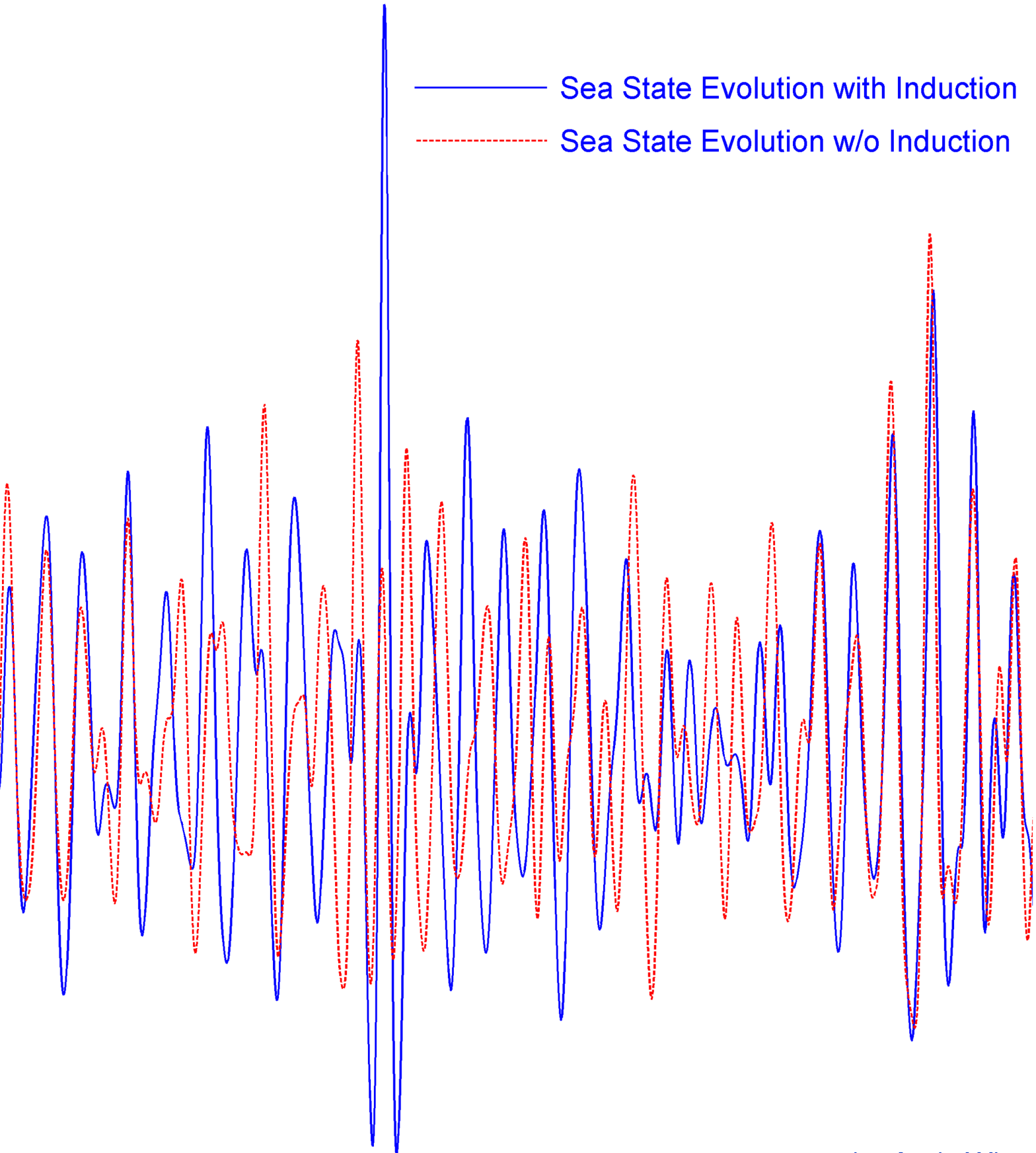
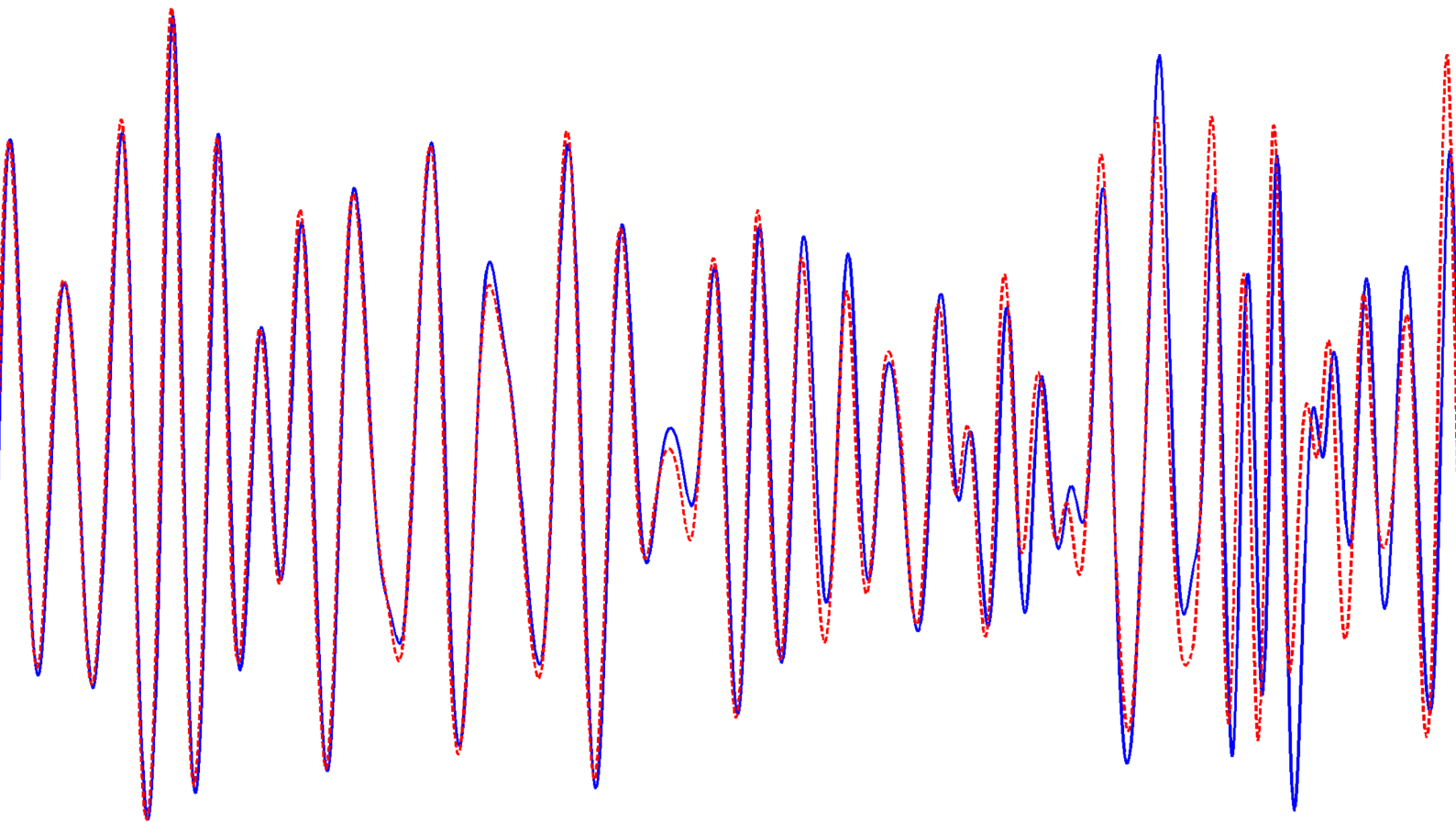


# Inducing Predefined Nonlinear Rogue Waves on Basis of Breather Solutions



The Peregrine Breather, an analytical solution of the Nonlinear Schroedinger Equation, is modified to induce locally and temporally accurate, predefined extreme wave events in an arbitrary directed sea state. To this end, a parameter study of the distortion term of the unstable Peregrine modulation is performed to enforce form, height, and steepness of the rogue wave. In addition, the phase modulation is identified to be the crucial perturbation for the nonlinear Breather dynamic. With this knowledge, the inducing of a predefined rogue wave in non-uniform carrier waves and even in irregular, directed sea states is presented, its limits determined, and the Breather dynamics analyzed by spectral and phase evolution analysis in time and space. The results are compared to the dynamics of real occurred extreme waves and a reverse engineering as well as a forecast model for nonlinear real rogue waves are depicted briefly.



---

# **Inducing Predefined Nonlinear Rogue Waves on Basis of Breather Solutions**

---

**Vom Promotionsausschuss der  
Technischen Universität Hamburg**

zur Erlangung des akademischen Grades  
Doktor der Naturwissenschaften (Dr. rer. nat.)

genehmigte Dissertation

von  
Andy Witt

aus  
Brunsbüttel

2019

## **Approved Doctoral Dissertation at the Hamburg University of Technology**

Examination Board Chairman: Prof. Dr. Wolfgang Mackens

1. Reviewer: Prof. Dr. rer. nat. habil. Norbert Hoffmann

2. Reviewer: Prof. Dr. rer. nat. Amin Chabchoub

Date of Oral Exam: 18 January 2019

## **Copyright by Andy Witt 2019**

e-mail: mail@Andy-Witt.com; ORCID iD: <https://orcid.org/0000-0002-5150-540X>

All rights reserved. No part of this publication may be reproduced, stored in a retrieval system, or transmitted, in any form or by any means, electronic, mechanical, photocopying, recording or otherwise, without the prior permission of the publisher.

1st edition 2019.

## **Bibliographic information published by the German National Library**

The German National Library lists this publication in the German National Bibliography. Uniform Resource Name (URN): urn:nbn:de:gbv:830-882.032845. Detailed bibliographic data are available in the Internet at [www.dnb.de/EN](http://www.dnb.de/EN).

## **Identifiers**

ISBN 978-3-748533-98-6

ORCID iD <https://orcid.org/0000-0002-5150-540X>

DOI <https://doi.org/10.15480/882.2224>

Handle <http://hdl.handle.net/11420/2497>

URN urn:nbn:de:gbv:830-882.032845

# Abstract

## Abstract English:

The Peregrine Breather, an analytical solution of the Nonlinear Schroedinger Equation, is modified to induce locally and temporally accurate, predefined extreme wave events in an arbitrary directed sea state. To this end, a parameter study of the distortion term of the unstable Peregrine modulation is performed to enforce form, height, and steepness of the rogue wave. In addition, the phase modulation is identified to be the crucial perturbation for the nonlinear Breather dynamic. With this knowledge, the inducing of a predefined rogue wave in non-uniform carrier waves and even in irregular, directed sea states is presented, its limits determined, and the Breather dynamics analyzed by spectral and phase evolution analysis in time and space. The results are compared to the dynamics of real occurred extreme waves and a reverse engineering as well as a forecast model for nonlinear real rogue waves are depicted briefly.

## Abstrakt Deutsch:

Der Peregrine Breather, eine analytische Lösung der Nichtlinearen Schroedinger Gleichung, wird modifiziert, um punkt- und zeitgenau eine zuvor in Form, Höhe und Steilheit definierte nicht-lineare Extremwelle in einen beliebigen gerichteten Seegang zu induzieren. Dazu wird zunächst eine Parameterstudie des Störungsterms der instabilen Peregrine Modulation zur Formgebung der Extremwelle durchgeführt. Dabei wird die Phasenmodulation als die entscheidende Störung für die nichtlineare, wachsende Breather-Instabilität identifiziert. Mit diesem Erkenntnisstand wird das Induzieren einer vorbestimmten Extremwelle in nicht uniforme Trägerwellen und sogar irreguläre, gerichtete Seegänge dargestellt, die Grenzen ermittelt und die Dynamiken mittels Phasen- und Spektralanalyse über Zeit und Raum analysiert. Die Ergebnisse werden mit einer realen, auf der Nordsee gemessenen Monsterwelle verglichen und zudem wird sowohl ein Reverse Engineering als auch eine Vorhersagemethode solcher nichtlinearer Extremwellen skizziert.



# Acknowledgments

First of all, I would like to thank my supervisor Prof. Dr. Norbert Hoffmann for his support, guidance, and trust in my work. Analyzing papers, researching, trying to bring a bit of new knowledge to this beautiful world, and calling this my work has been a true gift to me. My studies are based on the research of Prof. Dr. Amin Chabchoub from the University of Sydney which is why I am particularly grateful that he accepted to be my second reviewer. I am also obliged to the examination board chairman Prof. Dr. Wolfgang Mackens who has been a role model of viewing the lively beauty of mathematics and theories since my first lectures at the university.

This thesis would not have been possible without the cooperation with the Institute of Fluid Dynamics and Ship Theory. A special thank to the chief of the water wave tank experimental facilities Uwe Gietz who supported, questioned and trusted me in every wave experiment. Accordingly, I would also like to thank my colleagues, especially Gesa Ziemer, Dr.-Ing. Sönke Neumann, and Dr.-Ing. Arne Wenzel for all the discussions, hugs, and participations in my private as well as university life.

I would not have been prepared for this thesis without my mentor, friend, and business partner Wolfgang Sievers who taught me to trust myself and grow in my beliefs. In the same way my dear friends Pascal Bayer and Michael Wiring supported me in life, studies, and profession in unspeakable manners.

As a child of a fisher-family, I thank my grandparents for their love and the attraction to the sea, my beloved mom for our unbreakable connection, my father for the joyful perspective on this world, their spouses for their support, and my niece and nephew for the glance in their eyes while playing with me.

My nerdy life is broadened with the energetic, artistical world of my boyfriend Filipe. As a sunflower e-merges mathematics and beauty by nature, you are raising my life into an open and diversified being of fortunate hope.

Whomever I have forgotten, whoever will still come: Thank you all for being in my life. Love and carpe undam.

Hamburg, January 2019

Andy Witt



# Contents

<b>Abstract</b>	<b>v</b>
<b>Acknowledgments</b>	<b>vii</b>
<b>1 Introduction</b>	<b>1</b>
1.1 Motivation and Objective . . . . .	1
1.2 Current State of Research and Outline . . . . .	4
<b>2 The Nonlinear Schroedinger Equation and its Analytical Breather Solutions</b>	<b>7</b>
2.1 Derivation and Limits of the Nonlinear Schroedinger Equation . . . . .	8
2.2 Peregrine Breather Solution . . . . .	13
<b>3 Producing Waves in the Wave Basin</b>	<b>19</b>
3.1 Experimental Facilities . . . . .	19
3.2 Driving Uniform Waves, NLS Breather Solutions and Arbitrary Directed Sea States . . . . .	21
<b>4 Governing Equations and their Use Cases</b>	<b>27</b>
4.1 Temporal and Spatial versions of NLS, Dysthe, and NLSType3 . . . . .	27
4.2 Temporal and Spatial High Order Spectral Method . . . . .	31
<b>5 Effects of Variations in Peregrine Distortion Term on Breather Dynamics</b>	<b>33</b>
5.1 Controlling the Freak Index and Maximal Steepness by the Parameter of the Absolute Maximal Value of the Peregrine Distortion Term . . . . .	33
5.2 Controlling the Number of Waves in a Steep Wave Event by the Wave Steepness	37
5.3 Relocating of the Maximal Wave Peak by the Wave Number of the Peregrine Distortion Term . . . . .	41
5.4 Pure Phase Modulated Rogue Waves and Their Dynamics . . . . .	44
<b>6 Experimental Study on Robustness of Breather Dynamic to Changes in the Carrier Wave</b>	<b>53</b>
6.1 Robustness of Peregrine Breather Dynamics to Phase Shifts in the Carrier Wave	54
6.2 Breather Dynamics on Amplitude Shifted Carrier Waves . . . . .	56
6.3 Phase and Amplitude Shifted Breather Dynamics . . . . .	59
6.4 Using an Arbitrary Directed Sea State as Carrier Wave for the Breather Dynamic	62
6.4.1 JONSWAP: A Simulated North Sea . . . . .	63

6.4.2	Causing a Rogue Wave in the JONSWAP Wave by the Peregrine Distortion Term . . . . .	64
6.4.3	Reference to Real Extreme Waves . . . . .	70
<b>7</b>	<b>Further Possibilities of Injecting Breather Dynamics in an Irregular Wave Field</b>	<b>77</b>
7.1	Current State of Research . . . . .	77
7.2	Multiplying the Breather Phase Distortion to each Superposed Wave of the JONSWAP Wave Field . . . . .	78
7.3	Multiplying the Breather Distortion to each Superposed Wave of the JONSWAP Wave Field . . . . .	84
<b>8</b>	<b>Summary, Conclusion, and Future Work</b>	<b>89</b>
8.1	Summary and Conclusion . . . . .	89
8.2	Directions for Future Work . . . . .	92
	<b>References</b>	<b>95</b>
	<b>Curriculum Vitae</b>	<b>105</b>

# 1 Introduction

## 1.1 Motivation and Objective

Since mankind goes to sea, extreme waves have been reported as walls of water, three sisters, monsters, ghosts, freak waves, and rogue waves. A long though not complete list of accidents with high waves starting with the time of Christopher Columbus has been collected by Liu [Liu07]. Even famous paintings and woodcuts like 'The Great Wave off Kanagawa' by Hokusai in 1829 documented those extreme events, though rejected as nautical yarn often. It needed the first measured rogue wave occurring at the Draupner platform in the North Sea off the coast of Norway on 1 January 1995 (Draupner Wave, [ATY<sup>+</sup>11] and [Hav04]) to prove the existence of rogue waves finally, leading to intense researches and sensitivity in the construction of ships and offshore structures.

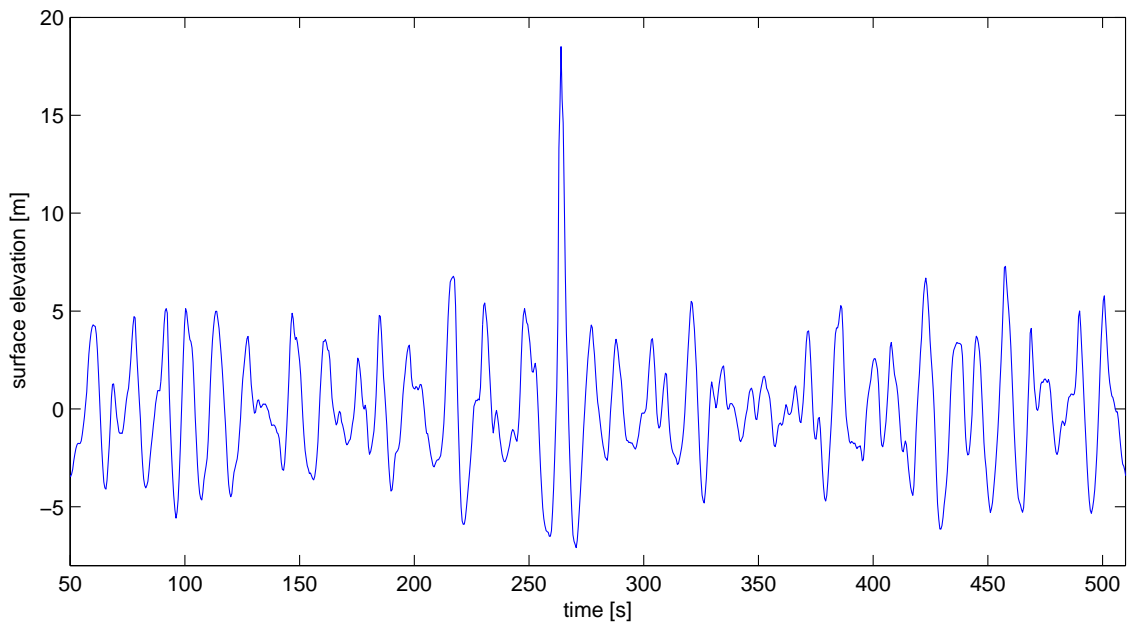


**Figure 1.1:** Draupner Wave Record on January 1<sup>st</sup> 1995 at 15:20:  
Significant Wave Height 11.9m, Wave Height of Extreme Event 25.6m,  
Norwegian North Sea with 70m water depth

Rogue waves are defined as extreme waves with a wave height (measured from crest to trough) higher than twice the significant wave height, i.e. twice the mean wave height of the highest

third of the surrounding waves of the considered time series. Typically they appear suddenly without any warning. They can cause massive damage to ships and other offshore structures and disappear untraceable as they would have had never existed. [Wik18] claims that one ship longer than 200m per month sunk in the last 20 years. Researchers believe that some sinkings may be caused directly or indirectly by these high rogue waves. The Draupner platform registered 466 freak waves in twelve years, i.e. one extreme wave every ten days on average.

Beside the height of the rogue waves, those waves are very steep and have high velocities due to nonlinear increases of the speed. Ships have high inertias and are not able to overrun these extreme waves. The waves roll over the ships causing high pressures in the structures and superstructures which are not designed for these high forces. In addition to this flooding, the small wavelength of the wave peak is headed and followed by deep troughs. This may lead to loads affected in one single point which may break the ship. Moreover, if the ship is hit by an extreme wave sideways, it may flip over.

While rogue wave events due to linear theory are widely understood [KPS09a], the nonlinear effects gaining automatically in importance with the wave steepness are unreasonable neglected in here. Furthermore, linear theory alone can not explain the number of rogue wave events in the world oceans and seas, underestimated up to hundreds of times [Mor04, Sta04, For03]. Therefore the nonlinear dynamics of rogue waves are still under intense research and have not been fully understood yet, though the area of impact of extreme wave events is not limited to gravity water waves only but also contains nonlinear optics, quantum mechanics, electrostatic and electromagnetic physics.

Hence, this thesis is dedicated to analyzing analytical, nonlinear Breather solutions of the Nonlinear Schroedinger Equation concerning whether they can be used to cause realistic rogue waves in properties like shape, height, and steepness occurring in regular and non-regular sea states. We question:

- How robust is the growing modulation instability of analytical Breather solutions, i.e. will the inherent distortion term lead to growing amplitudes and rogue waves, ...
  - ▷ ... even if the distortion term is modified severely? What are the limits?
  - ▷ ... even if the distortion term is applied to irregular wave fields which are much closer to the experimental reality of rogue wave phenomena in the open sea? Can we use any, arbitrary, maybe even random directed sea state?

- If so, can we modify the distortion term of the analytical Breather solutions to get predefined rogue waves of various, targeted shapes? In that case, what are the limits in targeted parameters like steepness and amplification factor?
- And how can we inject those specific rogue wave event in a predefined or random sea state?
  - ▷ Does this injection require much energy like an unrealistic amplitude modulation or is it naturally 'undiscoverable'?
  - ▷ Which effect has the carrier wave on the extreme event?
- Can we predict or even force the place and time of the occurrence of the extreme event enabling scientists to perform targeted wave-structure-experiments like in [FCKDO12, OPCK13]?
- And conversely, could we even enable scientists to forecast and rebuild the dynamics and disruptive forces of real rogue waves, i.e. are we able to predict steep wave events and subsequently reverse engineer a known rogue wave time series into an 'ordinary' sea state distorted by an 'undetectable' Breather distortion for reconstructing real wave-structure-impacts?

In case we can answer all these questions satisfactorily, we may understand better the dynamics of nonlinear rogue waves in realistic open sea situations. Those answers will provide us with a strong indication why nonlinear effects have to be taken into account to explain extreme wave events in the world oceans and seas. They will show why Breather solutions of the Nonlinear Schroedinger equation are relevant regarding extreme wave events in realistic sea states due to natural distortions. But most of all this study will provide future scientists with a box of bricks to reverse engineer known, real rogue waves and their impacts as well as to cause aimed space- and time-located nonlinear breathing freak wave events in any predefined or random directed sea state to investigate its dynamics and potential impacts in experimental, simulative, and analytical studies. This will hopefully lead to improved designs of marine structures and new approaches of forecasting extreme and possibly catastrophic events of water waves but also in nonlinear optics, quantum mechanics, electrostatic and electromagnetic physics.

## 1.2 Current State of Research and Outline

### State of Research

According to [KPS09a] 'there are various physical mechanisms generating rogue waves on the sea surface' but most of the researched effects are linear dynamics which are especially in steep wave events neglecting the inherent nonlinear mechanisms. Rogue waves may occur due to linear theory by

- wave-current interactions: Wind waves or swells which propagate against a current leading to a Doppler effect maybe even strengthened by opposed wind forces.
- geometrical and spatial focusing: Underwater topography may cause Doppler effects, branchings (see [YZHK11] and [HKS<sup>+</sup>10]) and caustics leading to superposed high waves.
- dispersive focusing: In a dispersive medium waves of different wavelengths propagate with different group velocities according to the related dispersion relation. Longer waves may catch shorter waves up and superpose to high waves.
- crossing seas: Two sea fields meet and interfere with each other leading to rogue waves.

and by nonlinear effects due to

- focusing of modulation instabilities: A Benjamin-Feir instability produces growing modulations of the envelope of wave groups ending in a nonlinear focusing of the wave energy by interactions of Fourier decomposed inherent uniform waves (which are independent in the linear point of view) before getting demodulated again.
- crossing seas which exchange energy and by that build localized wave packets which may be unstable to modulation instabilities.
- solitons (occurring from uniform wave trains under modulation instabilities) colliding with each other, plane waves, or other wave groups.

All these phenomena have been discussed in [DKM08] and [KP03] already. Hence, the linear theory does not explain all occurring rogue waves on the oceans solely. Furthermore, it does neglect the correlation between superposed waves. So wave statistics and physical dynamics are not met by linear theories in the chaotic and turbulent surface wave system.

Much research had been performed by various researchers who let the approach of inducing predefined rogue waves in arbitrary, directed sea states by Breather distortion terms appear promising: First of all, [CHA11] proved the existence of Peregrine Breathers in surface wave

dynamics by wave tank experiments. Also the robustness of the Peregrine Breather against small perturbations and external wind forces has been showed by [ADA09], [CHB<sup>+</sup>13], and [DT99]. Also, [Cha16] cut the standard Peregrine solution into an irregular wave field and could see the persistence of the Breather dynamic.

On the other hand, [OOS02] and [OOSB01] were able to change the JONSWAP spectrum parameters to increase the probability of occurring freak waves even if the parameters are unusual for natural ocean wave fields. However, [FBL<sup>+</sup>16] proved that the main qualitative behavior of real rogue waves can be described by weakly nonlinear equations and solutions (like the NLS solutions), though they doubt the importance of unstable modulations for rogue waves in real oceans. They analyzed several real occurred freak waves and found out that the ocean wave field was partly regular.

All these researches indicate the possibility that the analytical, 'breathing' NLS solutions may be a key to induce spatially and locally accurate, predefined extreme waves in an arbitrary, directed wave field. This will analyzed in the following chapters.

## Outline

This thesis analyzes the nonlinear effects of causing Breather type steep wave events on the basis of analytical solutions of the nonlinear Schroedinger equation (NLS). Therefore, in chapter 2 we first derive the NLS and discuss its limits. Furthermore, we reason the analytical Breather solution called Peregrine Breather to be the basis of our rogue wave injections. In chapter 3 we present the experimental facilities and the driving of wave fields of different types. We discuss the nonlinear Stokes effects and the error of measured to targeted wave time series. Beside this wave tank facilities, we extend our examination possibilities numerically by the simulation of several governing equations and discuss their use cases in chapter 4. We also introduce a new wave equation and some helpful analyzing tools.

With these facilities, we study the effects of variations in the Peregrine distortion term on the Breather dynamics in chapter 5. We will find controlling parameters for the freak index, maximal wave steepness, and the number of waves in the steep wave event. We will also find a parameter to relocate the maximal peak in the rogue wave group and make out the phase distortion as the crucial modulation for the induced nonlinear Breather dynamic. The latter will be underlined by analyzing the spatial evolution of the local wavelengths.

After that, chapter 6 presents an experimental study on the robustness of the Breather dynamics to changes in the carrier wave. The initially uniform carrier wave will be phase shifted as well as amplitude shifted in time. Combining this so far gathered knowledge we will be able to induce

a Breather type dynamic using the Peregrine distortion term in an arbitrary, directed sea state developed by a JONSWAP ocean spectrum. The results are compared to the Draupner wave - a real occurred freak wave - by spectral analysis. This will lead to a depiction of the reverse engineering of real ocean freak waves and a possible forecast model.

To extend the possibilities of inducing a nonlinear rogue wave to an irregular, directed carrier wave, we show further options of injecting a Breather dynamic in chapter 7 and examine them with a temporal and spatial spectral analysis. In chapter 8, we close with a summary and conclusion of the performed studies and sketch possible directions for future works.

## 2 The Nonlinear Schroedinger Equation and its Analytical Breather Solutions

The Nonlinear Schroedinger Equation (NLS) is the simplest equation describing the evolution of weakly nonlinear deep-water wave trains. Evolution equation taking into account higher-order nonlinearities are discussed in [Dys79, Osb10a, Slu05] and chapter 4.

Though relative simple, the NLS describes not only linear dispersion but also the nonlinear evolution in time and space of wave packets propagating in (sufficient) finite and infinite depth, as well as the phenomenon of Benjamin-Feir instability [Joh97a, New81] which is one of the solid proofs of necessity of using nonlinear equations for surface gravity wave propagation. Nevertheless, the NLS is still fully integrable [ZS72] and by this provides the possibility of comparing experimental results to theory without effort. Furthermore, analytical solutions of the NLS called Breathers are known which have a similar form of appearance as the reported rogue waves in the ocean [AAT09], i.e. extreme high waves, appearing from nowhere and disappearing without any trace. Those analytical solutions provide us with an initial starting point for driving extreme wave events of predefined shape and location on arbitrary sea states. Of course, using a just weakly nonlinear equation has some drawbacks which will be pointed out in 2.1. However, several papers proved the qualitative sufficiency of the NLS for propagating waves of moderate steepness [CSS92, Osb10a]. Comparing with fully nonlinear simulations and experiments the analytic NLS solutions are found to describe the actual wave dynamics of steep waves reasonably well [SPS<sup>+</sup>13, FBL<sup>+</sup>16]. In addition, the NLS is not only limited to gravity water waves only but also includes nonlinear optics [SRKJ07], quantum mechanics [DMEG82], electrostatic and electromagnetic physics [Lee12].

We will first show the derivation of the NLS and give some remarks to its limits in 2.1, followed by section 2.2 with the motivation and mathematical description of the used breathing analytical solution to solve our objectives in 1.1.

## 2.1 Derivation and Limits of the Nonlinear Schroedinger Equation

### Derivation

According to [KP01], an irrotational flow of an inviscid, incompressible fluid can be described by a scalar velocity potential function  $\Phi$  and the Bernoulli's equation:

$$\mathbf{u} = \nabla \Phi \quad (2.1)$$

$$\frac{\partial \Phi}{\partial t} + \frac{1}{2} (\nabla \Phi^\top \nabla \Phi) + \frac{p}{\rho} + gz = \text{const} \quad (2.2)$$

with  $\mathbf{u}$ : velocity vector,  $\Phi$ : scalar velocity potential function,  $\nabla$ : the nabla operator  $(\frac{\partial}{\partial x}, \frac{\partial}{\partial y}, \frac{\partial}{\partial z})^\top$ ,  $t$ : time,  $p$ : pressure at  $z = 0$ ,  $\rho$ : constant density,  $g$ : gravity acceleration, and  $z$ : vertical coordinate with  $z = 0$  at the equilibrium level of the surface.

For describing the surface waves (see [Dys79]), we insert the irrotational flow (2.1) into the mass continuity equation  $\frac{\partial \rho}{\partial t} + \nabla^\top (\rho \mathbf{u}) = 0$  where  $\frac{\partial \rho}{\partial t} = 0$ , and  $\nabla^\top \rho = 0$  as  $\rho = \text{const}$  (incompressible flow). Then we take the total time derivative of (2.2) as a boundary condition at  $z = \zeta$  where  $\zeta(x, y)$  is the surface elevation associated with the wave motion at constant atmospheric pressure. If we finally add the kinematic boundary condition at  $z = \zeta$  as a second boundary condition, we will get:

$$\nabla^2 \Phi = 0, z \leq \zeta \quad (2.3)$$

$$\frac{\partial^2 \Phi}{\partial t^2} + g \frac{\partial \Phi}{\partial z} + \frac{\partial}{\partial t} (\nabla \Phi)^2 + \frac{1}{2} \nabla \Phi^\top \nabla (\nabla \Phi)^2 = 0, z = \zeta \quad (2.4)$$

$$\frac{\partial \zeta}{\partial t} + \nabla \Phi^\top \nabla \zeta = \frac{\partial \Phi}{\partial z}, z = \zeta \quad (2.5)$$

with  $\nabla^2 = \nabla^\top \nabla$ ,  $(\nabla \Phi)^2 = \nabla \Phi^\top \nabla \Phi$ , and  $\nabla \zeta = (\frac{\partial \zeta}{\partial x}, \frac{\partial \zeta}{\partial y}, 0)^\top$ .

Having in mind the slow evolution of a wave train, Dysthe developed  $\Phi$  and  $\zeta$  around a mean flow  $\bar{\Phi}$  and a mean surface elevation  $\bar{\zeta}$  in [Dys79] and put this into the equations (2.3), (2.4), and (2.5). These equations may be developed until a certain order in wave steepness  $\varepsilon = k_0 a$ , where  $a$  is the wave amplitude averaged over one wavelength and  $k_0$  the wave number  $k_0 = \frac{2\pi}{\lambda_0}$  with averaged wavelength  $\lambda_0$  of the mean wave propagation direction.

If we neglect all terms of order  $\varepsilon^3$  or higher and assume  $x$  to be the spatial direction of the mean wave propagation and  $y$  to be the perpendicular spatial direction to  $x$ , we will get the

famous Nonlinear Schroedinger equation (NLS) for the complex envelope  $A(x, y, t)$  first derived by Zakhorov [Zak68]

$$i\left(\frac{\partial A}{\partial t} + \frac{\omega_0}{2k_0} \frac{\partial A}{\partial x}\right) - \frac{\omega_0}{8k_0^2} \frac{\partial^2 A}{\partial x^2} + \frac{\omega_0}{4k_0^2} \frac{\partial^2 A}{\partial y^2} - \frac{\omega_0 k_0^2}{2} |A|^2 A = 0 \quad (2.6)$$

where the free surface elevation in first order is given by

$$\zeta(x, y, t) = \text{Re}\{A(x, y, t)e^{i(k_0 x - \omega_0 t)}\} \quad (2.7)$$

or in second order by

$$\zeta(x, y, t) = \text{Re}\{A(x, y, t)e^{i(k_0 x - \omega_0 t)} + \frac{1}{2}k_0 |A(x, y, t)|^2 e^{2i(k_0 x - \omega_0 t)}\} \quad (2.8)$$

The NLS equation expresses a 2-dimensional weakly nonlinear flow around a main wave with wave frequency  $\omega_0 = \frac{2\pi}{T_0}$  and period  $T_0$  and wave vector  $\mathbf{k}_0 = (k_0, 0)^\top$  with  $k_0 = \frac{2\pi}{\lambda_0}$  and wavelength  $\lambda_0$  in x-direction. A different derivation of the Nonlinear Schroedinger equation which will also lead to higher order NLS type equations is presented in chapter 4.

Beside linear dispersion and by that dispersive focusing, the NLS describes a weakly nonlinear flow and by that is already capable of 'energy exchanging' frequency interaction leading to unstable growing modulations: By small perturbations in amplitude and phase of the uniform wave train solution of the NLS which recovers the Stokes wave ([Wik17]) the NLS may predict unstable growth for specific wavelengths. For example, taking the Benjamin-Feir side-band modulation ([YL82]) to the uniform wave train solution of the 1-dimensional NLS and linearizing predicts unstable growth rate for  $0 \leq k \leq 2\sqrt{2}k_0^2 a_0$  (see [Yue91]).

A deeper look into the NLS equation (2.6) let us determine the effects of each summand:  $\frac{\partial A}{\partial t}$  describes the (material) amplitude change in time while the second summand  $\frac{\omega_0}{2k_0} \frac{\partial A}{\partial x}$  disappears if the system of coordinates is defined as a moving reference of group velocity  $\frac{\omega_0}{2k_0}$ .  $\frac{\omega_0}{8k_0^2} \frac{\partial^2 A}{\partial x^2}$  and  $\frac{\omega_0}{4k_0^2} \frac{\partial^2 A}{\partial y^2}$  are diffusive terms who correlates to the dispersion, i.e. the spreading of wave packets due to different propagation velocities of the inherent wave components. The last term  $\frac{\omega_0 k_0^2}{2} |A|^2 A$  introduces the nonlinearity into the equation. It can be seen as an amplitude dispersion effect as with this term the amplitude change depends cubically on the amplitude itself.

The factors of the summands are also identified by a Taylor series of  $\omega(\mathbf{k}, |A|^2) = \sqrt{g|\mathbf{k}| + g|A|^2|\mathbf{k}|^3}$  (third order dispersion relation for long-crested deep water waves) about

$\mathbf{k}_0 = (k_0, 0)^\top$  and  $|A|^2 = 0$  according to [Deb94] and section 4.1, e.g. the group velocity  $\frac{\partial \omega}{\partial k_x}|_{(k_0, 0)^\top} = \frac{\omega_0}{2k_0}$ .

If we neglect all terms of order  $\varepsilon^4$  or higher, we will get the Dysthe equations which are more accurate and stable to modulation instabilities as shown in [SA13]. On the other hand, they are more complex in simulation and numerical solving processes. Therefore in chapter 4 a slightly different equation will be derived which tries to combine the simplicity in numerical solving procedures with higher order truncation in  $\varepsilon$ . This equation will give us more accuracy in locating the highest peaks of the rogue waves than the NLS without losing the simplicity of the numerical simulation.

### Limits of the Nonlinear Schroedinger equation

Beside the derivation assumptions (irrotational flow in an inviscid, incompressible fluid) there are some limits of use for the Nonlinear Schroedinger Equation which has to be taken into account when simulating wave evolution by this equation. First of all, by derivation, there is no term in the NLS for introducing an external potential, wind excitement, or interaction between the oceanic and atmospheric boundary layer. Second, as the NLS describes a weakly nonlinear flow around a main wave with wave frequency  $\omega_0$  and wave vector  $\mathbf{k}_0 = (k_0, 0)^\top$  in x-direction, it naturally comes along with some other limits:

- The NLS is narrow-band around the leading wave frequency  $\omega_0$ . Waves with a wide range of frequencies will lead to inaccurate propagation calculations by the NLS.
- By this the NLS is also directed to the wave vector  $\mathbf{k}_0 = (k_0, 0)^\top$ , i.e. the NLS is not sufficiently capable of non-directed sea-states. A coupled system of NLS equations may improve this, especially coupled systems of two NLS are under big research at the moment to investigate the behavior of two crossing seas (see [Oka84, OO06]).
- The NLS is derived by developing an irrotational flow until (and including) the second order of wave steepness  $\varepsilon$ . [Osb10a] showed the qualitative sufficiency of the NLS for propagating waves of just moderate steepness, i.e.  $\varepsilon \leq 0.15$ . A simple but effective numerical trick for steep initial wave data is presented in [HPD99]: The NLS is scalable in time and space and by that can adjust the initial wave steepness  $\varepsilon$  as the scaling transformation  $x \rightarrow cx, t \rightarrow c^2t, q \rightarrow \frac{q}{c}$  with  $c \in \mathbb{R}$  leaves the NLS invariant. Therefore the NLS is numerically not capable of waves evolving to very steep waves but for arbitrary steep initial waves. For steep evolving waves it is advisable to use higher order equations.

- [Su82] demonstrated experimentally that an initially symmetric wave packet evolves in an asymmetric manner. This asymmetric development is accelerated as the wave steepness (nonlinearity) is increased and can not be accounted for by the NLS which predicts symmetric evolution. As shown in chapter 4 higher order equations may solve this.
- A reason of this asymmetric evolution is the nonlinear increase in group velocity of steep envelopes. [HPD99] proved that the NLS does not account for this effect, i.e. for our consideration of rogue waves the spatial locating of the highest peak will be unprecise if done by the NLS. But as shown in chapter 4 higher order equations will solve this issue.
- An effect which correlates to the nonlinear group velocity increase by the dispersion relation is the so-called frequency down-shifting. Related to rogue waves Tulin shows in [Tul96] that a uniform wave with a growing modulation exhibits a longer wave period temporary close to the maximum amplitude and with that a reduced frequency. Tulin proves that the NLS is not capable of displaying this frequency down-shift. This effect has to be taken into account while comparing theoretically NLS waves to measured waves or considered by higher order equations like the Dysthe equations.
- Furthermore, the NLS overestimates the maximum peak of the extreme wave event modulated by a growing perturbation modulation. [HPD99] and [SA13] analyze this effect and compare the results to more accurate higher order equations.
- The NLS (2.6) is derived for deep water. Contrary to deep water, the contribution of the mean flow velocity potential becomes very important in shallow water and can not be neglected as done in the derivation above. [Joh97b] shows that the nonlinear coefficient of  $|A|^2 A$  changes if  $kd \gg 1$  is not fulfilled (deep water constraint) with  $d$ : water depth. For  $kd \approx 1.363$  the nonlinear coefficient turns to zero and thus the nonlinear effects just appear in higher levels. If the critical value gets even smaller then the related coefficient will get negative. Therefore the bifurcation value  $kd$  corresponds to a significant change in the nonlinear wave dynamics. For instance, [KM83] proves that a Benjamin-Feir instability modulation may not grow if the coefficient gets zero or negative. As we concentrate to deep water cases we have to ensure that the deep water constraint is fulfilled in all our NLS simulations and experiments.
- The NLS does not consider dissipation or wave breaking for steep waves.

Despite these drawbacks, the NLS is a numerically simple but powerful equation describing the wave dynamics qualitatively reasonable well ([SPS+13]). So, [FBL+16] argues that the main qualitative behavior of real rogue waves can be described by weakly nonlinear equations like

the NLS and its solutions. [HPD99] even proves that the NLS agrees excellently over a much longer timescale than expected, particularly for lower steepness. Beside this, the NLS provides us with analytical solutions of growing modulation instabilities which provide prototypes of real nonlinear rogue waves as pointed out in 2.2. And whenever a limit of the NLS is met, or quantitative values have to be forecasted we can ensure the NLS-data by higher order equations as described explicitly in chapter 4.

## 2.2 Peregrine Breather Solution

### Motivation of Basis Peregrine Breather Solution

As a starting point for our objectives outlined in 1.1 we need an analytical wave description which we can modify according to our needs. As we like to inject a not discoverable distortion to an arbitrary sea state to enforce a rogue wave event, this will not be the simple case of superposed waves leading to a dispersive focusing. [AAT09, HPD99] investigated several analytical solutions of the NLS and compared them to real rogue waves. It turns out that the breathing Peregrine solution also called the isolated Ma soliton '*is the most convenient approximation*' to several steep wave events. It does not only meet the qualitative behavior of appearing from nowhere, surging to a high wave and disappearing untraceable. But also, it already fits very well to wave records of real extreme wave events, though it is just a single distorted uniform wave train solution.

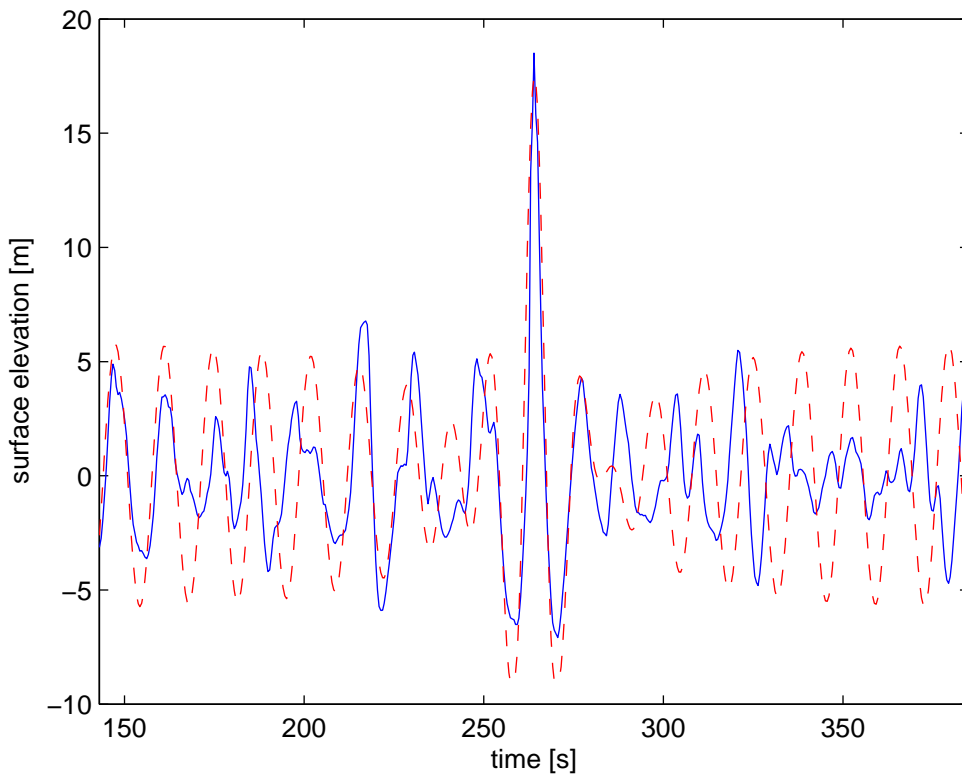


**Figure 2.1:** Draupner Wave (blue line) versus fitted Peregrine solution (dashed red line)

Exemplary, in figure 2.1 a 'best fit Peregrine model' to the Draupner wave was determined by the analysis tool presented in chapter 4. By reducing the relative error of the measured wave to

the parameterized Peregrine, it ascertains a Peregrine model with wave number  $k = 0.023 \frac{rad}{m}$  and steepness  $\varepsilon = ka$  (with  $a$ : amplitude) of the uniform carrier wave of  $0.1373 rad$  recorded 254.1m (almost one wavelength) before its maximum peak. We can see that the dashed red distorted uniform wave captures the general form of the real waves quite well before the freak event. Closer to the peak a temporary frequency down-shifting occurs. The Peregrine which is a solution of the NLS is incapable of this effect and therefore will not meet the general wave behavior after the steep wave event. Both, the Peregrine model as well as the wave record has a slightly deeper trough after the peak than before - for the regular Peregrine an indicator for not being in its maximum yet. The 'best fit Peregrine model' analysis tool of chapter 4.1 forecasts further wave height growth of 0.5m. Of course, a single distorted uniform wave will not model all properties of a complex real sea state. Nevertheless, the agreement of Peregrine model and Draupner wave is surprisingly strong. Chapters 6 and 7 will show how to model and compare freak wave events in real, complex sea states.

### The Peregrine Breather Solution

The Peregrine Breather first derived in [Per83] is a limiting case of two other well known pulsating solutions: The time periodically breathing solution of Kuznetsov and Ma (see [Ma79, Kuz77]) and the space-periodic solution of Akhmediev (see [AEK85, AK86]). The Peregrine Breather represents those two solutions for an infinite breathing period, i.e. the Peregrine Breather just pulsates once to a peak three times of the carrier wave amplitude and tends to the plane wave for  $x \rightarrow \pm\infty$  and  $t \rightarrow \pm\infty$ :

$$q_p(x, t) = a_0 e^{-\frac{ik_0^2 a_0^2 \omega_0}{2} t} * \left( 1 - \frac{4(1 - ik_0^2 a_0^2 \omega_0 t)}{1 + [2\sqrt{2}k_0^2 a_0(x - c_g t)]^2 + k_0^4 a_0^4 \omega_0^2 t^2} \right) \quad (2.9)$$

where  $t$  and  $x$  are the time and longitudinal coordinates,  $a_0$ ,  $k_0$  and  $\omega_0 = \omega(k_0)$  denote the amplitude, wave number and the wave frequency of the carrier wave, respectively.  $\omega_0$  and  $k_0$  are linked by the dispersion relation (see chapter 4). Accordingly, the group velocity is  $c_g := \frac{d\omega}{dk}|_{k=k_0} = \frac{\omega_0}{2k_0}$ . The surface elevation of the sea water is then given by  $\eta(x, t) = \text{Re} \left\{ q_p(x, t) e^{i(k_0 x - \omega_0 t)} \right\}$  with phase velocity  $\frac{\omega_0}{k_0} = 2c_g$  or in second-order  $\eta(x, t) = \text{Re} \left\{ q_p(x, t) e^{i(k_0 x - \omega_0 t)} + \frac{1}{2} k_0 |q_p(x, t)|^2 e^{2i(k_0 x - \omega_0 t)} \right\}$ . Linear, second order, or even higher order experimental driving is further investigated in section 3.2.

It is easily shown that (2.9) is an exact solution of the NLS (2.6). Looking at  $\eta(x, t)$  of order one it is the uniform wave train disturbed by the unstable modulation term in brackets of (2.9). As seen in figure 2.2 this disturbance moves at group velocity  $c_g$  and focuses wave energy on itself. The Peregrine solution is localized in space and time and as such describes a unique

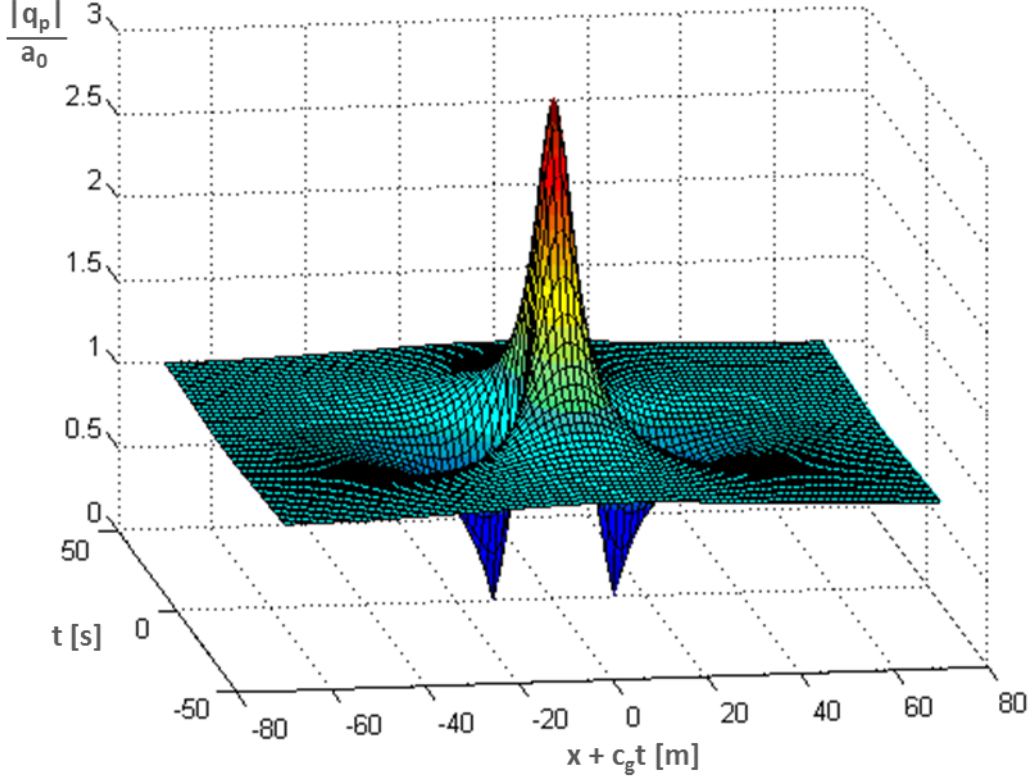


**Figure 2.2:** Peregrine Breather solution (2.9). Maximum amplitude amplification of three at  $x + c_g t = 0$  and  $t = 0$ . Minimum amplitude amplification of zero.  
Note: Moving reference system in  $x$ .

rogue wave event multiplying the carrier wave by a factor of three. It only breathes once and is untraceable afterward: 'A single wave of large amplitude that appears from nowhere and disappears without a trace.' Therefore it is a perfect prototype in qualitative behavior and form for a nonlinear rogue wave in the ocean as also explained in [DT99] and [SG10]. More analytical NLS solutions which are localized in space and time can be found in [AAT09].

Figure 2.3 presents the experiment of [CHA11] driving the Peregrine Breather Solution according to (2.9) with  $a_0 = 0.01m$ ,  $k_0 = 11.63 \frac{rad}{m}$ , and  $\omega_0 = 10.7 \frac{rad}{s}$  in a water wave tank. The driven surface elevation is given by  $\eta(x, t) = \text{Re} \{ q_p(x, t) e^{i(k_0 x - \omega_0 t)} \}$ . We see that the initial distortion focuses energy on itself growing to an extreme wave event with its maximal peak at  $9.1m$  distance from the wave maker.

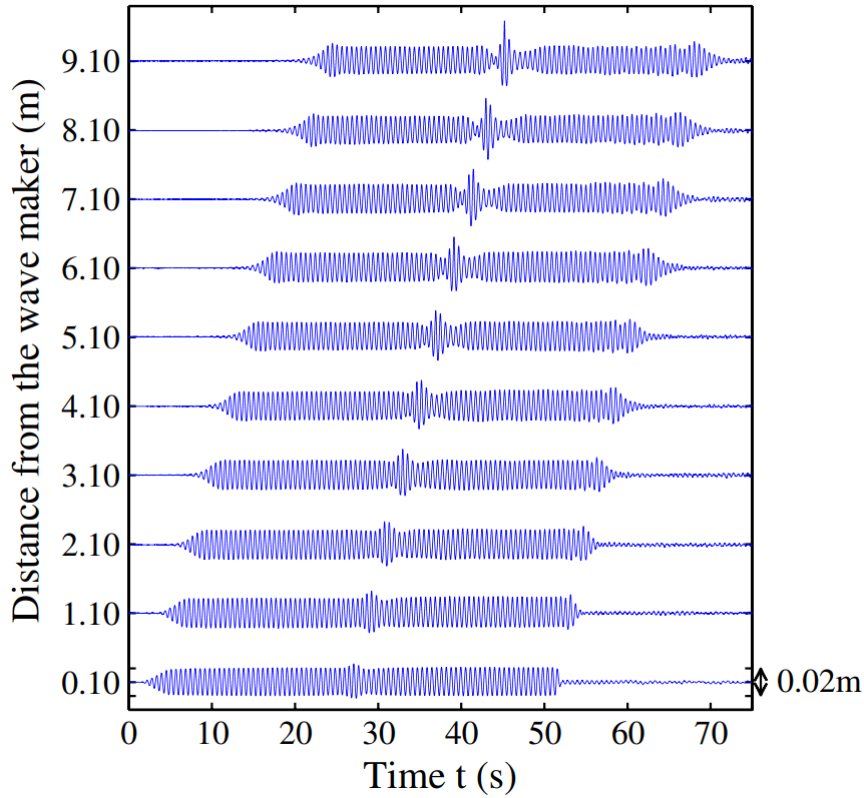


**Figure 2.3:** Temporal evolution of the water surface height of a wave driven by the Peregrine Breather solution at various distances from the wave maker.  
Figure from 'Rogue Wave Observation in a Water Wave Tank' from [CHA11].

Considering the Peregrine solution as a uniform wave disturbed by an unstable modulation term, we determine three main issues to achieve our objectives:

- Can we modify the carrier wave to an arbitrary sea state without destroying the growing modulation character of the distortion term?
- Can we change the parameters of the distortion term preserving the growing modulation character but shaping the rogue wave event in a specific predefined way in properties like height, steepness, and speed?
- Can we still forecast the rogue wave event by our governing equations?

Next to the general question of how to inject those modulation instabilities to real wave fields and the reverse engineering of real rogue wave events, we will answer these questions in chapter 5, 6 and 7 and will even sketch the results of the instability propagating into different wave domains (neighboring waves) in the outlook of further studies in chapter 8.

However, before that, we will have a closer look at how to produce waves in a wave basin to run fine-tuned experiments in chapter 3 first. And second, we will specify the governing equations and programmed analyzing tools in chapter 4.





$\prod_{l=1}^m(1 - \frac{is}{Z_l})/\prod_{k=1}^n(1 - \frac{is}{P_k})$  to flap motions for generating the aimed wave. The filter  $H(s)$  determined by the complex poles  $P_k$  and complex zeros  $Z_l$  changes the amplitudes and inserts phase shifts increasing with radial frequency  $s$  (see [Del12]). From measurements it was possible to compute those complex parameters, called the wave board characteristics, that define the transfer function.

This thesis uses this process to drive arbitrary analytical wave functions: A Matlab file has been created which transforms an analytical wave function to a file of wave data points of 25 Hz. We initiate a dummy wave by the standard Bosch software. Then, the related motion data file of step (2) is replaced by the Matlab produced file. Therefore in step (3) the driving facility reads the wave data points of our aimed wave function and transfers them to flap kinematics to produce the targeted wave train. Furthermore, in this way we are also able to write individual data points for each flap and by that drive every flap individually.

This procedure even allows us to extend the wave tank length artificially. To this end, we measure the surface motion near the beach (but before affected by reflecting waves) with a frequency of 25 Hz. These recorded data points are written to a wave motion file. This file is used to trigger the driving facility of the flaps for the next run. By repeating this process, we can prolong the wave tank theoretically to an arbitrary length (considering slight wave dynamics changes due to the retriggering as shown in section 3.2).

All experiments are conducted in deep water conditions (see chapter 2.1), i.e. the water depth 2.4m times the wave number is always much larger than one.

#### Ultrasound Probes and Vicon System

The Hamburg Ship Model Basin provides two possibilities of measuring the surface motion:

- There are four free movable ultrasound probes. These gauges measure the surface elevation with ultrasound frequency and return averaged data points of 50 Hz without influencing the water. The recorded data points are written into a text file which can be analyzed as explained in chapter 4. The four probes are free to move to arbitrary positions along the wave tank.
- As a second measuring facility the Hamburg Ship Model Basin has a Vicon system. This system consists of three tracking cameras, arbitrary positionable float objects, and an analyzing software. The camera system captures optically the x (direction of tank length), y (direction of tank width), and z (surface elevation) movements of almost arbitrary many float objects in an area of 4m x 2m. The Vicon software converts those movements to 50

Hz data points. With this measurement device, we can capture the surface elevation of an area of 4m x 2m discretely.

## 3.2 Driving Uniform Waves, NLS Breather Solutions and Arbitrary Directed Sea States

### Uniform Wave Train

We take the plane wave solution  $u_{NLS} = a_0 e^{-\frac{ik_0^2 a_0^2 \omega_0}{2} t}$  of the NLS with  $a_0 = 0.02m$ ,  $k_0 = 5 \frac{rad}{m}$ , and  $\omega_0$  determined by the deep water dispersion relation of first order  $\omega_0 = \sqrt{gk_0}$  with  $g$ : gravitational constant (see chapter 4). We drive the flaps in first order with the surface elevation  $\eta(x, t) = \text{Re} \{ u_{NLS}(t) e^{i(k_0 x - \omega_0 t)} \}$  at  $x = 0m$ .

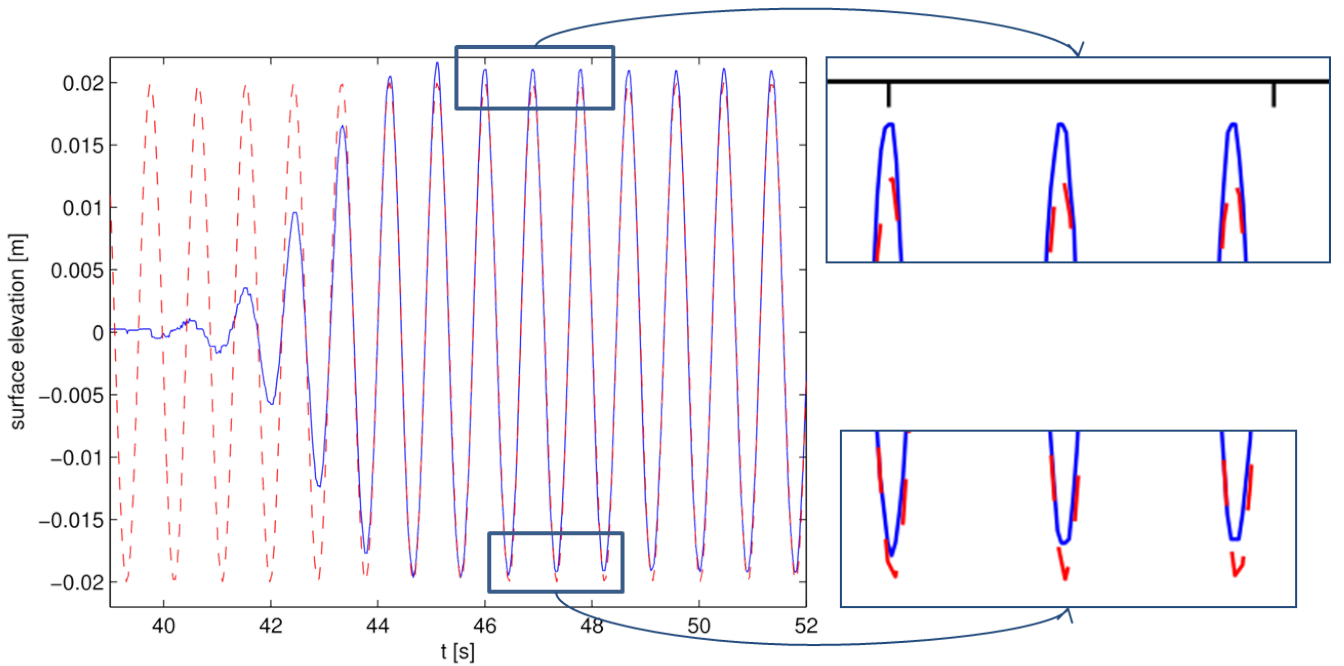


**Figure 3.2:** Uniform Wave Driven with Order 1: Wave Record 1m behind flap (blue line) versus Uniform Wave 1st Order (red dashed line)

Figure 3.2 compares the resulting wave in the wave basin 1m (not even 1 wavelength) after the flap (blue line) against the theoretical first order driven wave  $\eta(1, t)$  (red dashed line). The wave record is given by an ultrasound probe. We see some key features:

- The flap driving is started with a smooth transition from no movement to the full amplitude and phase movement within 5s.

- This starting process leads naturally to an initial overshooting of the amplitude.
- The comparison of the two waves returns an averaged absolute error  $\frac{\sum_{i=1}^N |\eta(1, t_i) - f(t_i)|}{N}$  [in m] of  $5.5886e^{-4}$ , with  $f(t)$ : wave record and  $t_i$ :  $N$  time steps starting at the first peak after the overshooting crest for in total 50 wave periods. Though the agreement is already very good, all crests of the measured wave are higher and all troughs flatter than the theoretical wave. This is the typical nonlinear Stokes behavior (see [Wik17]) occurring though the flaps are driven in order 1.
- Figure 3.3 compares the measured wave to the theoretical surface elevation  $\eta(x = 1, t) = \text{Re} \left\{ u_{NLS}(t) e^{i(k_0 x - \omega_0 t)} + \frac{1}{2} k_0 |u_{NLS}(t)|^2 e^{2i(k_0 x - \omega_0 t)} \right\}$  of order 2. Therefore the crests and troughs are met better reducing the averaged absolute error to  $4.0731e^{-4}$ . Visually it is already hard to see a difference between the two wave lines after the overshooting peak.
- If we even drive the flaps by order 2, i.e.  $\eta(x = 0, t) = \text{Re} \left\{ u_{NLS}(t) e^{i(k_0 x - \omega_0 t)} + \frac{1}{2} k_0 |u_{NLS}(t)|^2 e^{2i(k_0 x - \omega_0 t)} \right\}$  and compare the resulting wave to the theoretical wave 1m behind the flap we will reduce the averaged absolute error to  $3.5389e^{-4}$ .
- A comparison to third order or even driving the flaps by the theoretical uniform NLS solution with order 3 does not reduce significantly the averaged absolute error anymore.

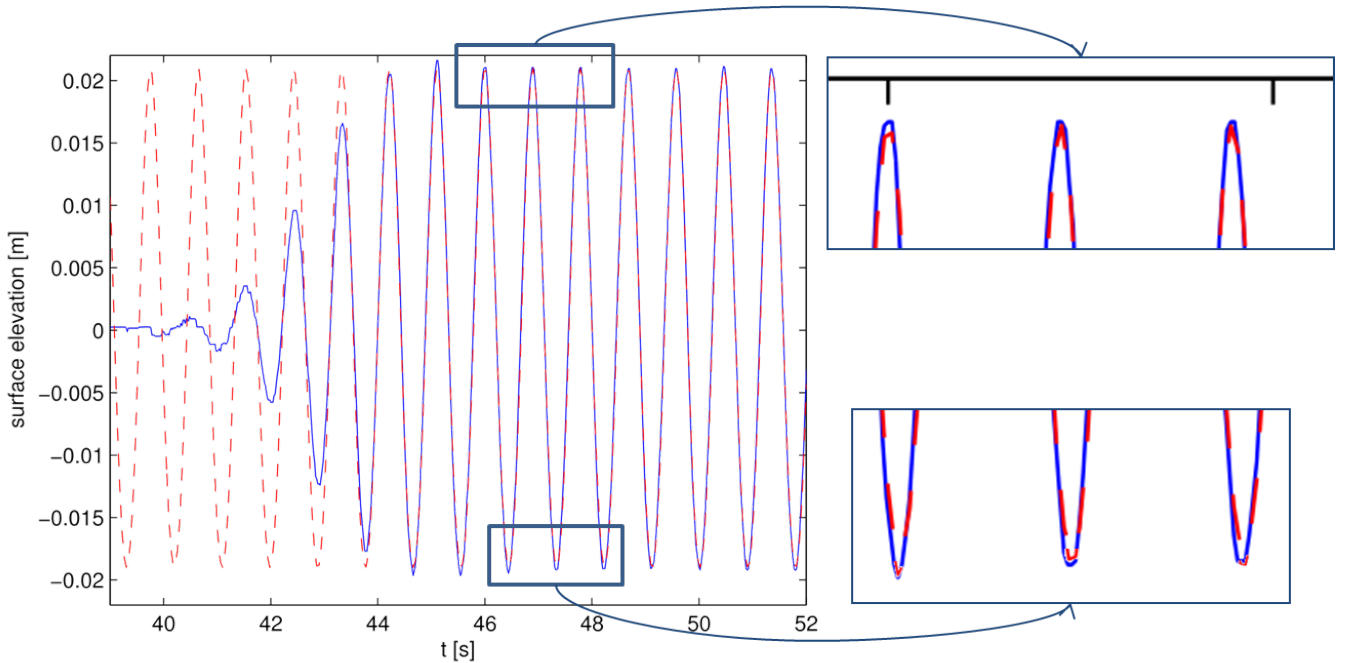


**Figure 3.3:** Uniform Wave Driven with Order 1: Wave Record 1m behind flap (blue line) versus Uniform Wave 2nd Order (red dashed line)

We conclude that the generated wave is close to the theoretically driven wave. For the uniform NLS wave driving and comparing of order 2 is sufficient and advisable.

The same key features are determined 30m behind the flap. Figure 3.4 compares the theoretical uniform wave of order 2 against the measured wave driven by order 2. The transition zone from zero to full movement and the overshooting amplitude grew due to dispersion. The averaged absolute error after the transition zone is adequate with  $3.9478e^{-4}$ . Furthermore, the dissipation is not noticeable: The amplitude attenuation of the wave trains in all experiments with regular wave trains is not measurable or just marginal. However, if we drive an irregular wave field the dissipation has to be taken into account as we will see in section 6.4 and chapter 7.

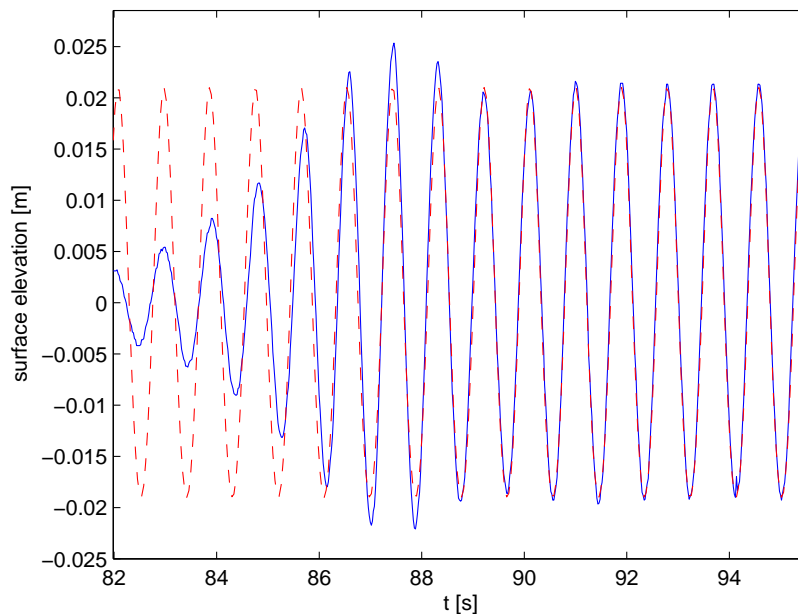


**Figure 3.4:** Uniform Wave Driven with Order 2: Wave Record 30m behind flap (blue line) versus Uniform Wave 2nd Order (red dashed line)

### Nonlinear Schroedinger Equation Breather Solutions

We drive exemplary the Peregrine Breather solution according to equation (2.9) with first order driving, i.e.  $\eta(x, t) = \text{Re} \left\{ q_p(x, t) e^{i(k_0 x - \omega_0 t)} \right\}$  with  $a_0 = 0.01m$ ,  $k_0 = 7.3 \frac{\text{rad}}{m}$ , and  $x = -17.72m$ . We measure the highest peak after  $27.98m$  and determine the 'best fit Peregrine model' according to chapter 4 which is  $\eta(-0.01m, t)$ . Figure 3.5 presents the measured wave elevation (blue solid line) and the 'best fit Peregrine model' (red dashed line).

Beside the 'Stokes effect' of higher crests and flatter troughs of the measured wave we can see some of the constraints of the Nonlinear Schroedinger equation as described in section 2.1:

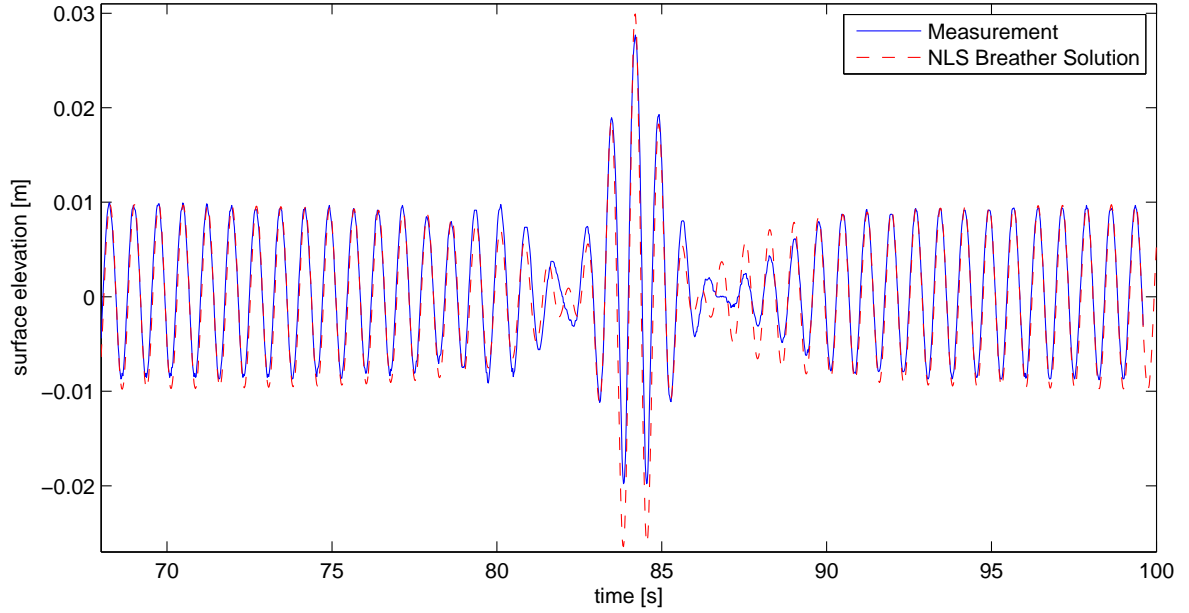


**Figure 3.5:** Measured Breather Wave driven by  $\eta(x = -17.72m, t)$  after  $27.98m$  in its Maximal Peak (blue solid line) compared to the 'Best Fit Peregrine Model' (red dashed line)

- Next to the horizontal asymmetry we also see the vertical asymmetry of the wave evolution. The initially symmetric wave packet evolves partly due to the nonlinear increase of the group velocity in an asymmetric manner. The NLS Peregrine Breather solution does not map this.
- Furthermore, we see the frequency down-shifting of the real measured wave near its maximal peak. The NLS does not account for this.
- In addition, the maximal peak of the extreme wave is overestimated by the Peregrine Breather model. Hence, the theoretical freak index of  $AI = 3$  reduces to  $AI = 2.4$ . This effect depends on the initial steepness  $\varepsilon_0 = a_0 k_0$  of the wave as shown in [SA13].
- Moreover, the Peregrine was driven with  $x = -17.72m$  and should have its maximum peak after  $17.72m$  consequently. Yet, its maximal peak evolves after  $27.98m$  which is in agreement with the studies of [SA13]. The spatial locating can be improved by higher order simulations of the Peregrine Breather model.

Nevertheless, we see the good alignment of the measured wave and the relating theoretical NLS Peregrine Breather solution. However, to quantify changes by modification of the distortion term in equation (2.9) and of the carrier wave, we will have to perform high order simulations

or execute real wave tank experiments. Yet, we can use the NLS solutions to drive the targeted wave as the wave field 'adjusts' quickly to the related high order natural dynamics.

### JONSWAP Wave and Extending Wave Tank Artificially

---

In order to test an arbitrary directed sea state as well as the procedure to extend the wave tank length artificially (see section 3.1), we drive a wave field simulating a possible North Sea state according to [HPBB<sup>+</sup>73]. To this end, we generate a JONSWAP spectrum by the Wave Analysis for Fatigue and Oceanography (WAFO, based on [HPBB<sup>+</sup>73]) project: a toolbox of Matlab routines for statistical analysis and simulation of random waves and random loads [WAF09]. According to WAFO

' the JONSWAP spectrum is assumed to be especially suitable for the North Sea [...].

It is a reasonable model for wind generated sea when  $3.6\sqrt{H_s} < T_p < 5\sqrt{H_s}$  ,

, where  $H_s$  is the significant wave height, and  $T_p$  the peak wave period. To relate to our standard experiment cases, we use a significant wave height of  $H_s = 0.04m$ , peak wave period  $T_p = \frac{2\pi}{\sqrt{gk}}s$  with  $k = 5\frac{rad}{m}$ , and peak enhancement factor according to [TFH<sup>+</sup>84]  $\gamma = e^{3.484*(1-0.1975*D*T_p^4/(H_s^2))} = 1.5729$  with  $D = 0.036 - 0.0056 * T_p/\sqrt{H_s}$ . The related ocean wave spectra considering 256 wave frequencies is shown in figure 3.6.

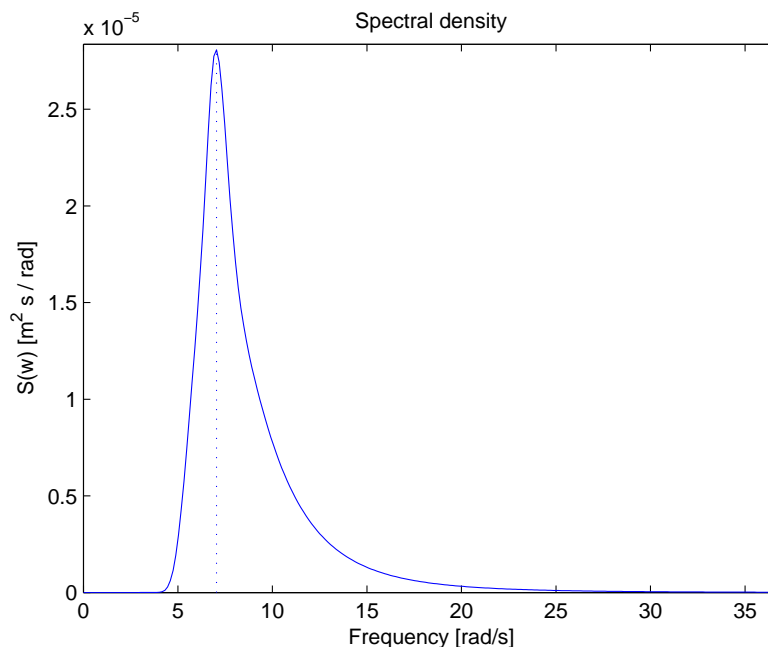


**Figure 3.6:** JONSWAP Ocean Wave Spectrum with significant wave height of  $H_s = 0.04m$ , peak wave period  $T_p = 0.89714s$ , and peak enhancement factor  $\gamma = 1.5729$ .

Let  $S_l$  be the spectral density to the wave frequency  $\omega_l$ ,  $k_l$  the related wave number determined by the deep water dispersion relation of first order  $\omega_l = \sqrt{gk_l}$ ,  $d\omega$  the step width of the uniform distributed wave frequencies, and  $\theta_l \in [0; 2\pi)$  a random phase offset. We superpose the related waves by

$$\eta(x, t) = \text{Re} \left\{ \sum_l \left( A_l e^{i(k_l x - \omega_l t - \theta_l)} + \frac{1}{2} k_l A_l^2 e^{2i(k_l x - \omega_l t - \theta_l)} \right) \right\}, \text{ with } A_l = \sqrt{S_l * 2d\omega} \quad (3.1)$$

or in the sense of the NLS the uniform wave solutions

$$\eta(x, t) = \text{Re} \left\{ \sum_l \left( u_l(t) e^{i(k_l x - \omega_l t - \theta_l)} + \frac{1}{2} k_l |u_l(t)|^2 e^{2i(k_l x - \omega_l t - \theta_l)} \right) \right\} \quad (3.2)$$

, where  $u_l(t) = \sqrt{S_l * 2d\omega} e^{-\frac{ik_l^2 \sqrt{S_l * 2d\omega}^2 \omega_l}{2} t}$

$\eta(0, t)$  gives us an analytical function to drive a wave. Figure 3.7 compares the measured JONSWAP wave (3.2) 2m behind the flaps against the simulated wave evolution by a High Order Spectral (HOS) method (see section 4.1). The averaged absolute error is  $2.05e^{-3}$  which is 5.1% of the significant wave height  $H_s$ . Indeed, in all experiments and HOS simulations of irregular waves, we could determine an averaged error of roughly 5% of the significant wave height  $H_s$ . Of course, this value is worse than for regular waves. Nevertheless, the main properties and dynamics of the irregular wave are met, and the averaged error is still small. We conclude we may even trigger irregular waves with an acceptable accuracy to perform experiments in arbitrary directed sea states or to extend the wave tank artificially.

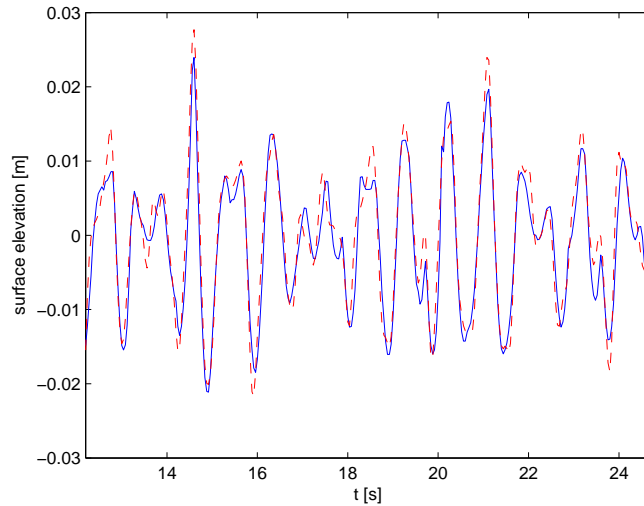


**Figure 3.7:** Measured JONSWAP wave (blue line) against HOS simulated wave (red dashed line) 2m behind flap.

## 4 Governing Equations and their Use Cases

### 4.1 Temporal and Spatial versions of NLS, Dysthe, and NLSType3

As pointed out in chapter 2.1 the Nonlinear Schroedinger Equation (NLS) (2.6) has some drawbacks. For simulating and analyzing waves, it is in some cases advisable to use higher order equations and simulation processes than given by the NLS. Following the used equations and simulation implementations are presented:

#### Temporal and Spatial Nonlinear Schroedinger Equation

The NLS (2.6) and its spatial analog is used to be able to make a fast and numerical efficient comparison of a measured and a theoretical wave:

- A 'best fit model' analysis tool for the NLS to a measured wave is determined by minimizing the averaged absolute or relative error of the recorded wave to a parametrized theoretical NLS solution wave (e.g. Peregrine Breather). To this end, an iteration is run over the parameters wave number, steepness, and either location or time. The averaged absolute error of each iteration is then found by the sum of absolute errors divided by the number of compared time steps or spatial steps, respectively.
- A split step ([WH86, Sua15]) based simulation of a given initial wave according to the 2D and 3D NLS has been implemented by Graphics Processing Unit (GPU) Computing based on CUDA (see [NVI18a]). GPU Computing uses the real parallel nature of graphics processing to accelerate the computational speed of a simulation as described in [NVI18b]. The standard (temporal) NLS delivers the possibility of time integrating an initial wave given at a specific time over all spatial dimensions. To be able to evolve numerically a given wave time series at a specific local point (e.g. wavemaker), we will need a spatial analog to the temporal NLS. To this end, we adapt a simple, heuristic derivation of the temporal NLS presented in [Yue91] and [Deb94]. For reasons of clarity and comprehensibility, we present the one spatial dimensional case:

We determine the inverse function of the third order Stokes dispersion relation (see

[Wik17])  $\omega = \sqrt{gk + ga^2k^3}$  resulting in  $k(\omega, a)$  and expand the wave number  $k$  to second order in wave amplitude  $a$  and perturbation wave frequency  $(\omega - \omega_0)$

$$-(k - k_0) + \frac{2k_0}{\omega_0}(\omega - \omega_0) + \frac{k_0}{\omega_0^2}(\omega - \omega_0)^2 - k_0^3 a^2 = \mathcal{O}(a^{p_1}(\omega - \omega_0)^{p_2}), \text{ with } p_1 + p_2 \geq 3 \quad (4.1)$$

Recalling a direct correspondence between the dispersion relation and this equation, the following associations can be made based on the theories of the Fourier transform:  $-i(\omega - \omega_0) \rightarrow \frac{\partial}{\partial t}$ ,  $i(k - k_0) \rightarrow \frac{\partial}{\partial x}$ . Thus, it can be argued that the operator to be applied to the complex wave envelope function  $A$  takes the form

$$\hat{P} = i \frac{\partial}{\partial x} + i \frac{2k_0}{\omega_0} \frac{\partial}{\partial t} - \frac{k_0}{\omega_0^2} \frac{\partial^2}{\partial t^2} - k_0^3 a^2 \quad (4.2)$$

Since  $a = |A|$ , we obtain a spatial analog to the (temporal) NLS (2.6) for  $A$ :

$$i \left( \frac{\partial A}{\partial x} + \frac{2k_0}{\omega_0} \frac{\partial A}{\partial t} \right) - \frac{k_0}{\omega_0^2} \frac{\partial^2 A}{\partial t^2} - k_0^3 |A|^2 A = 0 \quad (4.3)$$

A direct derivation of this spatial NLS out of the temporal NLS is presented in [LM85].

The 'best fit Peregrine model' analysis tool provides a surprisingly useful tool to determine the distance to the maximum of the growing modulation for regular and irregular waves distorted by Peregrine type modulations. In addition, the simulation of an initial wave field by the temporal or spatial NLS can provide the qualitative behavior of a growing instability. However, [SA13] showed that the NLS forecasts the maximum peak of a Peregrine Breather too early and too high. And of course, all other limits of the NLS presented in chapter 2.1 have to be taken into account using these weak nonlinear governing equations.

#### Dysthe Equations and Third Order NLS Type Equation

If we take in the derivation using (2.3) to (2.5) in chapter 2.1 one more steepness order into account than in the NLS, we will get the Modified Nonlinear Schroedinger Equations, also known as Dysthe equations. It is a coupled system of equations which for clarity will be presented here neglecting the flow direction perpendicular surface space coordinate  $y$  according to [SD08]:

$$\begin{aligned} i \left( \frac{\partial A}{\partial t} + \frac{\omega_0}{2k_0} \frac{\partial A}{\partial x} \right) - \frac{\omega_0}{8k_0^2} \frac{\partial^2 A}{\partial x^2} - \frac{\omega_0 k_0^2}{2} |A|^2 A - i \frac{\omega_0}{16k_0^3} \frac{\partial^3 A}{\partial x^3} + i \frac{\omega_0 k_0}{4} A^2 \frac{\partial A^*}{\partial x} \\ + i \frac{3}{2} \omega_0 k_0 |A|^2 \frac{\partial A}{\partial x} - k_0 A \frac{\partial \phi}{\partial x} \Big|_{z=0} = 0 \end{aligned} \quad (4.4)$$

$$\frac{\partial^2 \phi}{\partial x^2} + \frac{\partial^2 \phi}{\partial z^2} = 0 \text{ for } (-h < z < 0) \quad (4.5)$$

where  $A^*$  is the complex conjugate of the complex envelope  $A(x, t)$ ,  $\phi(x, z, t)$  is the potential of the induced mean current,  $h$  is the water depth, and  $z$  the (x,y)-perpendicular space coordinate in the direction of the water depth with  $z = 0$  is the location of the free surface. These equations may be subjected to the boundary conditions at the free surface and at the bottom:

$$\frac{\partial \phi}{\partial z} = \frac{\omega_0}{2} \frac{\partial |A|^2}{\partial x} \text{ at } (z = 0) \quad (4.6)$$

$$\frac{\partial \phi}{\partial z} = 0 \text{ for } (z \rightarrow -\infty) \quad (4.7)$$

It is easily seen that the temporal NLS is recovered from the first four terms of (4.4). A spatial version of the Dysthe equations is presented in [SD08], too. Nevertheless, the coupled equations are a bit more complex and thus more time-consuming in simulation and numerical solving process than the NLS. As the below presented more accurate High Order Spectral Method (HOS) is highly parallelizable by GPU Computing and therefore already fast in simulation, the Dysthe equation is more interesting in analyzing the effects of taking one order nonlinearity more into account in comparison to the NLS. However, for comparing measured waves to simulated data, the HOS is the more powerful tool.

Therefore a slightly different NLS type equation is derived to combine the simplicity in numerical solving procedures with higher order truncation in steepness. As in the derivation of the spatial NLS above, we expand the wave frequency  $\omega$  taking the third order Stokes dispersion relation  $\omega = \sqrt{gk + ga^2k^3}$  with  $k = \sqrt{k_x^2 + k_y^2}$ . But this time, we expand analog to the Dysthe equations derivation to third order in wave amplitude  $a$  and perturbation wave number:

$$\begin{aligned} & -(\omega - \omega_0) + \frac{\omega_0}{2k_{x_0}}(k_x - k_{x_0}) - \frac{\omega_0}{8k_{x_0}^2}(k_x - k_{x_0})^2 + \frac{\omega_0}{4k_{x_0}^2}k_y^2 + \frac{\omega_0 k_{x_0}^2}{2}a^2 + \frac{\omega_0}{16k_{x_0}^3}(k_x - k_{x_0})^3 \\ & - \frac{3\omega_0}{8k_{x_0}^3}k_y^2(k_x - k_{x_0}) + \frac{5}{4}\omega_0 k_0(k_x - k_{x_0})a^2 = \mathcal{O}(a^{p_1}(k_x - k_{x_0})^{p_2}k_y^{p_3}), \text{ with } p_1 + p_2 + p_3 \geq 4 \end{aligned} \quad (4.8)$$

Again, we make following associations according to theories of Fourier transform:  $-i(\omega - \omega_0) \rightarrow \frac{\partial}{\partial t}$ ,  $i(k_x - k_{x_0}) \rightarrow \frac{\partial}{\partial x}$ ,  $i(k_y) \rightarrow \frac{\partial}{\partial y}$ . If we apply the resulting operator to the complex wave envelope  $A(x, y, t)$ , we will obtain a third order NLS type equation (NLSType3) for  $A$ :

$$\begin{aligned} & i \left( \frac{\partial A}{\partial t} + \frac{\omega_0}{2k_{x_0}} \frac{\partial A}{\partial x} - \frac{\omega_0}{16k_{x_0}^3} \frac{\partial^3 A}{\partial x^3} + \frac{3\omega_0}{8k_{x_0}^3} \frac{\partial^3 A}{\partial y^2 \partial x} \right) - \frac{\omega_0}{8k_{x_0}^2} \frac{\partial^2 A}{\partial x^2} + \frac{\omega_0}{4k_{x_0}^2} \frac{\partial^2 A}{\partial y^2} - \frac{\omega_0 k_{x_0}^2}{2} |A|^2 A \\ & + i \frac{5}{2} \omega_0 k_{x_0} |A|^2 \frac{\partial A}{\partial x} + i \frac{5}{4} \omega_0 k_{x_0} A^2 \frac{\partial A^*}{\partial x} = 0 \end{aligned} \quad (4.9)$$

Likewise, we can develop a spatial version of this (temporal) NLSType3 equation as for the NLS (see above). The similarity to the Dysthe equations is apparent, except of the factors in front of the two last terms and of course the missing potential of the induced mean current.

As Dysthe and the NLSType3 are still developed around a leading wave frequency  $\omega_0$  and wave number  $\mathbf{k}_0 = (k_0, 0)^\top$ , both equations are still not capable of non-directed sea states and wide ranges of frequencies. However, as we take one order in steepness more into account, the equations are capable of steeper wave evolutions than the NLS.

Furthermore, both equations show a nonlinear dependency of the group velocity to the wave steepness directly. While the group velocity of the NLS is given by  $\frac{\partial \omega}{\partial k_x}$  evaluated at the expanding point giving  $\frac{\omega_0}{2k_{x0}}$ , Dysthe with (4.4) and NLSType3 with (4.9) add a nonlinear steepness factor to  $\frac{\partial A}{\partial x}$ . In fact, the factors of the new nonlinear terms in (4.9) are determined by  $\frac{\partial^3 \omega}{\partial k_x \partial a^2}$  which is interpretable as the change in the group velocity due to changes in the amplitude  $a = |A|$ . This is also self-evident by analyzing the wave number domain step of the split step method (presented here in one spatial dimension) to solve the NLSType3 equation:

$$\hat{\mathbf{A}}(\mathbf{k}, t_i + \frac{\Delta t}{2}) = \hat{\mathbf{A}}(\mathbf{k}, t_i) e^{i \frac{\Delta t}{2} (-c_g \mathbf{k} + c_{\text{diff}} \mathbf{k}^2 - c_{\text{curve}} \mathbf{k}^3 - c_{\text{nl2}} \mathbf{k} |\hat{\mathbf{A}}(\mathbf{k}, t_i)|^2)} \quad (4.10)$$

, where  $\hat{\mathbf{A}}$  is the amplitude vector of the discrete Fourier transform of the complex wave envelope  $A$  in the wave number domain specified by the wave vector  $\mathbf{k}$ .  $\Delta t$  specifies the time step from  $t_i$  to  $t_{i+1}$ , and  $c_g = \frac{\omega_0}{2k_{x0}}$ ,  $c_{\text{diff}} = \frac{\omega_0}{8k_{x0}^2}$ ,  $c_{\text{curve}} = \frac{\omega_0}{16k_{x0}^3}$ , and  $c_{\text{nl2}} = \frac{5}{4}\omega_0 k_{x0}$ . While  $c_{\text{curve}} \mathbf{k}^3$  adds a fixed velocity depending on the wave numbers,  $c_{\text{nl2}} \mathbf{k} |\hat{\mathbf{A}}(\mathbf{k}, t_i)|^2$  is a varying extra velocity depending on the steepness of the actual wave. Therefore, Dysthe and NLSType3 are capable of the nonlinear increase in group velocity of steep envelopes and by that also of the frequency down-shifting presented in chapter 2.1. (The frequency down-shifting may be a persisting effect which will be only detected in 3D volume models including the potential of the induced mean current  $\phi(x, z, t)$ ; see [HPD99, Tul96]). This may lead to an asymmetric evolution of an initially symmetric wave packet of which the NLS is not capable. Therefore, both Dysthe and NLSType3 are capable of determining the location of the maximum peak much more accurate as the cubic NLS. Exemplary, [SD08] and [SA13] shows these feature differences by comparing simulations of wave evolutions based on the NLS to the Dysthe equations. Nevertheless, the NLSType3 lacks the detuning effect and restraining forces due to the spatially differentiated potential of the induced mean current in the Dysthe equations. [Dys79] argued this detuning effect leading to a more stable behavior of the modified NLS. Therefore, the NLSType3 is as accurate as the Dysthe equations in determining the spatial location of the maximum peak but - in contrast to the Dysthe equations - will still overestimate the amplitude of the maximum peak in the same way as the NLS.

## 4.2 Temporal and Spatial High Order Spectral Method

For a high order simulation which is not limited to narrow-band domains and by this neither to a directed sea state a high order spectral (HOS) method (see [Boy00]) is used. The HOS simulates an irrotational flow of an incompressible, inviscid fluid. According to section 2.1 we apply the potential flow theory leading to the Laplace's equation (2.3) and following [Zak68] the fully-nonlinear free surface boundary conditions are given by the dynamic boundary condition (2.4) and the kinematic boundary condition (2.5).

In the most common way of the HOS, the scalar velocity potential function  $\Phi(x, y, z, t)$  is Fourier expanded in  $x$  and  $y$  with time-dependent Fourier coefficients and multiplied real exponential functions in  $z$  (see [DBLTF07], for  $x, y, z$ : see figure 4.1). This leads to periodic boundary conditions in  $x$  and  $y$  and solves (2.3) by construction. For every time step the expansion of the velocity potential  $\Phi(x, y, z, t^*)$  (with  $t^*$  is the actual time step) is formed and the vertical derivative  $\frac{\partial \Phi}{\partial z}$  is determined order-consistently. The two surface quantities  $\zeta(x, y, t^*)$  and  $\Phi(x, y, z = \zeta, t^*)$  are then marched in time by an efficient temporal discretization scheme in which the linear parts of the equations are integrated analytically.

The Ecole Centrale de Nantes has developed a 2D and 3D HOS simulation since 2007 free available at [Nan18]. As a temporal version, we use the HOS-ocean toolbox ([DBTF16, DBLTF07, BDTF11]) which simulates the time evolution of an initial given wave field. The spatial version is given by the numerical wave tank toolbox called the HOS-NWT ([DBTF12]) in which the spatial evolution of a located wave time series is simulated.

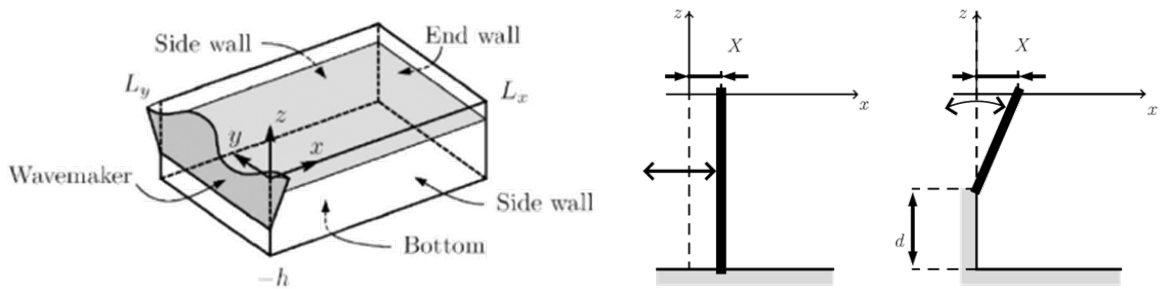


**Figure 4.1:** Numerical wave tank (left) and wave maker (right) of the HOS-NWT toolbox.

To meet the need of this thesis, the time expensive calculation parts have been changed to a GPU Computing version to accelerate the simulation. Furthermore, the HOS-NWT transfer function of the wavemaker to the induced waves in the numerical wave tank has been adapted to the HSVA facilities. Besides, the possibility of forcing a wave time series in a specific location of the wave tank without a wave maker transfer function has been added. To complete the

simulation possibilities, also a backward spatial evolution of a located wave time series and a backward time evolution of an initial wave state have been implemented. By this, we can determine a wave field temporally and spatially before a measured extreme wave.

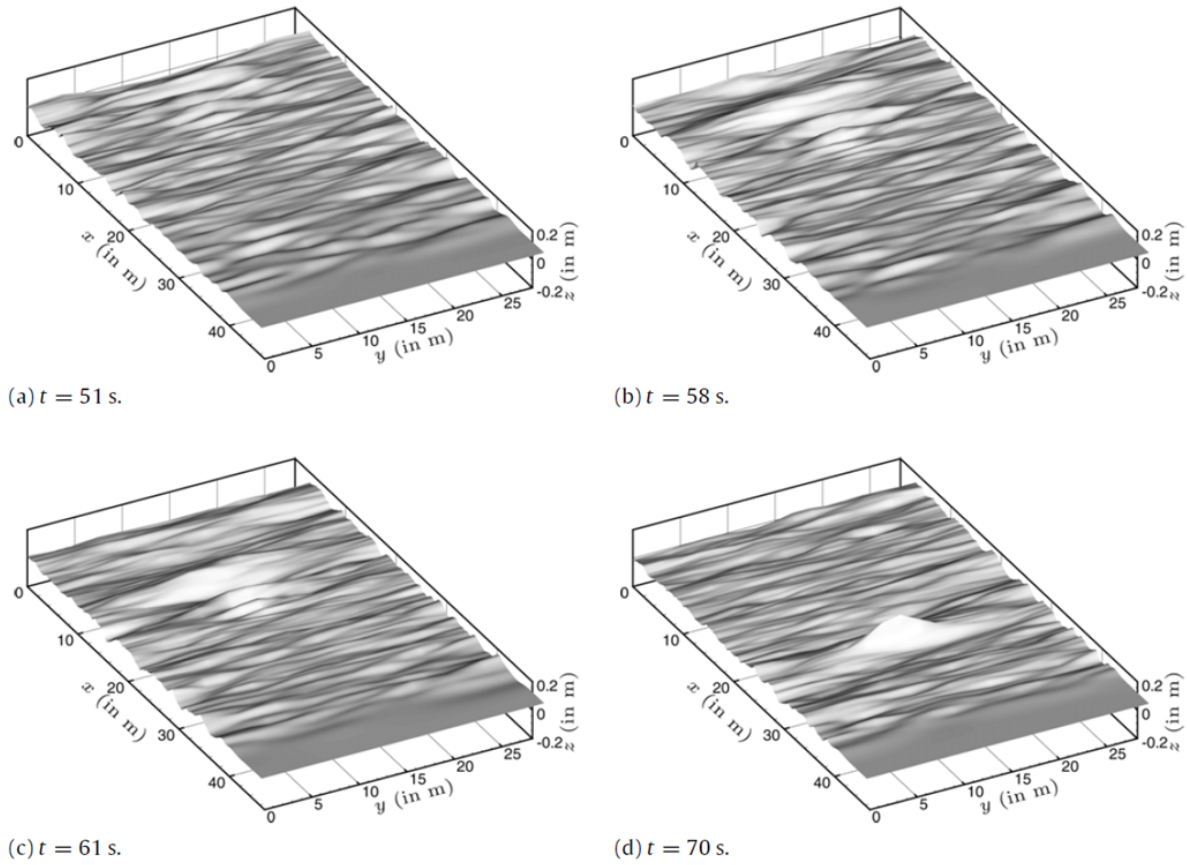


**Figure 4.2:** Visual output of the HOS-NWT toolbox:  
Wave maker at  $x=0$ m and beach with full absorption at  $x=40$ m.

## 5 Effects of Variations in Peregrine Distortion Term on Breather Dynamics

The Peregrine Breather solution (2.9) delivers an initial starting point for causing extreme wave events of predefined shape and location. This chapter presents an experimental study on the Breather distortion term. [ADA09] proved that the Peregrine Breather is robust against small perturbations staying spatially and temporal localized, i.e. representing a modified single steep wave event. Therefore, we question how robust is the growing modulation instability against perturbations itself? What are the limits? Are we able to modify the distortion term to get predefined rogue waves of targeted shapes, height, and steepness? To this end, in section 5.1, 5.2, and 5.3 we will determine three parameters of the distortion term to modify the resulting extreme wave event according to our targeted wave shapes. After that, in section 5.4 we will observe that not the amplitude but the phase modulation is the key feature of the growing Breather type instability. Hence, it is possible to induce a Breather modulation 'energy conservatively' and therefore so to say 'undiscoverable'.

### 5.1 Controlling the Freak Index and Maximal Steepness by the Parameter of the Absolute Maximal Value of the Peregrine Distortion Term

Following we consider the maximal steepness  $s_{max} = \max_i \left\{ \frac{H_i}{L_i} \right\}$  with  $i = 1, 2, \dots, m$  and  $m$  : number of crests in time series,  $H_i$  is the wave height to the  $i^{th}$  wave crest and  $L_i$  is the related local wavelength. A wave height is defined as the vertical distance between a wave crest and the deepest trough preceding or following the crest (see figure 5.1). The local wavelength  $L_i$  is determined by the related local wave period  $T_{local}$  of the  $i^{th}$  crest by the deep water dispersion relation  $\omega = \sqrt{gk}$ .

Hint: We use the steepness definition  $s = \frac{H}{L}$  depending on the wave height and wavelength instead of  $\varepsilon = ak = a \frac{2\pi}{L}$  to be more accurate in the term 'steepness'. However, both quantities are linked by  $H \approx 2a$ , i.e.  $s\pi \approx \varepsilon$ .

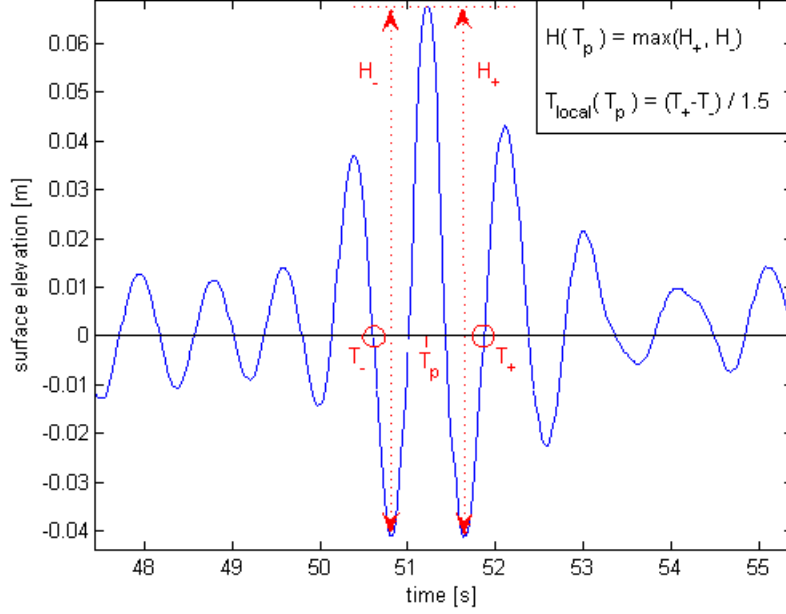


**Figure 5.1:** Visual Explanation of the Wave Height  $H$  and the Local Wave Period  $T_{local}$  related to the Peak Crest at  $T_p$ .

Furthermore, we consider the freak index  $AI$  defined as the quotient of the maximal wave height  $H_{max}$  of all considered waves to the significant wave height  $H_s$  which is the mean wave height of the highest third of the waves in a time series. A rogue wave exceeds per definition at least twice the significant wave height, i.e.  $AI > 2$ .

To control the steepness and freak index value, we investigate the theoretically maximal absolute value of the Peregrine distortion term (at  $x = 0$  and  $t = 0$ ), i.e. we change the factor  $\Gamma$  in

$$q_p(\Gamma, x, t) = a_0 e^{-\frac{ik_0^2 a_0^2 \omega_0}{2} t} * \left( 1 - \frac{\Gamma(1 - ik_0^2 a_0^2 \omega_0 t)}{1 + [2\sqrt{2}k_0^2 a_0(x - c_g t)]^2 + k_0^4 a_0^4 \omega_0^2 t^2} \right) \quad (5.1)$$

which recovers the Peregrine Breather solution for  $q_p(\Gamma = 4, x, t)$ . If we change the value of  $\Gamma$  we will cause extreme wave events with higher or reduced maximal steepness  $s_{max}$  and freak index  $AI$ .

Figure 5.2 illustrates the change in the maximal steepness and freak index for wave tank experiments with a carrier wave of  $a_0 = 0.01m$  and wave number  $k_0 = 7.3 \frac{rad}{m}$ . The maximal wave steepness in figure 5.2 is normalized by the experimentally determined wave breaking threshold steepness 0.142. This value is in agreement with the wave breaking threshold for unidirectional waves in [TBOW10]. Likewise, the freak index is normalized by the maximal experimentally measured freak index  $AI_{max} = 5.3$  on the chosen carrier wave while changing  $\Gamma$ .

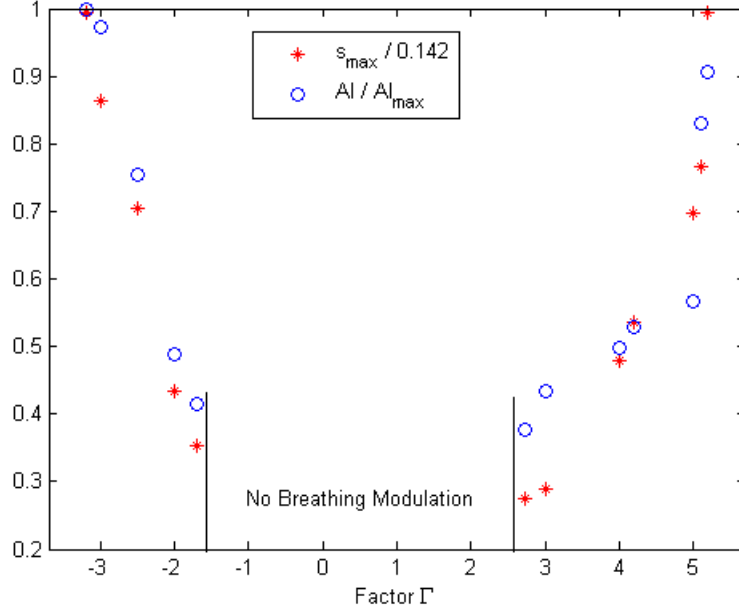


**Figure 5.2:** Experimental Parameter Study on  $\Gamma$  for carrier wave with  $a_0 = 0.01m$  and wave number  $k_0 = 7.3 \frac{rad}{m}$ .  
 Maximal Steepness  $s_{\max} = \max_i \{ \frac{H_i}{L_i} \}$  (red stars) normalized by wave breaking limit 0.142  
 Freak Index  $AI = \frac{H_{\max}}{H_s}$  (blue open circles) normalized by  $AI_{\max} = 5.3$

By varying the parameter  $\Gamma$  we detect a way to control the maximal steepness of the extreme wave events in the experiments. It is possible to increase the maximal steepness until the wave breaking limit of  $s = 0.142$  for  $\Gamma = 5.2$ . On the other hand, a reduction of the Peregrine value of  $\Gamma$  causes a reduced maximal steepness. A further reduction below  $\Gamma = 2.72$  will even suppress the distortion, i.e. there is no breathing modulation or growing instability anymore.

The same way the freak index is controllable. Considering the carrier wave with  $a_0 = 0.01m$  and wave number  $k_0 = 7.3 \frac{rad}{m}$  the maximal reached freak index in the experiments is 5.3.

It is remarkable that the same behavior is observed for negative values of  $\Gamma$  also, though the range of values leading to a non-breaking breathing modulation is much smaller ( $\Gamma \in [-3.2; -1.71]$ ). Moreover, in all our related experiments and simulations the maximal and minimal value of  $\Gamma$  leading to a non breaking breathing modulation are connected by the theoretical maximal absolute distortion value  $q_{dist}^0(\Gamma) := |\frac{q_p(\Gamma, x=0, t=0)}{a_0}|$ :

The maximal positive value of  $\Gamma$  before wave breaking is 5.2 leading to a maximal absolute distortion value of  $q_{dist}^0(5.2) = 4.2$ . On the other hand, the minimal  $\Gamma$  value before wave breaking is  $-3.2$  leading to a maximal absolute distortion value of  $q_{dist}^0(-3.2) = 4.2$  which is

the same value as for the positive range. However, this symmetry is not detectable for the non breathing modulation thresholds:  $q_{dist}^0(2.72) = 1.72 \neq q_{dist}^0(-1.71) = 2.71$ .

Qualitatively, these observations hold for any regular carrier wave in our experiments and simulations. However, quantitatively the behavior changes. Figure 5.3 presents the experimental study on  $\Gamma$  for a less steep carrier wave with  $a_0 = 0.01m$  and wave number  $k_0 = 5.0 \frac{rad}{m}$ .

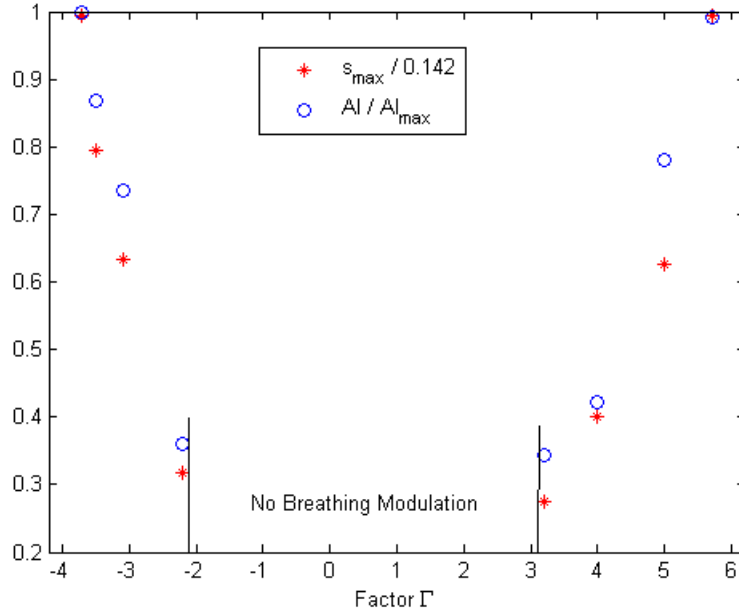


**Figure 5.3:** Experimental Parameter Study on  $\Gamma$  for carrier wave with  $a_0 = 0.01m$  and wave number  $k_0 = 5.0 \frac{rad}{m}$ :

Maximal Steepness  $s_{max} = \max_i \{ \frac{H_i}{L_i} \}$  (red stars) normalized by wave breaking limit 0.142

Freak Index  $AI = \frac{H_{max}}{H_s}$  (blue open circles) normalized by  $AI_{max} = 6.4$

The maximal wave steepness  $s_{max}$  before wave breaking and the minimal wave steepness to cause a breathing modulation are the same, i.e. 0.142 and 0.039 respectively. Also, the width of the positive and negative  $\Gamma$  ranges causing non-breaking breathing modulations are alike. However, the ranges are shifted to bigger absolute numbers of  $\Gamma$  ( $\Gamma \in \{[-3.7; -2.2] \cup [3.2; 5.7]\}$ ). But again, the maximal and minimal value of  $\Gamma$  leading to a non breaking breathing modulation are connected by the theoretical maximal absolute distortion value  $q_{dist}^0(\Gamma)$ :  $q_{dist}^0(5.7) = 4.7 = q_{dist}^0(-3.7)$ . Like in the former case, this symmetry is not detectable for the non breathing modulation thresholds:  $q_{dist}^0(3.2) = 2.2 \neq q_{dist}^0(-2.2) = 3.2$ .

The maximal freak index  $AI_{max}$  is raised to 6.4, i.e. the maximal wave height  $H_{max}$  exceeds the significant wave height  $H_s$  by 6.4. In all our experiments we observed that the less steep

the carrier wave is, the higher is the maximal possible freak index  $AI_{max}$  before wave breaking. This is in agreement with [CLSY81] who proves a higher growth rate of an unstable modulation the smaller the carrier wave steepness is. In contrast, the freak wave probability indicator for long crested wave fields (like in our experiments) called Benjamin-Feir index will not forecast these possible 'super freak waves' for small steepnesses as the index is proportional to the mean wave steepness:

$$I_{BF} = \sqrt{2} \frac{\varepsilon_{mean}}{\Delta\omega/\omega_p} \quad (5.2)$$

, with  $\varepsilon_{mean} = a_{rms} * k_p$ : mean wave steepness as the product of the root mean-square amplitude and the peak wave number,  $\Delta\omega$ : spectral bandwidth, and  $\omega_p$ : peak wave frequency.  $I_{BF}$  is normalized here by the factor  $\sqrt{2}$  such that a random (long crested) wave train is (said to be) unstable if  $I_{BF} > 1$  (see [GT07]).

In the other direction, the restabilization of the system for sufficient high values of the steepness mentioned in [CLSY81] is of interest for simulations only as the given stabilization threshold value of  $\varepsilon_0 = a_0 k_0 > 0.5rad$  corresponds to  $s_0 = \frac{H_0}{L_0} > 0.159$  ( $H_0$  : wave height of carrier wave,  $L_0$  : wavelength of carrier wave) which is bigger than the wave breaking threshold  $s = 0.142$  for unidirectional real wave dynamics anyways and even almost the value of the wave breaking threshold for arbitrary sea states of  $\varepsilon_{wave\ breaking} = (a_0 k_0)_{wave\ breaking} \geq 0.55rad$  which corresponds to  $s_{wave\ breaking} = (\frac{H_0}{L_0})_{wave\ breaking} \geq 0.175$  (see [TBOW10]).

## 5.2 Controlling the Number of Waves in a Steep Wave Event by the Wave Steepness

To control the number of the waves in the steep wave event and to motivate the following section 5.3, we follow [HPD99] and investigate the steepness of the carrier wave, i.e.

$$q_p(\varepsilon_0, x, t) = a_0 e^{-\frac{i\varepsilon_0^2 \omega_0}{2} t} * \left( 1 - \frac{4(1 - i\varepsilon_0^2 \omega_0 t)}{1 + [2\sqrt{2}\varepsilon_0 k_0(x - c_g t)]^2 + \varepsilon_0^4 \omega_0^2 t^2} \right) \quad (5.3)$$

, with steepness  $\varepsilon_0 = a_0 k_0$ . This is not a change in the distortion term, solely. However, its effect is to reduce the affected area of the (still) uniform carrier wave by the perturbation. Recalling figure 2.2 to mind as the absolute value of the complex envelope of the analytical Peregrine Breather solution (5.3) of the NLS,  $\varepsilon_0$  includes without limitation the control of the number of waves of the related surface elevation in the distortion area.

Figure 5.4 shows four measured Peregrine waves in their maximal peaks with  $\varepsilon_0 = 0.06rad$ ,  $\varepsilon_0 = 0.073rad$ ,  $\varepsilon_0 = 0.1rad$ , and  $\varepsilon_0 = 0.112rad$ , respectively.

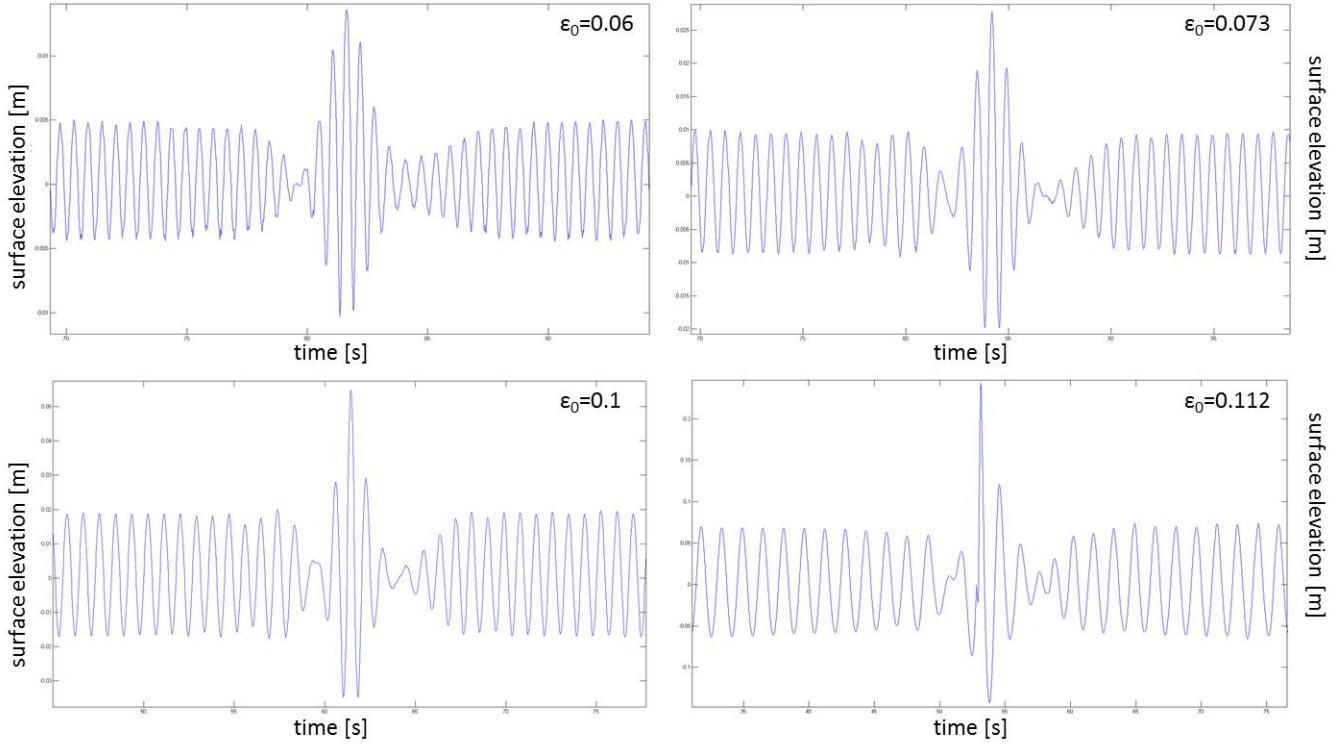


**Figure 5.4:** Experimental Parameter Study on  $\varepsilon_0$  [rad]

It is easy to see from (5.3) that the less steep the carrier wave is, the more waves are included in the 'significant' distortion area leading to steep wave events with more included waves higher than the significant wave height. In figure 5.4 the number of waves in the steep wave event rises from four waves for  $\varepsilon_0 = 0.06rad$  to three waves with less and less high neighboring waves ( $\varepsilon_0 = 0.073rad$  and  $\varepsilon_0 = 0.1rad$ ) to two waves for  $\varepsilon_0 = 0.112rad$ . The maximal local wave steepness in case of  $\varepsilon_0 = 0.112rad$  is  $s_{max} = 0.14$ , i.e. close to wave breaking. It is possible to go even further and reduce the number of waves higher than  $H_s$  to a single wave only, but this leads to a slightly breaking freak wave with foam which is not measurable adequately with the ultrasound probes. Therefore, a picture of an experiment with this so-called 'White Wall' event for a carrier wave with  $\varepsilon_0 = 0.12rad$  is presented in figure 5.5. It is a very steep wave with white capping followed by a deep trough. An interesting fact is that this slightly wave breaking seems to stabilize the steep wave event leading to a qualitatively longer time period of the maximal wave peak. This effect has to be analyzed further in proceeding experiments.



**Figure 5.5:** 'White Wall' event for Peregrine Breather with Carrier Wave of  $\varepsilon_0 = 0.12rad$

Another typical eyewitness report is the case of the 'Three Sisters': Three high waves succeeding one another with narrow troughs preventing the buoyancy for ships which will be overrun by the second or latest third wave, therefore. This event may relate to the three waves in figure 5.4 with a carrier wave of  $\varepsilon_0 = 0.073rad$ .

It is to underline that the number of high waves in the steep wave event relates to the steepness  $\varepsilon_0$  of the carrier wave and not to the amplitude  $a_0$  or the wave number  $k_0$  only. A change in the wave amplitude or wave number does not change the qualitative behavior of the freak wave event if the steepness is constant.

To quantify the change of the steep wave event (SWE) by changing the steepness  $\varepsilon_0$  we measure the surface of the freak wave, i.e.

$$A_{SWE} = \sum_{t_{left}}^{t_{right}} \frac{|\eta(t_i)| \Delta t}{H_s/2} \quad (5.4)$$

$t_{left}$  : first  $t_i$  with  $|\eta(t_i)| > H_s/2$  in SWE,  $t_{right}$  : last  $t_i$  with  $|\eta(t_i)| > H_s/2$  in SWE

, with  $\eta(t_i)$  is the surface elevation to the  $i^{th}$  sampling time  $t_i$  and  $\Delta t = 1/f_{\text{Ultrasound Probe}}$  the reciprocal of the ultrasound probe sampling rate. Exemplary, figure 5.6 presents the surface elevation considered in  $A_{SWE}$  by the dashed red line.

Figure 5.7 shows the experimentally determined steep wave event surface  $A_{SWE}$  for different carrier wave steepnesses  $\varepsilon_0$ . Analogously to the four pictured waves in figure 5.4, we see that

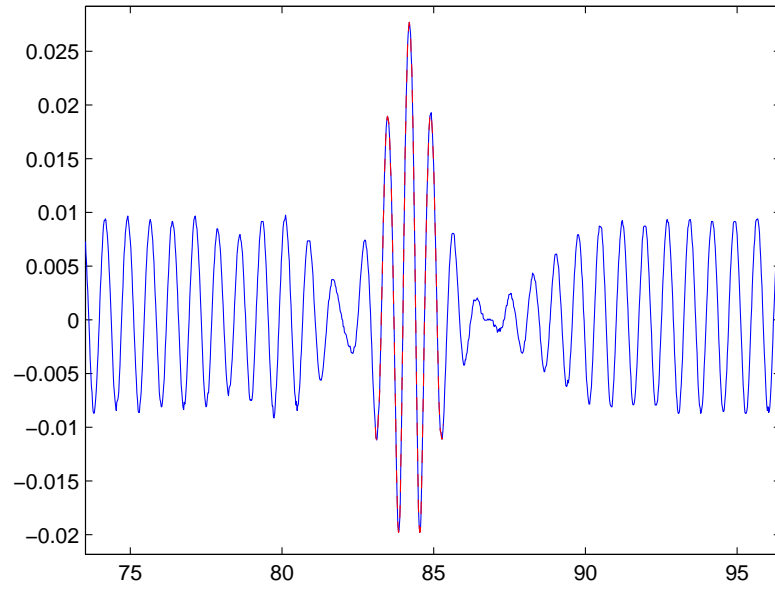


**Figure 5.6:** Explanation of  $A_{\text{SWE}}$ : Considered Surface Elevation (dashed red line)

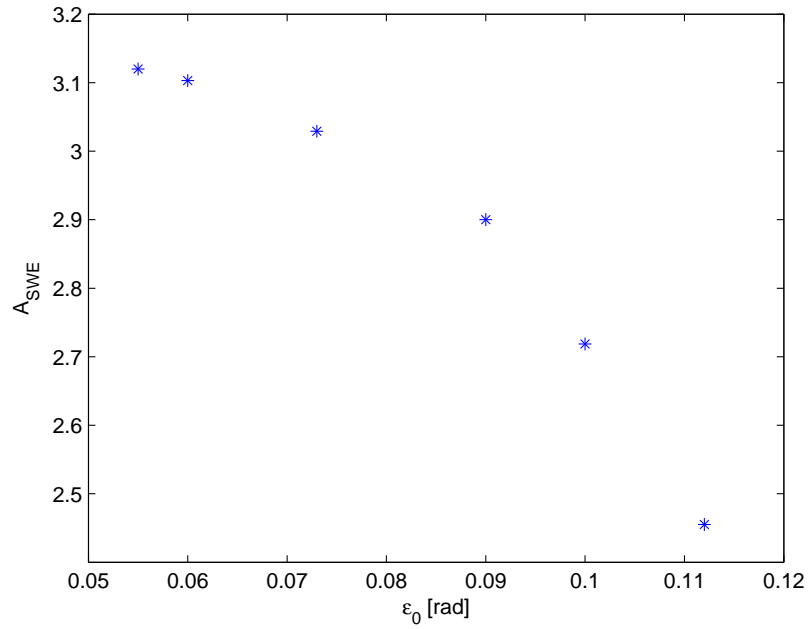


**Figure 5.7:** Experimental Parameter Study on  $\varepsilon_0$ :  $A_{\text{SWE}}$  against carrier wave steepness  $\varepsilon_0$

the number of waves measured by the surface of the rogue wave event reduces more and more. Therefore, the steepness parameter  $\varepsilon_0$  of the carrier wave is an easy way to control the number of waves in the steep wave event.

The problem remains that this is not a change in the distortion term, solely. If the carrier wave has a given, fixed steepness or if it is even an arbitrary directed sea state, we can not use this parameter. Furthermore, the steepness influences the effect of the  $\Gamma$  shaping parameter of section 5.1. Therefore, we will determine a similar, but distortion term only shaping parameter in the following section.

### 5.3 Relocating of the Maximal Wave Peak by the Wave Number of the Peregrine Distortion Term

Next, we question if we can produce phenomena like White Walls without changing the steepness of the carrier wave and if we can increase freak indexes and maximal steepnesses without changing the maximal value of the Peregrine distortion term. Furthermore, we like to control the range widths of reduced wave amplitudes before and after the steep wave event. To this end, we investigate the wave number  $k_1$  in the Peregrine distortion term, i.e.

$$q_p(k_1, x, t) = a_0 e^{-\frac{ik_0^2 a_0^2 \omega_0}{2} t} * \left( 1 - \frac{4(1 - ik_1^2 a_0^2 \omega_1 t)}{1 + [2\sqrt{2}k_1^2 a_0(x - c_{g1}t)]^2 + k_1^4 a_0^4 \omega_1^2 t^2} \right) \quad (5.5)$$

with  $\omega_1(k_1) = \sqrt{gk_1}$  according to the dispersion relation, and  $c_{g1} = \frac{\omega_1}{2k_1}$ .  $q_p(k_1 = k_0)$  recovers the Peregrine Breather solution. By changing the value of  $k_1$ , we change the wavelength and by that the steepness value of the distortion term only. This allows us to shift the maximum peak of the steep wave event in time within the distortion area (figure 5.8) or even into the domain of the not amplitude reduced uniform carrier wave (figure 5.9). In this manner, we may increase the maximal peak, change the amplitude reduced range width, and produce different wave shapes like a White Wall.

Figure 5.8 pictures two steep wave events in their maximal peaks for different  $k_1$  values (carrier wave with  $a_0 = 0.02m$  and  $k_0 = 5 \frac{rad}{m}$ ). We see that the number of waves in the non-uniform wave range remains but the maximal peak is shifted for  $k_1 = 0.5k_0$ . By this we prolong the reduced amplitude range behind the peak, increase the freak index  $AI$  from 2.31 to 3.32 as well as the maximal wave steepness  $s_{max}$  from 0.0882 to 0.1133. Furthermore, the rogue wave shape for  $k_1 = 0.5k_0$  looks similar to figure 5.4 in case of  $\varepsilon_0 = 0.112rad$ , i.e. a White Wall.

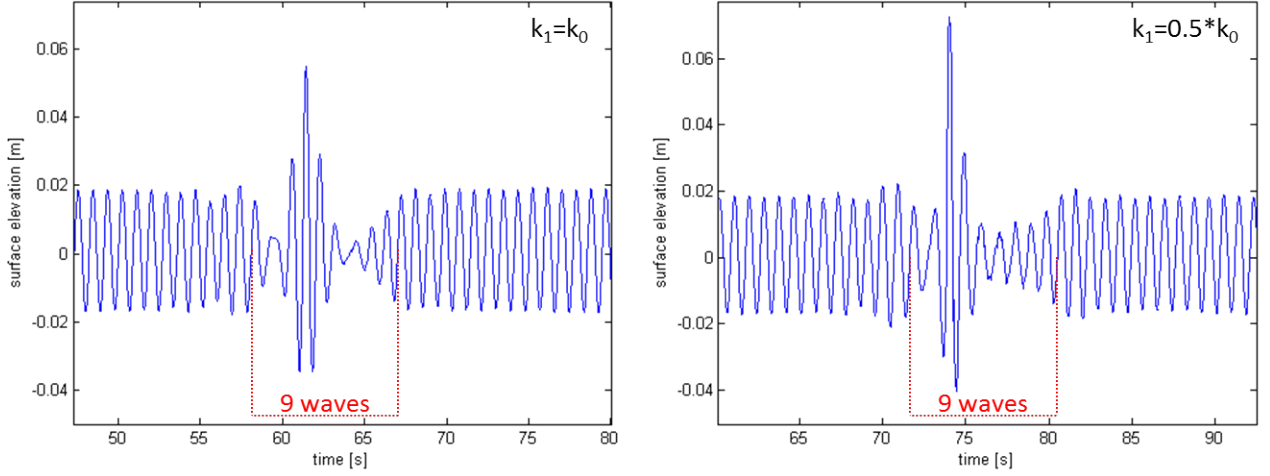


**Figure 5.8:** Experimental Parameter Study on  $k_1$ : Two Examples

Analogously, we can increase  $k_1$  so that  $k_1 > k_0$ . In that case, the peak is shifted to the right on the time axis prolonging the reduced amplitude range width in front of the peak.

For the experimentally analyzed modulation instabilities it exists a threshold number  $\vartheta_{\varepsilon_0} \in \{\mathbb{R} | \vartheta_{\varepsilon_0} > 1\}$  depending on the steepness  $\varepsilon_0$  of the carrier wave. In case of  $\frac{k_1}{k_0} \notin [1/\vartheta_{\varepsilon_0}; \vartheta_{\varepsilon_0}]$ , there is no amplitude reduced range in front ( $\vartheta_{\varepsilon_0} k_1 < k_0$ ) or behind ( $k_1 > \vartheta_{\varepsilon_0} k_0$ ) the maximal peak, but we introduce a triangle shape of the wave envelope from the maximal peak to the persisting reduced amplitude area. Figure 5.9 pictures two steep wave events in their maximal peaks with carrier wave amplitude  $a_0 = 0.01m$  and wave number  $k_0 = 7.3 \frac{rad}{m}$ . In case of  $k_1 = 3k_0$ , there is no reduced amplitude area behind the peak but a prolonged one before the peak. Furthermore, due to the case of 'entering' the uniform wave train, a triangle envelope shape between reduced amplitude area and the maximal peak occurs. The freak index  $AI$  is increased from 2.64 to 4.28 as well as the maximal wave steepness  $s_{max}$  from 0.068 to 0.1125.

In the experiments, the behavior of  $k_1 = ck_0$  with  $c \in \{\mathbb{R} | c > 1\}$  is qualitatively symmetric to  $k_1 = \frac{1}{c}k_0$  in the sense of the maximal peak is shifted in the same way to the right (for  $k_1 > k_0$ ) as to the left (for  $k_1 < k_0$ ) on the time axis. Quantitatively, this is shown in figure 5.11 which presents the experiments  $q_p(k_1 = ck_0, x, t)$  on carrier waves with  $\varepsilon_0 = 0.073rad$  (blue stars) and  $\varepsilon_0 = 0.1rad$  (red open circles). To be able to quantify the changes in the reduced amplitude

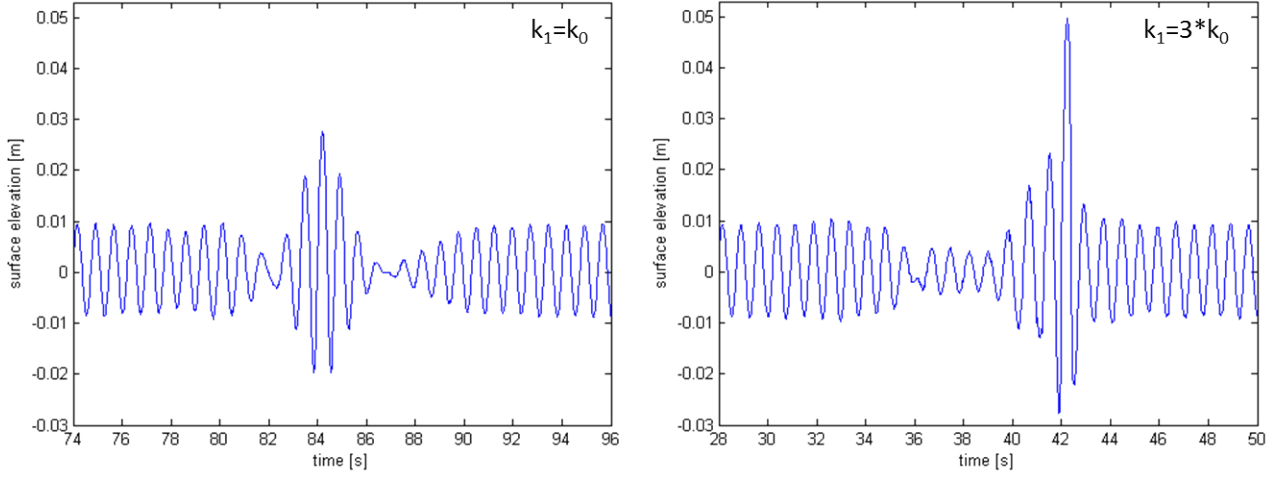


**Figure 5.9:** Experimental Parameter Study on  $k_1$ : Two Examples

area widths we introduce the surfaces of the reduced amplitude areas before and behind the maximal peak of the steep wave event, i.e.

$$A_{\text{beforePeak}} = \sum_{t_{\text{left1}}}^{t_{\text{right1}}} \frac{|\eta(t_i)| dt}{H_s/2} \quad (5.6)$$

$t_{\text{left1}}$  : first  $t_i$  with 'is local extremum' and  $|\eta(t_i)| < 0.85H_s/2$   
 $t_{\text{right1}}$  : first  $t_i > t_{\text{left1}}$  with  $|\eta(t_i)| > 0.9H_s/2$

and  $A_{\text{afterPeak}}$  analogously, whereby the values 0.85 and 0.9 are chosen as experienced values. Exemplary, figure 5.10 presents the contours of both surfaces visually. We take the value of  $n_1(\frac{A_{\text{afterPeak}}}{A_{\text{beforePeak}}})$  where  $n_1$  indicates the normalization of the surface quotient for  $k_1 = k_0$ .

As already seen in figure 5.8 and 5.9 the surface of the reduced amplitude area before the maximal peak decreases for  $k_1 < k_0$  and increases for  $k_1 > k_0$ . In the opposite way the area of the reduced amplitude after the maximal peak is controllable. The thresholds to terminate the reduced amplitude areas are  $\vartheta_{0.073} = 2.41$  and  $\vartheta_{0.1} = 2.7$ . The values  $\frac{A_{\text{afterPeak}}}{A_{\text{beforePeak}}}$  for  $c = \frac{1}{\vartheta_{\varepsilon_0}}$  are not displayed in figure 5.11 as  $\frac{A_{\text{afterPeak}}}{A_{\text{beforePeak}}} \rightarrow \infty$  for  $c \rightarrow \frac{1}{\vartheta_{\varepsilon_0}}$ .

It has not been analyzed yet whether the connection of the thresholds terminating the reduced amplitude areas before ( $k_1 < \frac{1}{\vartheta_{\varepsilon_0}}$ ) and behind the maximal peak ( $k_1 > \vartheta_{\varepsilon_0}$ ) for the cases  $\varepsilon_0 = 0.073$  and  $\varepsilon_0 = 0.1$  are always reciprocal values for  $\varepsilon_0 \notin \{0.073, 0.1\}$ .

As an explanation of the  $k_1$  parameter effect, we may interpret the Breather dynamic as the nonlinear interactions of an envelope soliton with a background plane wave (see [KPS09b]). Therefore, the change of the wave number  $k_1$  (and by this the change of the 'group velocity'

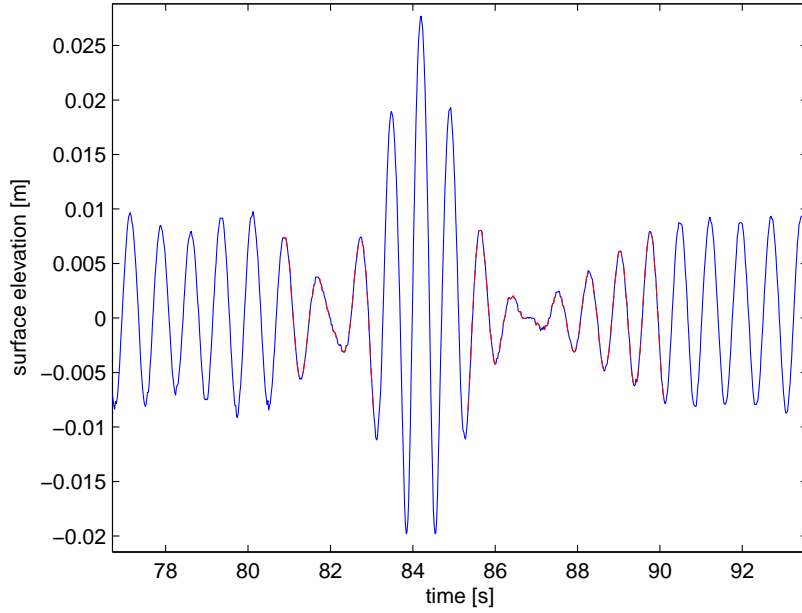


**Figure 5.10:** Visual Explanation of Included Sampling Points in  $A_{\text{beforePeak}}$  and  $A_{\text{afterPeak}}$  (red dashed line)

of the distortion) can be also interpreted as the modification of the soliton velocity leading to the described dynamics. Furthermore, the soliton interacts with more or fewer waves. Thus, a simulation and comparison of solitons with different velocities on plane waves is envisaged in proceeding studies.

## 5.4 Pure Phase Modulated Rogue Waves and Their Dynamics

Next, we question whether the amplitude and phase modulation of the Peregrine distortion term is both necessary to cause a Breather dynamic or if the phase or amplitude modulation solely is sufficient to provoke a growing modulation instability. In case of the pure phase modulation, we would be able to induce Breather dynamics 'energy conservatively' and therefore so to say 'undiscoverable'. To this end, we define the pure phase modulated Breather

$$q_{\text{phase}}(x, t) = a_0 \frac{q_p(x, t)}{|q_p(x, t)|} \quad (5.7)$$

with  $q_p(x, t)$  according to (2.9).

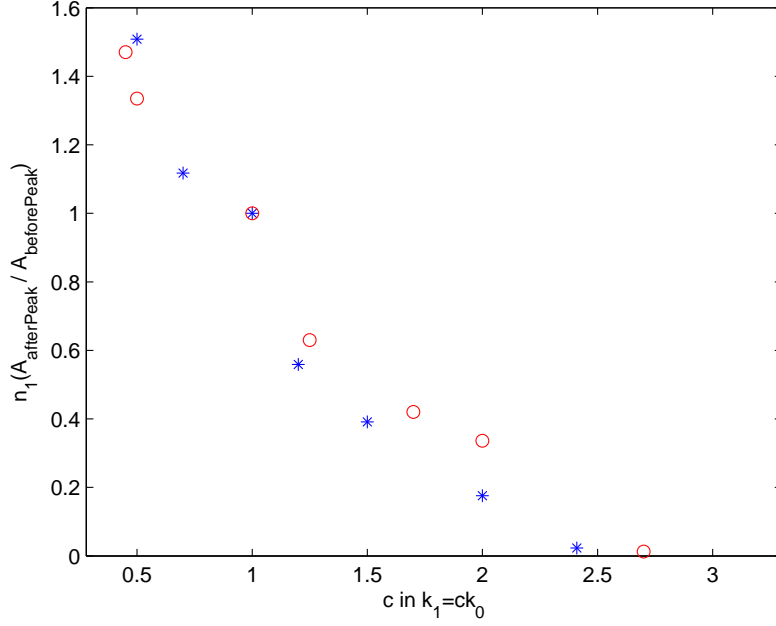


**Figure 5.11:**  $n_1(\frac{A_{\text{afterPeak}}}{A_{\text{beforePeak}}})$  versus Factor  $c$  in  $q_p(k_1 = ck_0, x, t)$  for a carrier wave with  $\varepsilon_0 = 0.073$  (blue stars) and a carrier wave with  $\varepsilon_0 = 0.1$  (red open circles)

In figure 5.12 we present the order 1 flap triggering of  $q_{\text{phase}}$  for a carrier wave of  $a_0 = 0.02m$  and  $k_0 = 5 \frac{\text{rad}}{m}$  (blue solid line) and the carrier wave without distortion (red dashed line).

Indeed, this leads to a Breather dynamic as shown in figure 5.15, whereas

- $x$  is the direction of the propagation.
- The measurements to  $x = 50m$  and  $x = 80m$  are done by an artificially extending of the wave tank. For this purpose, the recorded surface elevation in  $x = 40m$  is retriggered into the wave flaps in a separate experiment (see section 3.2).

Of course, we have to analyze whether this effect is mainly a dispersive focusing dynamic rather than a nonlinear modulation instability. If we plot the local wavelengths over the time of  $q_{\text{phase}}(x = \text{flap position}, t)$  relating to figure 5.12 we see that shorter waves are followed by longer waves which looks like a upcoming dispersive focusing process. Figure 5.13 pictures the local wavelengths of the flap triggering by determining numerically the local wave periods  $T_{\text{local}}$  leading to the local wavelengths by  $L_{\text{local}} = \frac{T_{\text{local}}^2 g}{2\pi}$  (with  $g$  : gravitational acceleration) according to the dispersion relation of first order.

However, if we plot the local wavelengths for different locations (see figure 5.14) we see that the 'potential of the dispersive effect' grows and the wave length modulation area is almost

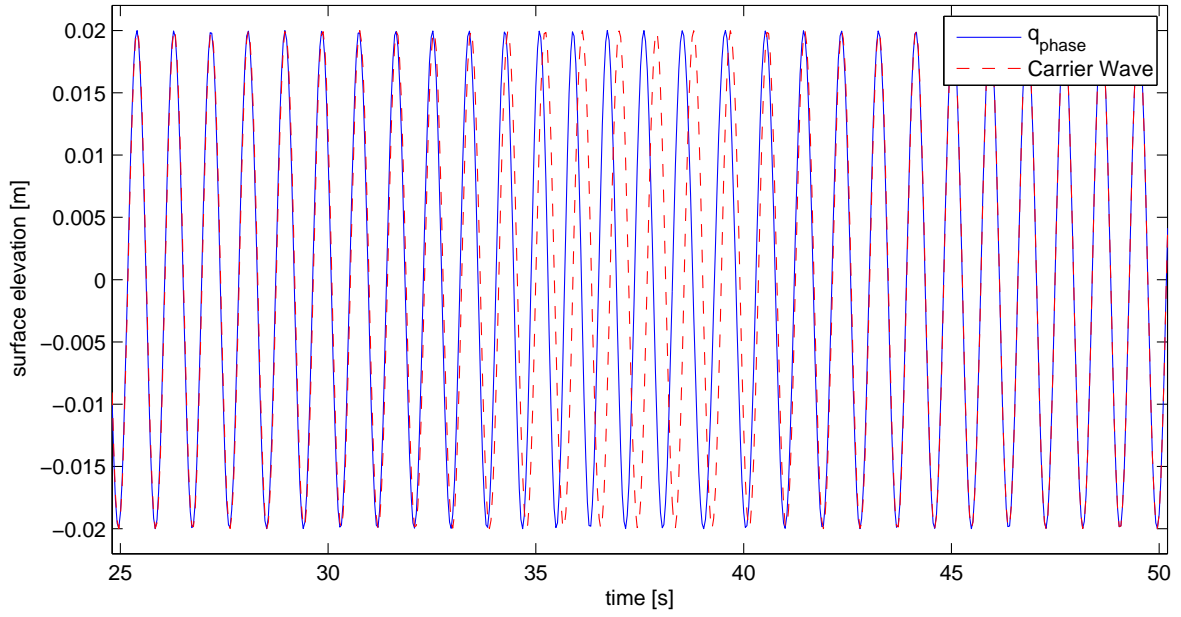


**Figure 5.12:** Flap Triggering: Pure Phase Modulated Breather (blue solid line) against Carrier Wave (red dashed line); both Driven with Order 1

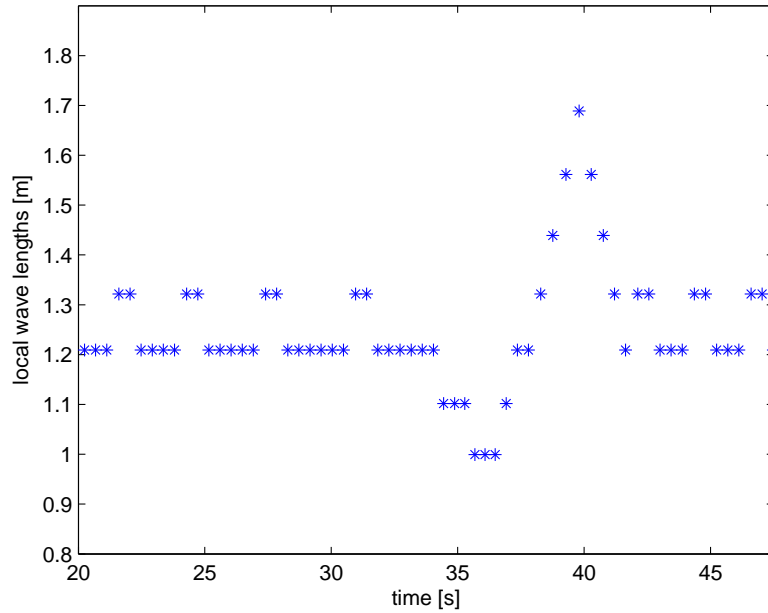


**Figure 5.13:** Local Wavelengths over Time for  $q_{\text{phase}}(x = \text{flap position}, t)$

constant until the maximal peak at  $x = 26m$ . (Hint: The vibrating of the local wavelength in the picture of  $x = 26m$  right in front of the peak is a numerical effect of the very small wave hook right in front of the peak in figure 5.15.) Hence, the nonlinear effects of the Peregrine model phase modulation do not only suppress the dispersive effects but also raise the 'dispersive potential'.

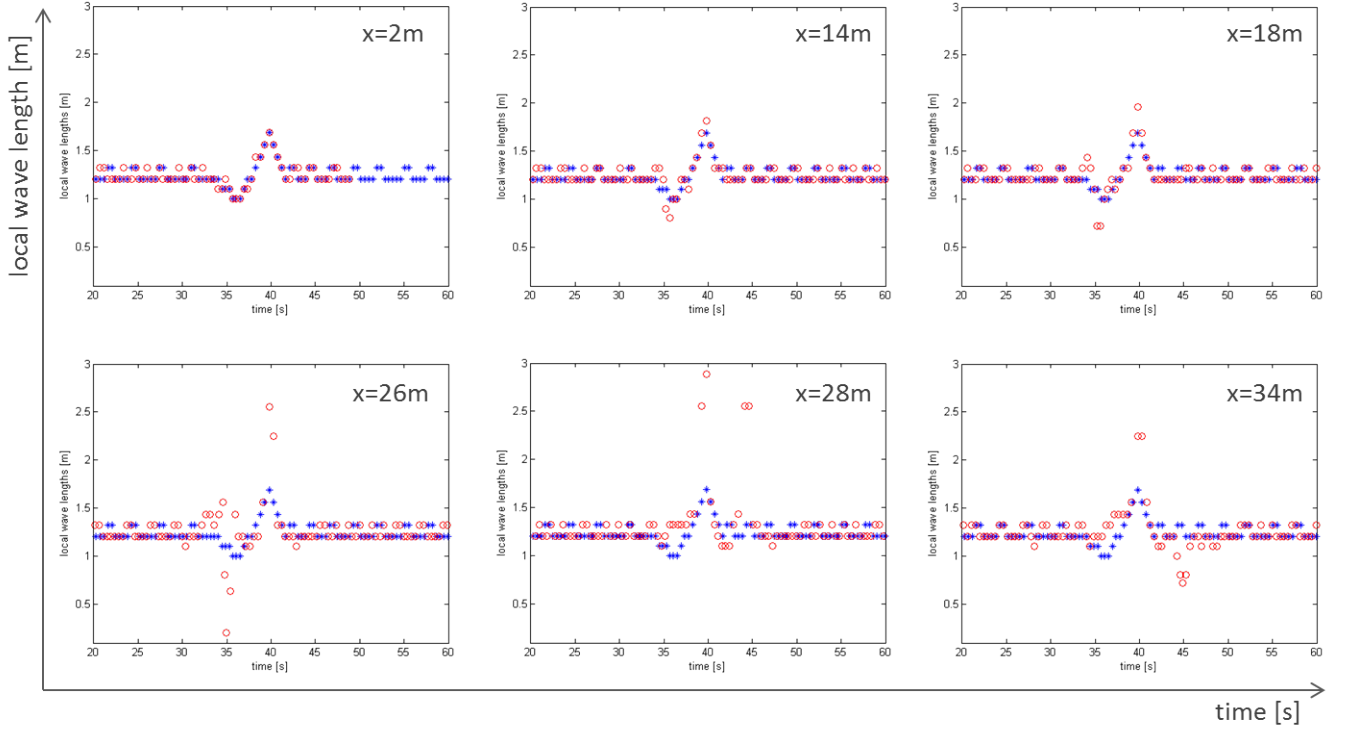


**Figure 5.14:** Local Wavelengths over Time for  $q_{\text{phase}}(x = \text{flap position}, t)$  (stars in blue) and Different Measurement Locations (red open circles)  
Hint: Wavelengths for Measurement Locations are Shifted in Time for Better Comparison

This is a nonlinear effect as the short waves have not been 'overrun' by the long waves, the width of the distortion area is constant until the maximal peak. To validate this, we simulated  $q_{\text{phase}}(x = \text{flap position}, t)$  in a linear and nonlinear Schroedinger equation. The simulations showed that the peak rising due to the dispersive effect would need much longer: The emergence of the maximal peak due to dispersive focusing needs 6.73 times longer than the emergence in the nonlinear case. Actually, the linear Schroedinger equation has no quantifiable amplitude increase at the location of the maximal nonlinear peak. Furthermore, the linear Schroedinger equation forecasts a freak index of  $AI = 1.2$  in its (much later occurring) maximal peak while the nonlinear peak has  $AI = 2.665$  in the simulation and  $AI = 2.1$  in the real wave tank

experiment. Therefore, the pure phase modulated Breather is (mainly) driven by nonlinear effects.

However, right behind the location of the maximal peak ( $x = 26m$ ) the dispersive focusing starts to act (see figure 5.14), the smaller and longer wavelengths are no longer in balance so that a wave is 'dispersed' in the others which may higher/stabilize the remaining waves and the peak for a longer distance before the dispersion leads to a decaying of the peak.

It should be mentioned that the evolution of the local wavelengths in different locations are qualitatively the same for the standard Peregrine Breather, though the Peregrine Breather has already its maximal wavelength and the 'dispersed' wave fully developed in its peak while the pure phase modulated Breather is still in the process of a growing maximal wavelength and of dispersing a wave after its peak. This may imply a higher maximal wave peak in case of the amplitude and phase modulation but a longer 'peak survival' in case of the pure phase modulated Breather which will be seen in the wave evolution analysis below, indeed.

Besides, already in  $x = 34m$ , we can see some additional very small wavelength outliers. These slight outliers will persist, drive apart, and get smaller and smaller until just a slight 'pumping' remains (see figure 5.15 for  $x = 80m$ ) which we also notice in the Peregrine Breather dynamic. This may be minor unstable Stokes waves according to Benjamin-Feir (see [BF67, BF72]) leading to quasiperiodic slight pumping wave modulations.

If we have a deeper look to the evolution of the pure phase modulated Breather in figure 5.15, we see that the Breather evolution is qualitatively similar to the related standard Peregrine Breather. The rogue wave occurs, breaths once, has three waves in its steep wave event, and remains with a slight wave 'pumping' after decaying.

However, there are also differences to the related standard Peregrine Breather dynamic, of course. First of all, the freak index  $AI = 2.1$  of the maximal peak reached at  $x = 26m$  is much smaller which will be affiliated with the missing amplitude distortion. However, sections 5.1 and 5.3 gives us parameters to allow us to increase the freak index and maximal steepness.

Another change in the dynamic is how fast the peak rises to its maximum. While the related standard Peregrine  $q_p(x_{flaps}, t)$  (with  $x_{flaps} < 0$  theoretical position of the flaps before the maximal peak at  $x = 0$ ) for  $a_0 = 0.02m$  and  $k_0 = 5 \frac{rad}{m}$  for the smallest possible initial modulation with experimentally resulting Breather dynamic ( $x_{flaps} := x_{min}$ ) needs  $65.12m$  (after 51.82 wavelengths) to reach its final peak, the related pure phase modulated Breather reaches its maximal peak already at  $x = 26m$  (after 20.69 wavelengths) as if it had been driven with a much higher initial modulation, i.e.  $q_{phase}(x_{min} + \Delta x, t)$ . The pure phase modulated Breather behaves

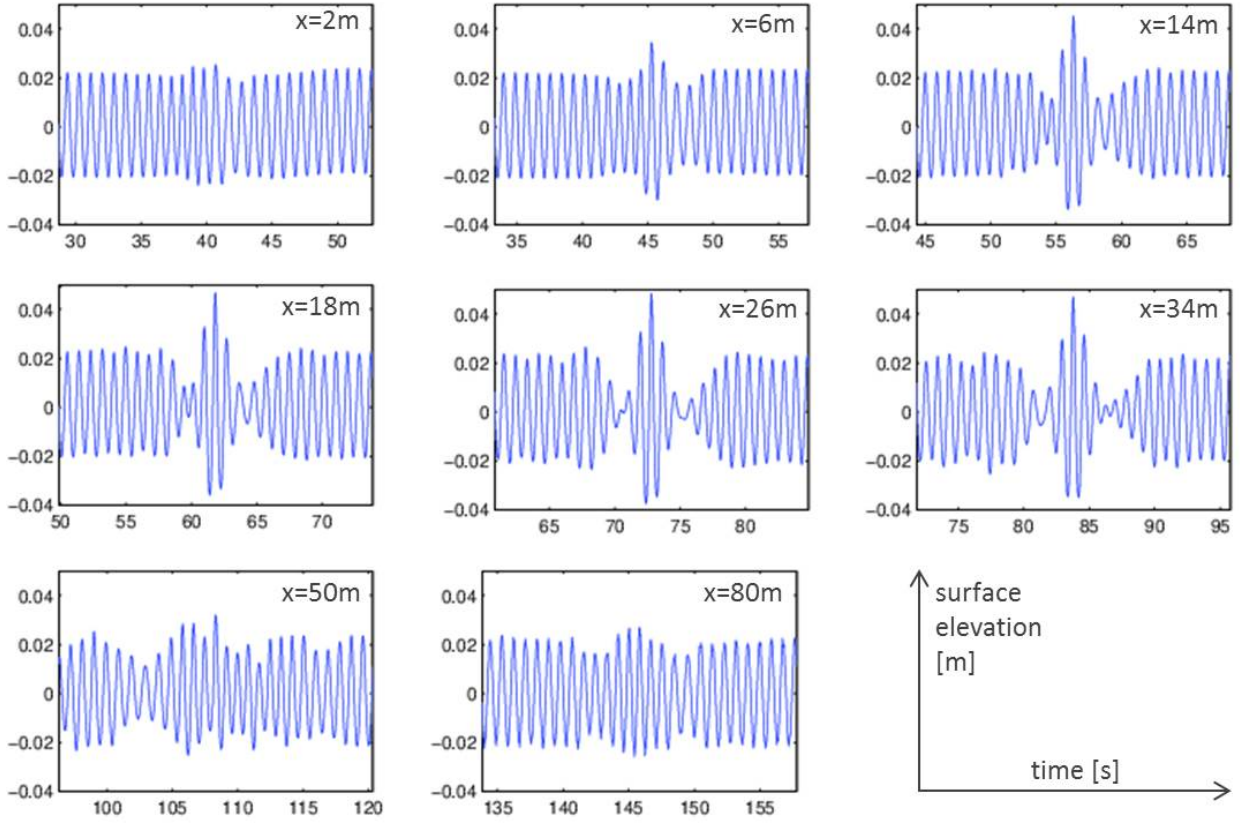


**Figure 5.15:** Pure Phase Modulated Breather Measured in Different Locations

here like a Peregrine Breather on a much steeper carrier wave ( $\varepsilon_0 = 0.1\text{rad} \rightarrow \hat{\varepsilon}_0 = 0.1337\text{rad}$ ). However, this has to be quantified still in proceeding studies.

On the other hand, the peak 'survives' in the pure phase modulated Breather much longer than in the related Peregrine Breather. If we compare the spatial range width of all  $x$  with a peak of at least 90% of the maximal rogue peak, i.e. all  $x \in \{x^* | \max_t \eta(x^*, t) \geq 0.9 * \max_{x,t} \eta(x, t)\}$ , we will see that for the related standard Peregrine Breather the width is  $10.38\text{m}$  while for the pure phase modulated Breather the width is  $20\text{m}$  (for all  $x \in [14\text{m}; 34\text{m}]$ ). This is almost double as long as for the related standard Peregrine Breather or in terms of the wavelength: The related standard Peregrine Breather has a peak of at least 90% of the maximal peak for 8.26 wavelengths while the pure phase modulated Breather can keep this high peak for 15.916 wavelengths. Therefore, the pure phase modulated Breather behaves like a Peregrine Breather on a much less steep carrier wave ( $\varepsilon_0 = 0.1 \rightarrow \hat{\varepsilon}_0 = 0.0805$ ).

As described above, it could be suggested that a dispersive focusing after the maximal peak stabilize the pure phase modulated Breather in its high peak distance. Anyway, the quantitative differences of the local wavelengths over time in different spatial positions between the

pure phase modulated Breather and the related Peregrine Breathers will have to be analyzed further in proceeding studies to determine whether this explanation is a complete answer to the occurrence of a longer 'high peak life'.

Both effects of rising faster to the maximal peak and 'surviving' longer in its high peak combined with the control parameters of section 5.1 and 5.3 enable steep wave events with even more risks to marine structures than the standard Peregrine Breather.

The possibility of combining the control parameters with the pure phase modulated Breather has been proven by experiments on carrier waves of  $\varepsilon_0 = 0.1rad$  and  $\varepsilon_0 = 0.073rad$  but has to be still quantified in processing studies. Especially, that the parameter  $\Gamma$  (see section 5.1) increases the maximal peak is surprising as the factor mainly amplify the amplitude modulation which does not work for a pure phase modulated Peregrine. But if we compare the pure phase modulated Breather with  $\Gamma = 4$  and  $\Gamma = 5$  in figure 5.16 and 5.17 we see that the area of distortion is widened, though not amplified. But the widened distortion relates to the behavior of a less steep carrier wave (see section 5.2) which may cause higher growth rates of the unstable modulation according to [CLSY81]. Even if this has still to be validated and deeper analyzed the wider area of distortion indicates an increased modulation.

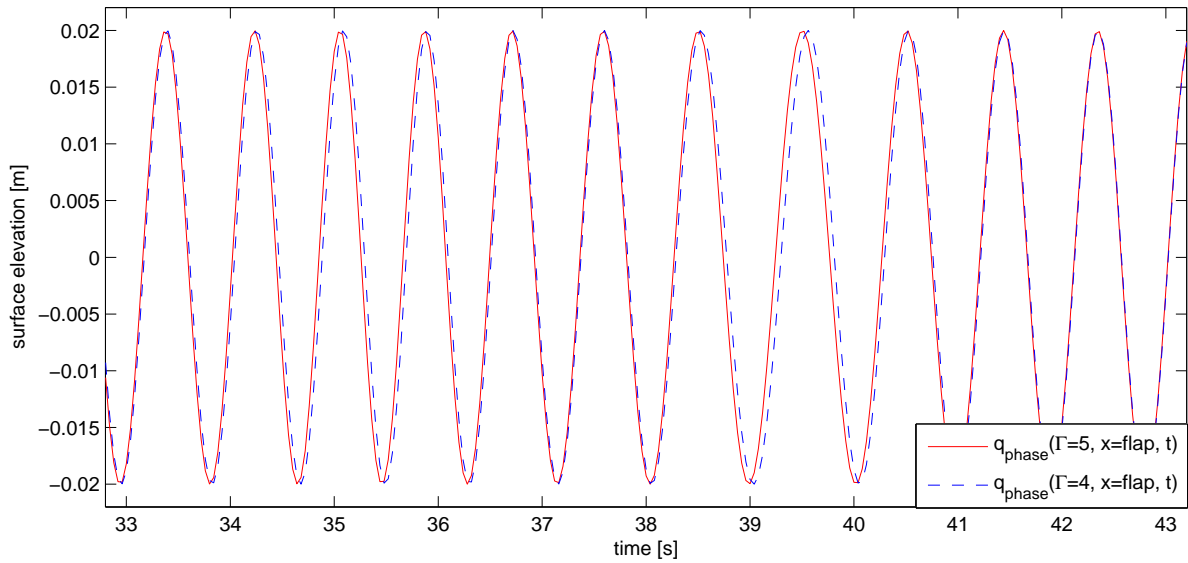


**Figure 5.16:** Flap Triggering:  $q_{\text{phase}}(\Gamma = 4, x = \text{flap position}, t)$  (red dashed line) against  $q_{\text{phase}}(\Gamma = 5, x = \text{flap position}, t)$  (blue solid line)

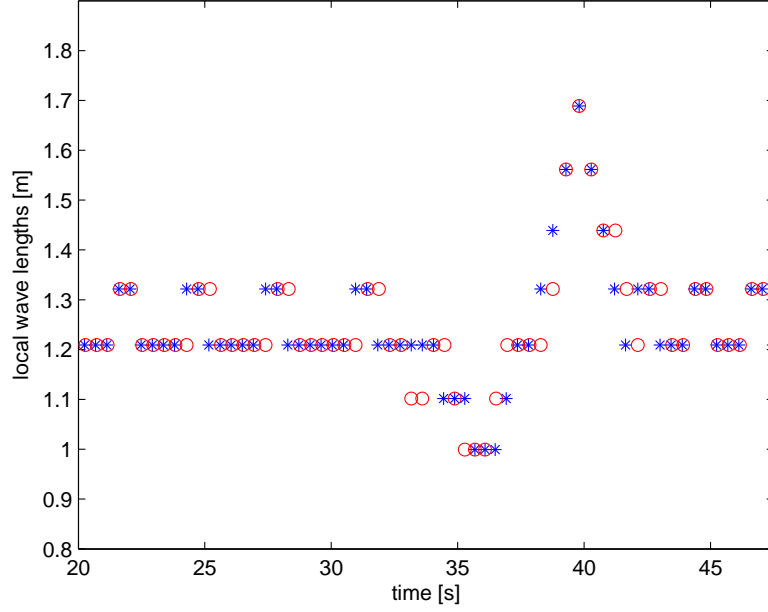


**Figure 5.17:** Local Wavelength over Time for  $q_{\text{phase}}(\Gamma = 4, x = \text{flap position}, t)$  (blue stars) and  $q_{\text{phase}}(\Gamma = 5, x = \text{flap position}, t)$  (red open circles)

#### Pure Amplitude Distortion

It seems natural to question whether a pure amplitude distortion is also able to cause a growing modulation instability. Therefore, we define

$$q_{\text{amplitudeV1}}(x, t) = |q_p(x, t)| \quad (5.8)$$

, with  $q_p(x, t)$  according to (2.9) and

$$q_{\text{amplitudeV2}}(x, t) = a_0 e^{-\frac{ik_0^2 a_0^2 \omega_0}{2} t} \left| \left( 1 - \frac{4(1 - ik_0^2 a_0^2 \omega_0 t)}{1 + [2\sqrt{2}k_0^2 a_0 (x - c_g t)]^2 + k_0^4 a_0^4 \omega_0^2 t^2} \right) \right| \quad (5.9)$$

Driving the flaps with  $\eta(x, t) = \text{Re} \left\{ q_{\text{amplitudeVi}}(x, t) e^{i(k_0 x - \omega_0 t)} \right\}$  or  $\eta(x, t) = \text{Re} \left\{ q_{\text{amplitudeVi}}(x, t) e^{i(k_0 x - \omega_0 t)} + \frac{1}{2} k_0 |q_{\text{amplitudeVi}}(x, t)|^2 e^{2i(k_0 x - \omega_0 t)} \right\}$ ,  $i \in \{1, 2\}$  will not cause a Breather dynamic. Even high driven modulations with  $\eta(x^*, t)$ ,  $x^* \approx -5 * \text{wave length of carrier wave}$  do not lead to an increasing peak but the modulation disperse in time and space. Therefore, the phase modulation is the key feature of the Peregrine Breather distortion term and is even sufficient to cause a growing modulation instability solely. This will be reasoned and further analyzed in chapter 6.



## 6 Experimental Study on Robustness of Breather Dynamic to Changes in the Carrier Wave

One of the striking differences of the so far analyzed Breather dynamics to real freak waves is the carrier wave: Up to now, we have assumed them to be uniform. But a natural sea state is at least slightly aperiodic or even irregular and turbulent. Furthermore, natural directed sea states have not uniform crested waves, but its crests also change in the perpendicular direction of the mean wave propagation. [ADA09], [CHB<sup>+</sup>13] and [DT99] analyzed the robustness of the Peregrine model to initial small perturbations and forcing wind. The results show the persistence of the Breather evolution dynamics.

Therefore, in this chapter, we analyze whether it is possible to change the carrier wave in a designated forced way with a persisting predefined localized Breather dynamic. To this end, we will analyze a smooth phase shift (section 6.1) and a smooth amplitude shift (section 6.2) over time in the carrier wave of the standard Peregrine Breather model as well as the combination of both, phase and amplitude shift (section 6.3) as a feasibility study of the robustness of the growing modulation instability injected by the Peregrine distortion term. This will lead to a fundamental prerequisite of the carrier wave for injecting a growing modulation instability by the (modified) Peregrine Breather distortion term.

With this knowledge combined with the studies of chapter 5 we will be able to inject a Breather dynamic on an arbitrary directed carrier wave modulated by the JONSWAP spectrum and compare the results to real occurred extreme waves and even indicate a forecast model for this type of nonlinear rogue waves (section 6.4).

## 6.1 Robustness of Peregrine Breather Dynamics to Phase Shifts in the Carrier Wave

First, we analyze whether it is possible to change the phase of the carrier wave, i.e. an 'energy conservatively' change of the carrier wave. [CHA12] has already shown that by changing the carrier wave by an angle of  $\phi = \pi$  we cause - instead of a high peak - a rogue wave hole:

$$\eta_{\text{hole}}(x, t) = \text{Re} \left\{ q_p(x, t)(x, t) e^{i(k_0 x - \omega_0 t)} e^{i\phi} \right\} \text{ with } \phi = \pi \quad (6.1)$$

which is also interpretable as the change of the sign in the distortion term of  $q_p(x, t)$  according to (2.9). Actually, in all experiments, this angle change led always to an 'upside down' qualitatively behavior of the related Breather with angle  $\phi = 0$ . Also, all other  $\phi$  did not destroy the Breather dynamic which will be comprehensible after the following analysis.

For a feasibility study of changing the carrier wave by a temporal phase shift without losing the Breather dynamic, we define a smooth phase change transition of the carrier wave directly in the Peregrine distortion domain:

$$\eta_\phi(\phi, n, x, t) = \text{Re} \left\{ q_p(x, t) e^{i(k_0 x - \omega_0 t)} e^{i \left( (1 + \tanh \frac{3(t-t_{\text{peak}})}{nT_0}) \phi \right)} \right\} \quad (6.2)$$

, with  $t_{\text{peak}}$  is the time point of the maximal peak of  $q_p(x, t)$ ,  $T_0$  is the period of the carrier wave, and  $n \in \mathbb{R}$  is a parameter to control the width of the phase shift.

Figure 6.1 shows a flap driving of  $\eta_\phi(\frac{\pi}{4}, 1, -40.865, t)$  (blue solid line) for  $a_0 = 0.02m$  and  $k_0 = 5 \frac{\text{rad}}{m}$  compared with the related standard Peregrine Breather  $\eta_p$  without phase shift in the carrier wave (red dashed line) and the resulting phase shift over time  $\Phi(t) = \left( (1 + \tanh \frac{3(t-t_{\text{peak}})}{nT_0}) \phi \right)$ .

Neither the HOS-NWT simulations (see section 4.2) nor the experiment can identify a Breather dynamic. Even if we trigger the flaps with a already high developed distortion, i.e.  $\eta_\phi(\frac{\pi}{4}, 1, -5 * \text{wavelengths}, t)$  or with different parameters  $\phi$  or  $n$ , a Breather dynamic is not detectable as long as the phase shift is 'noticeable' ( $n \ll \infty$ ,  $\phi > 0$ ) in the distortion area. Limits of this 'noticeable' have not been analyzed yet.

The destroying of the Breather dynamic is not surprising as the crucial instability modulation of the Peregrine Breather distortion is the phase modulation (see section 5.4). If we just change the phase by a constant phase over all time like in [CHA12], the Breather dynamic is persistent. But a change of the phase distortion by a phase shift  $\Phi(t)$  changing in time destroys the growing modulation instability feature of the Breather dynamic and results in a decaying behavior, only.

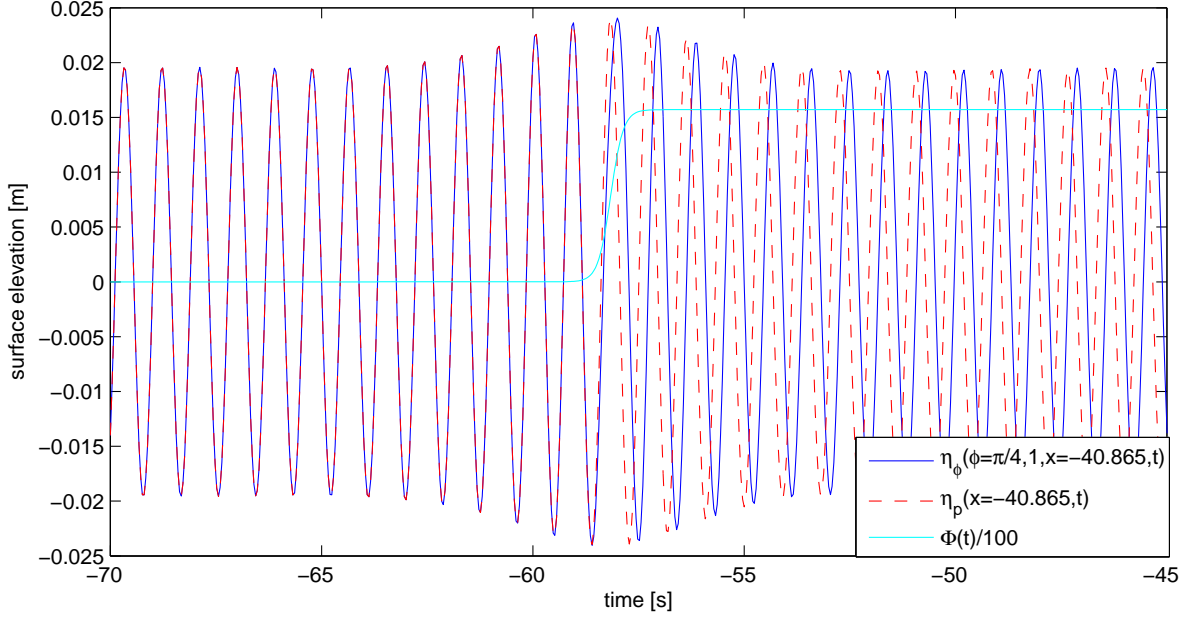


**Figure 6.1:** Flap Driving  $\eta_\phi(\frac{\pi}{4}, 1, -40.865, t)$  (blue solid line) compared to the Related Peregrine Breather  $\eta_p$  without Phase Shift in Carrier Wave (red dashed line), and resulting Phase Shift over Time  $\Phi(t)$  (cyan solid line)

In this sense, the temporal phase shifted Stokes wave is a dispersive wave group leading to a detuning effect of the Peregrine distortion term. If we drive the Stokes wave with the temporal phase shift solely, i.e.

$$\text{StokesWave}_\phi(\phi = \frac{\pi}{4}, n = 1, x = -40.865, t) = \text{Re} \left\{ e^{i(k_0 x - \omega_0 t)} e^{i \left( (1 + \tanh \frac{3(t-t_{\text{peak}})}{nT_0}) \phi \right)} \right\} \quad (6.3)$$

, we can picture the local wavelengths over time of different spatial positions. Exemplary, figure 6.2 compares the local wavelengths for two spatial positions with 12m distance to each other. (The plot for the second spatial position is time-shifted for better comparison.)

We see that this 'carrier wave' has a dispersive wave group in the area of the targeted Breather distortion injection: The phase shift distortion width increases and the local wavelength in here decreases in space. This dispersive wave group will detune the phase modulation of the Breather perturbation and therefore prevent a Breather dynamic. Calling section 5.4 to mind, this is not surprising as the phase modulation of the Peregrine distortion is the key feature to cause a growing modulation instability. Therefore, also a temporal phase shift not exactly at the maximal distortion peak will destroy the Breather dynamic. Nevertheless, the limits of a

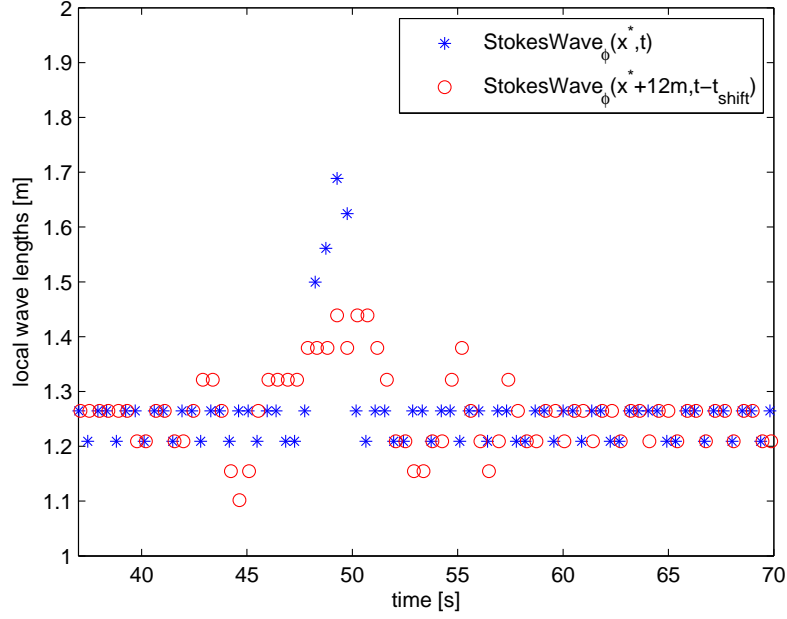


**Figure 6.2:** Measured Local Wavelengths of  $\text{StokesWave}_\phi$  for a position  $x^*$  (blue stars) and a position 12m further on in the wave tank (red open circles)

maximal possible phase shift without suppressing the growing modulation instability have to be determined in further studies still.

## 6.2 Breather Dynamics on Amplitude Shifted Carrier Waves

If the key feature of the Peregrine Breather distortion is the phase modulation (see section 5.4), we question if it is possible to perform an amplitude shift in the carrier wave without losing the Breather dynamic. To this end, we define a smooth amplitude transition of the carrier wave directly in the Peregrine distortion domain:

$$\begin{aligned} \eta_{\delta A}(\delta A, n, x, t) &= \text{Re} \left\{ (a_0 + \Delta A(t)) q_{pnorm}(x, t) e^{i(k_0 x - \omega_0 t)} \right\} \\ \Delta A(t) &= \frac{\delta A}{2} \left( 1 + \tanh \frac{3(t - t_{\text{peak}})}{nT_0} \right) \end{aligned} \quad (6.4)$$

, with  $t_{\text{peak}}$  is the time of the maximal peak of  $q_{pnorm}(x, t) = \frac{q_p(x, t)}{a_0}$ ,  $T_0$  is the period of the carrier wave, and  $n \in \mathbb{R}$  is a parameter to control the width of the amplitude shift.

Figure 6.3 shows a flap driving of  $\eta_{\delta A}(0.0037, 1, -40.865, t)$  (blue solid line) for  $a_0 = 0.01m$  and  $k_0 = 7.3 \frac{\text{rad}}{m}$  compared to the related standard Peregrine Breather  $\eta_p$  without amplitude shift

in the carrier wave (red dashed line) and the resulting amplitude shift  $\Delta A(t)$  over time. Like

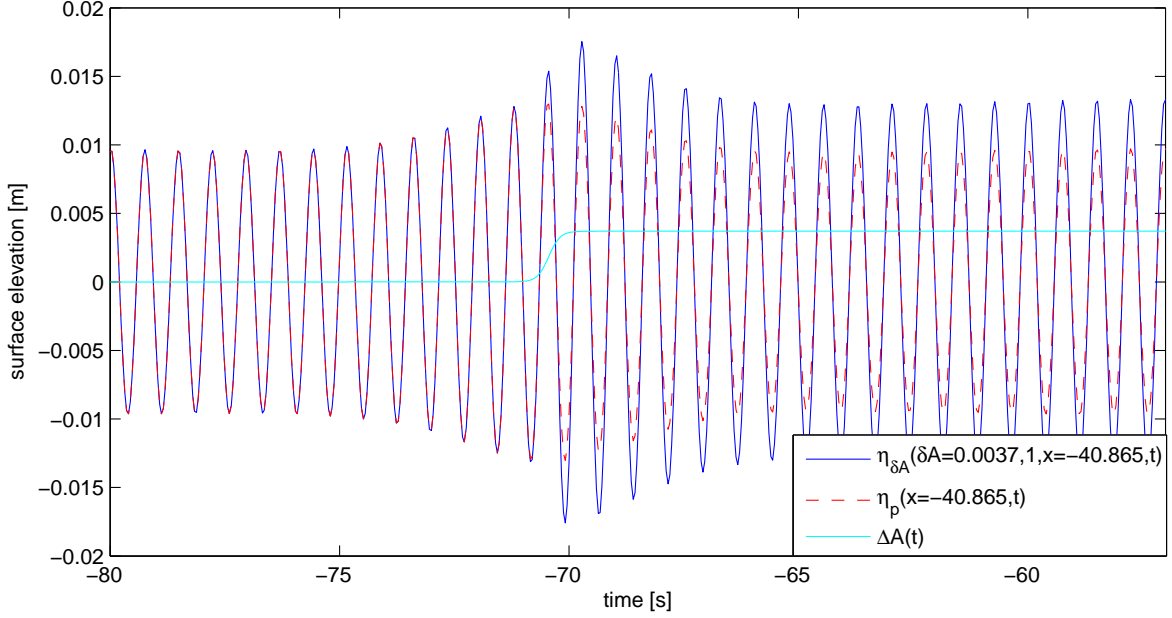


**Figure 6.3:** Flap Driving  $\eta_{\delta A}(0.0037, 1, -40.865, t)$  (blue solid line) compared with Related Peregrine Breather  $\eta_p$  without Amplitude Shift in the Carrier Wave (red dashed line), and resulting Amplitude Shift over Time  $\Delta A(t)$  (cyan solid line)

this, the carrier wave of  $\eta_{\delta A}$  increases its steepness from  $\varepsilon_0 = 0.073 \text{ rad}$  to  $\varepsilon_0 = 0.1 \text{ rad}$ .

If we measure the surface elevation after  $64.57 \text{ m}$  behind the flap (done by artificially prolonging the wave tank; see section 3.2) we see that the Breather dynamic occurs (figure 6.4; blue solid line). Actually, at this spatial position, we measure the highest peak of the amplitude shifted Breather. The peak has a freak index of  $AI_{\varepsilon_0=0.073} = 3.505$  relating to the carrier wave with steepness  $\varepsilon_0 = 0.073$  and a freak index of  $AI_{\varepsilon_0=0.01} = 2.61$  relating to the carrier wave with steepness  $\varepsilon_0 = 0.01$ .

Furthermore, figure 6.4 pictures the measurement of a stokes wave (driven in order 1; red dashed line) with the related amplitude shift solely, i.e. the measurement at  $x = 64.57 \text{ m}$  for the flap triggering

$$\text{StokesWave}_{\delta A}(\delta A, n, x, t) = \text{Re} \left\{ (a_0 + \Delta A(t)) e^{i(k_0 x - \omega_0 t)} \right\} \quad (6.5)$$

, with  $\delta A = 0.0037, n = 1, x = -40.865$ . If we compare the measured surface elevation with  $\eta_{\delta A}$  (blue solid line) we will see that the Breather distortion changes the dynamics in a localized area. Though the shape of the maximal steep wave event is changed by the amplitude shift, we see the persistence of the Breather dynamic.

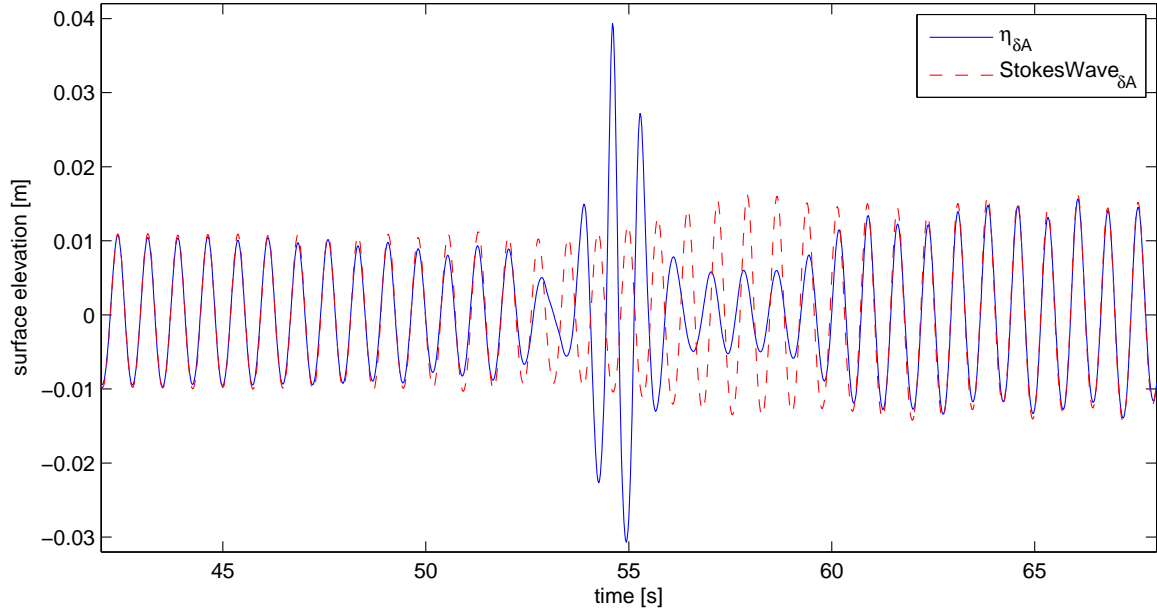


**Figure 6.4:** Measurement of  $\eta_{\delta A}$  in Maximal Occurring Peak (blue solid line) and Amplitude Shifted Stokes Wave at the Same Position (red dashed line)

Hints:

- The temporal amplitude shifted carrier wave does not add any dispersive effects of first order as an amplitude shift does not change the wavelengths / phases.
- So, the analysis of the local wavelengths of  $\eta_{\delta A}$  over time in different spatial locations determines a constant temporal width in all  $x$  until the spatial position of the maximal Breather peak.
- If we consider higher order dispersion relations like  $\omega = \sqrt{gk + ga^2k^3}$  and the group velocity  $c_g = \frac{\partial \omega}{\partial k}$ , the phase velocity  $c_p = 2c_g$ , as well as the Taylor series derivation of the NLS according to [Deb94] (the factor in front of the diffusive term  $\frac{\partial^2 a}{\partial x^2}$  correlates to  $\frac{\partial^2 \omega}{\partial k^2}$ , the factor of the 'nonlinear amplitude dispersion'  $|a|^2 a$  correlates to  $\frac{\partial \omega}{\partial |a|^2}$ ), we realize that the amplitude is taken into account only in higher orders, e.g. an amplitude shift in  $a$  may lead to (additional) dispersion but 'just in higher orders'. This is the reason, why smooth amplitude shifts (or even a forced constant wave height according to the pure phase modulated rogue waves of section 5.4) preserve and phase shifts destroy the growing modulation instability in simulations and wave tank experiments.
- Hint: The ' $2\pi$  phase loop' in the distortion area of figure 6.4 is typical for the perturbation in  $q_p$  in (2.9).

This feasibility study of changing the carrier wave of the Peregrine solution by a temporal amplitude shift without losing the Breather dynamic can be executed successfully for different  $n$  and  $\delta A$ . Likewise, the change from a higher amplitude to a reduced one does not suppress the growing modulation instability. Also, a temporal amplitude shift not exactly at the maximal distortion peak will preserve the Breather dynamic. Hence, a smooth amplitude change of the carrier wave does not destroy the Breather dynamic though it changes its shape and peak height (freak index and steepness). To quantify these changes and limits more experiments will have to be executed in further studies.

### 6.3 Phase and Amplitude Shifted Breather Dynamics

We saw in section 6.1 that a temporal phase shift of the carrier wave may destroy a growing modulation instability. However, a moderate amplitude shift in the carrier wave of a Breather in the area of the distortion will keep the growing modulation instability, though it will change the shape of the steep wave event. Therefore, we question whether it is possible to combine an amplitude with a phase shift in time so that they 'balance' the dispersive and detuning effect of the phase shift on the one hand, and maybe even stabilize the steep wave event shape relating to the corresponding standard Peregrine Breather. For that reason, we define an amplitude and phase shifted Breather according to

$$\eta_{a(t)}(\delta A, n, x, t) = \text{Re} \left\{ a(t) e^{-\frac{ik_0^2 a(t)^2 \omega_0}{2} t} * \left( 1 - \frac{4(1 - ik_0^2 a(t)^2 \omega_0 t)}{1 + [2\sqrt{2}k_0^2 a(t)(x - c_g t)]^2 + k_0^4 a(t)^4 \omega_0^2 t^2} \right) e^{i(k_0 x - \omega_0 t)} \right\}$$

$$a(t) = a_0 + \frac{\delta A}{2} \left( 1 + \tanh \frac{3(t - t_{\text{peak}})}{nT_0} \right)$$
(6.6)

, with the same parameters as in section 6.2. This leads to a smooth amplitude and phase shift transition in the main peak of the related standard Peregrine Breather  $\eta_p$ . In figure 6.5 we see the flap driving of  $\eta_{a(t)}$  (blue solid line) for  $a_0 = 0.01m$  and  $k_0 = 7.3 \frac{\text{rad}}{m}$  compared to the related Peregrine Breather  $\eta_p$  without amplitude and phase shifts (red dashed line) as well as the time depending amplitude change  $\Delta A(t) = a(t) - a_0$  (cyan solid line). The amplitude as well as the related phase shift to the standard Peregrine Breather is visible though cannot be interpreted as a change in the carrier wave only.

If we measure the surface elevation in its maximal peak behind the flap, we picture the steep wave event (figure 6.6; blue solid line). The shape, maximal steepness, and freak index is very

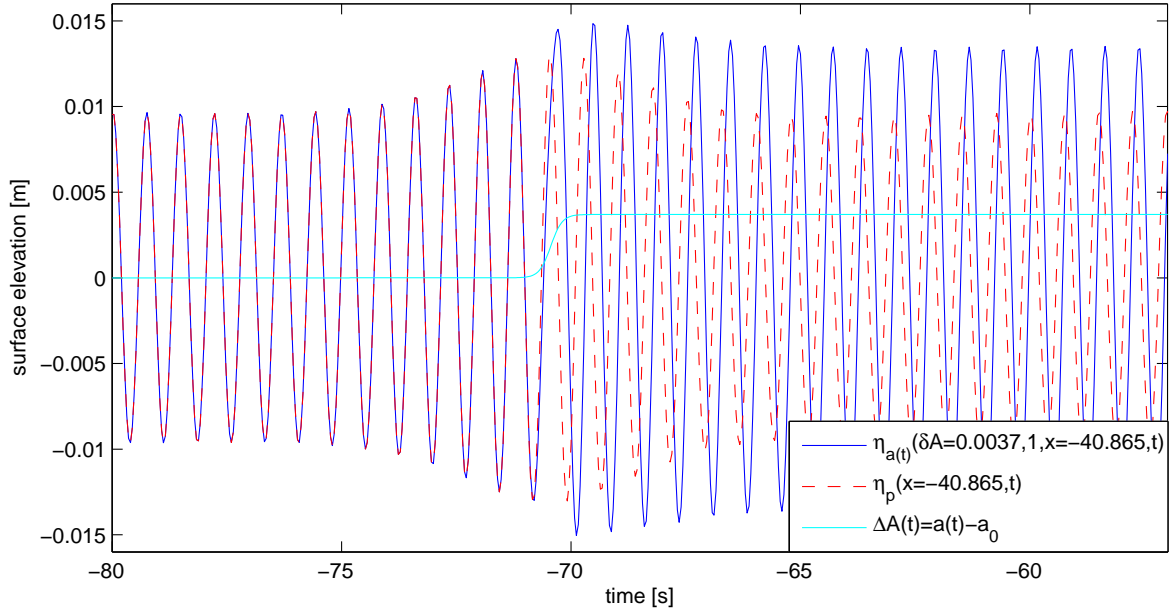


**Figure 6.5:** Flap Driving  $\eta_{a(t)}(0.0037, 1, -40.865, t)$  (blue solid line) compared with Related Peregrine Breather  $\eta_p$  without Shifts in Carrier Wave (red dashed line), and  $\Delta A(t) = a(t) - a_0$  over Time (cyan solid line)

close to the related Peregrine Breather with  $\varepsilon = 0.073rad$  (red dashed line), but the frequency down-shifting is much higher after the peak.

Therefore, in figure 6.7 we compare the amplitude and phase shifted Breather  $\eta_{a(t)}$  (blue solid line) with the related Peregrine Breather with  $\varepsilon = 0.1rad \approx (0.01m + \delta A) * 7.3 \frac{rad}{m}$  (red dashed line). This time we see the difference in the shape of the steep wave event (freak index, maximal steepness) but we realize the almost equivalent phase behavior in time. Therefore, the amplitude and phase shifted Breather  $\eta_{a(t)}$  behaves like a combination of the related Peregrine Breathers with  $\varepsilon = 0.073rad$  (for the steep wave event shape) and  $\varepsilon = 0.1rad$  for the phase behavior in time (e.g. frequency down-shifting).

If we change  $a(t)$  to shifting from the higher amplitude to the smaller, the resulting Breather behaves in the opposite way: It behaves in the steep wave shape (freak index, maximal local wave steepness) like the related Peregrine Breather with  $\varepsilon = 0.1rad$  and phase-wise like the related Peregrine Breather with  $\varepsilon = 0.073rad$ . In the end, this enables us to combine several Peregrine models to one extreme wave event.

Again, this feasibility study can be executed without losing the Breather dynamics and even the freak wave shape for different  $n$  and  $\delta A$ . So, a smooth amplitude change in the whole Peregrine Breather (2.9) leading to a combined temporal amplitude and phase shift does not destroy the

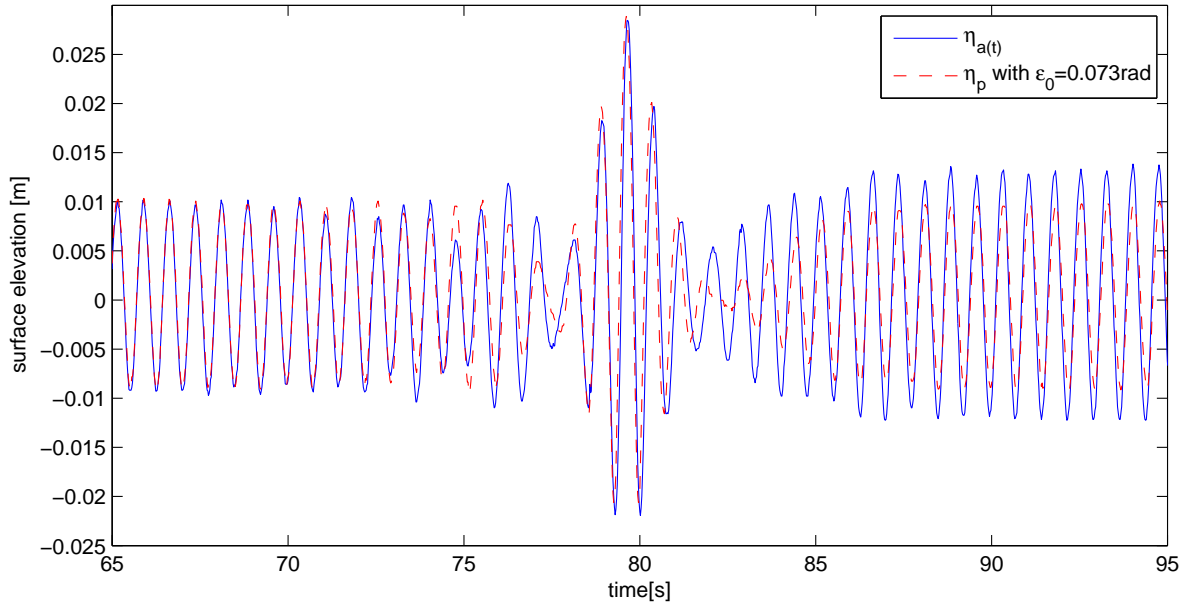


**Figure 6.6:** Measurement of  $\eta_{a(t)}$  (blue solid line) and Related Measured Peregrine Breather  $\eta_p$  with  $\varepsilon_0 = 0.073 \text{ rad}$  (red dashed line)  
Hint: Both in Maximal Peak.  $\eta_p$  shifted in Time for Better Comparison.

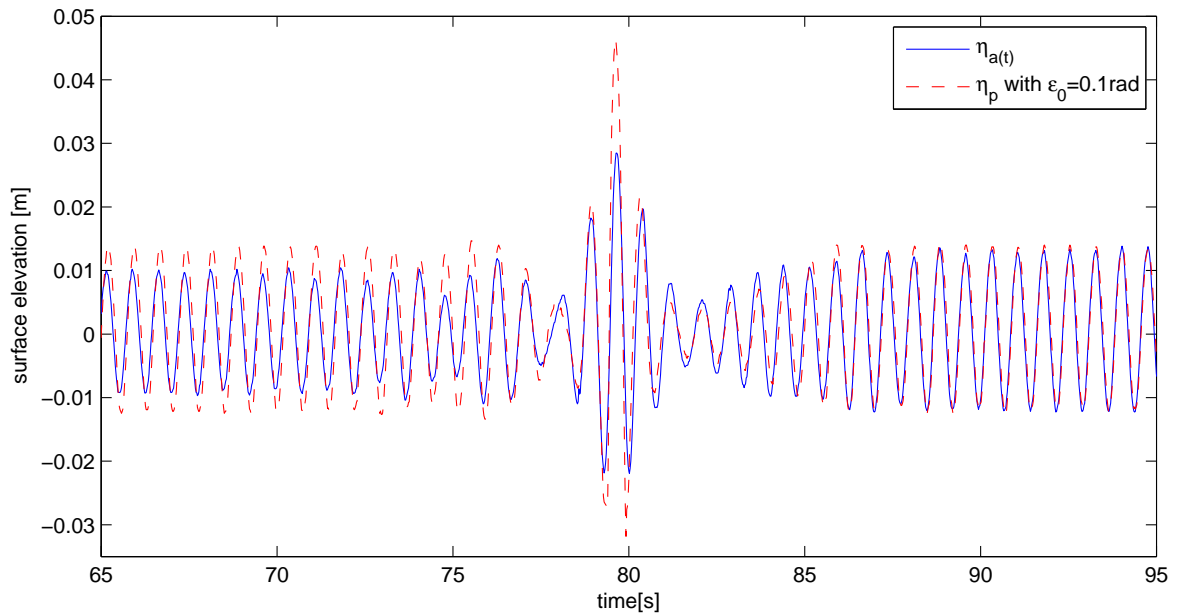


**Figure 6.7:** Measurement of  $\eta_{a(t)}$  (blue solid line) and Related Measured Peregrine Breather  $\eta_p$  with  $\varepsilon_0 = 0.1 \text{ rad}$  (red dashed line)  
Hint: Both in Maximal Peak.  $\eta_p$  shifted in Time for Better Comparison.

Breather dynamic but even retain its shape (freak index and maximal local steepness) and frequency down-shifting properties. However, the limits have to be quantified in proceeding studies still.

Yet, it is interesting that this specific temporal phase shift does not prevent the Breather dynamic and does not even change the Breather peak shape. A look to the wavelengths over time measured in different spatial positions shows that the distortion width is despite the extra phase modulation constant until the maximal rogue wave peak. Furthermore, the phases behave almost like the related Peregrine with  $\varepsilon = 0.1rad$  as also seen in figure 6.7 who is also 'non-dispersive' until its maximal peak. We conclude that a temporal phase shift may be stable with respect to the growing modulation instability if it is performed with a balancing temporal amplitude shift. This 'balancing' is defined by the Peregrine perturbation term.

Therefore a non-dispersive carrier wave group or at least a non-dispersive distortion area after the modulation with the (modified) Peregrine perturbation term is the fundamental prerequisite to preserve this growing modulation instability and is the proof of the nonlinear effects. The limits of this 'non-dispersive wave group' (necessary number of proceeding waves with the same phase, possible phase perturbation until growing instability modulation is prevented) has still to be determined by further studies but the following section 6.4 will give a guidance for injecting a steep wave event by the (modified) Peregrine Breather perturbation even in irregular carrier waves, i.e. in arbitrary directed sea states.

### 6.4 Using an Arbitrary Directed Sea State as Carrier Wave for the Breather Dynamic

Following, we will show how to inject a nonlinear Breather dynamic in an arbitrary directed sea state by the results from the sections and chapters before. To this end, we will first recap the basic idea of a JONSWAP spectrum to simulate an irregular directed wave field (subsection 6.4.1). This wave field is then taken as the carrier wave which will be disturbed according to the Peregrine Breather to cause a steep wave event (subsection 6.4.2). To classify how realistic this nonlinear rogue waves in real oceans are, we proceed with a comparison to real occurred freak waves and even indicate a reverse engineering and a new forecast model of/for this type of nonlinear rogue waves in subsection 6.4.3.

### 6.4.1 JONSWAP: A Simulated North Sea

In order to use an arbitrary directed sea state as carrier wave we produce a wave field simulating a possible North Sea state according to [HPBB<sup>+</sup>73]. We recap section 3.2 shortly:

First, we generate a JONSWAP spectrum by the Wave Analysis for Fatigue and Oceanography (WAFO, based on [HPBB<sup>+</sup>73]) project: a toolbox of Matlab routines for statistical analysis and simulation of random waves and random loads [WAF09]. According to WAFO

' the JONSWAP spectrum is assumed to be especially suitable for the North Sea [...].

It is a reasonable model for wind generated sea when  $3.6\sqrt{H_s} < T_p < 5\sqrt{H_s}$  ,

, where  $H_s$  is the significant wave height, and  $T_p$  the peak wave period. To relate to our standard experiment cases, we use a significant wave height of  $H_s = 0.04m$ , peak wave period  $T_p = \frac{2\pi}{\sqrt{gk}}s$  with  $k = 5\frac{rad}{m}$ , and peak enhancement factor according to [TFH<sup>+</sup>84]  $\gamma = e^{3.484*(1-0.1975*D*T_p^4/(H_s^2))} = 1.5729$  with  $D = 0.036 - 0.0056 * T_p/\sqrt{H_s}$ . The related ocean wave spectra considering 256 wave frequencies is shown in figure 6.8.

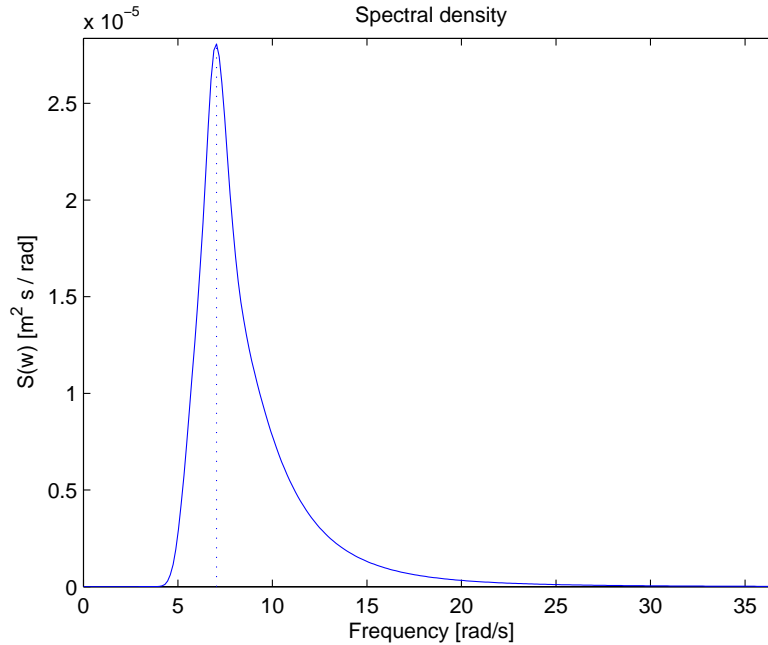


**Figure 6.8:** JONSWAP Ocean Wave Spectrum with significant wave height of  $H_s = 0.04m$ , peak wave period  $T_p = 0.89714s$ , and peak enhancement factor  $\gamma = 1.5729$ .

Let  $S_l$  be the spectral density to the wave frequency  $\omega_l$ ,  $k_l$  the related wave number determined by the deep water dispersion relation of first order  $\omega_l = \sqrt{gk_l}$ ,  $d\omega$  the step width of the uniform

distributed wave frequencies, and  $\theta_l \in [0; 2\pi)$  a random phase offset. We superpose the related waves by

$$\eta_{\text{JONSWAP}}(x, t) = \text{Re} \left\{ \sum_l \left( A_l e^{i(k_l x - \omega_l t - \theta_l)} + \frac{1}{2} k_l A_l^2 e^{2i(k_l x - \omega_l t - \theta_l)} \right) \right\}, \text{ with } A_l = \sqrt{S_l * 2d\omega} \quad (6.7)$$

or in the sense of the NLS the uniform wave solutions

$$\eta_{\text{JONSWAP}}(x, t) = \text{Re} \left\{ \sum_l \left( u_l(t) e^{i(k_l x - \omega_l t - \theta_l)} + \frac{1}{2} k_l |u_l(t)|^2 e^{2i(k_l x - \omega_l t - \theta_l)} \right) \right\} \quad (6.8)$$

, where  $u_l(t) = \sqrt{S_l * 2d\omega} e^{-\frac{ik_l^2 \sqrt{S_l * 2d\omega}^2 \omega_l}{2} t}$

$\eta_{\text{JONSWAP}}(0, t)$  gives us an analytical function to drive a wave train in the wave tank with an averaged error about roughly 5%.

#### 6.4.2 Causing a Rogue Wave in the JONSWAP Wave by the Peregrine Distortion Term

The natural first try to inject a Breather dynamic into the JONSWAP sea state is to multiply the Peregrine distortion term to the analytical JONSWAP wave, i.e.

$$\eta_{\text{dist}}(x, t, a_d, \omega_d) = \text{Re} \left\{ \hat{\eta}_{\text{JONSWAP}} * \left( 1 - \frac{4(1 - ik_d^2 a_d^2 \omega_d t)}{1 + [2\sqrt{2}k_d^2 a_d (x - \frac{\omega_d}{2k_d} t)]^2 + k_d^4 a_d^4 \omega_d^2 t^2} \right) \right\} \quad (6.9)$$

, with  $\hat{\eta}_{\text{JONSWAP}}$  is the complex version of (6.7) or (6.8). If  $\eta_{\text{JONSWAP}}$  is measured and just available as a real-time series, we apply  $\hat{\eta}_{\text{JONSWAP}} = \mathcal{H}(\eta_{\text{JONSWAP}})$  which indicates the transformation of the time series to an analytical signal by taking the Hilbert transform of the real part as the imaginary part.

The wave number and wave frequency are linked by  $k_d = \frac{\omega_d^2}{g}$  ( $g$ : gravitational constant) according to the deep water dispersion relation of first order. Hence, the main question is how to choose  $a_d$  and  $\omega_d$ . We have driven experiments with  $a_d = \frac{H_s}{2}$  and  $\omega_d = \frac{2\pi}{T_p}$  as well as parameters according to spectral analysis of the Draupner wave in [ATY<sup>+</sup>11] who determined a second peak wave frequency  $\omega_{\text{second}} = \frac{2\pi}{T_{\text{second}}}$  next to the main frequency of the Draupner wave field (see figure 6.15). None of the experiments led to a Breather dynamic. Which is understandable if we recap that the phase distortion of the Peregrine perturbation is the crucial property to inject a growing instability modulation. The arbitrary wave field destroys the phase shape of the perturbation and by that suppresses the Breather dynamic.

If the Peregrine distortion is multiplied to the wave field so that the main distortion acts on an 'almost regular wave group', the Breather dynamic occurs in our experiments if driven with an already highly developed modulation, i.e.  $\eta_{dist}(x = -5 * \text{main wavelength} = -5 \frac{T_p^2 g}{2\pi}, t, \frac{H_s}{2}, \frac{2\pi}{T_p})$ . Though interesting, this case limits the injection to an 'almost regular wave area' (which correlates mainly to the phase regularity as we will see below) and to unrealistic high injection modulations. However, it intuites the way to inject a Breather dynamic in an arbitrary directed sea state with the knowledge of the preceding chapters and sections:

We take the JONSWAP wave at the spatial position of injecting a Breather modulation (e.g. flap position). Then we decide for a wave area which should evolve a freak wave and determine its main roots for as many waves as manipulated by the Peregrine distortion term comparing  $\eta_p(x_{flap}, t) = \text{Re} \{ q_p(x, t) e^{i(k_0 x - \omega_0 t)} \}$  and  $\eta_{uniform}(x_{flap}, t) = \text{Re} \left\{ a_0 e^{-\frac{ik_0^2 a_0^2 \omega_0}{2} t} e^{i(k_0 x - \omega_0 t)} \right\}$  according to section 2.2. Figure 6.9 visualize this process.

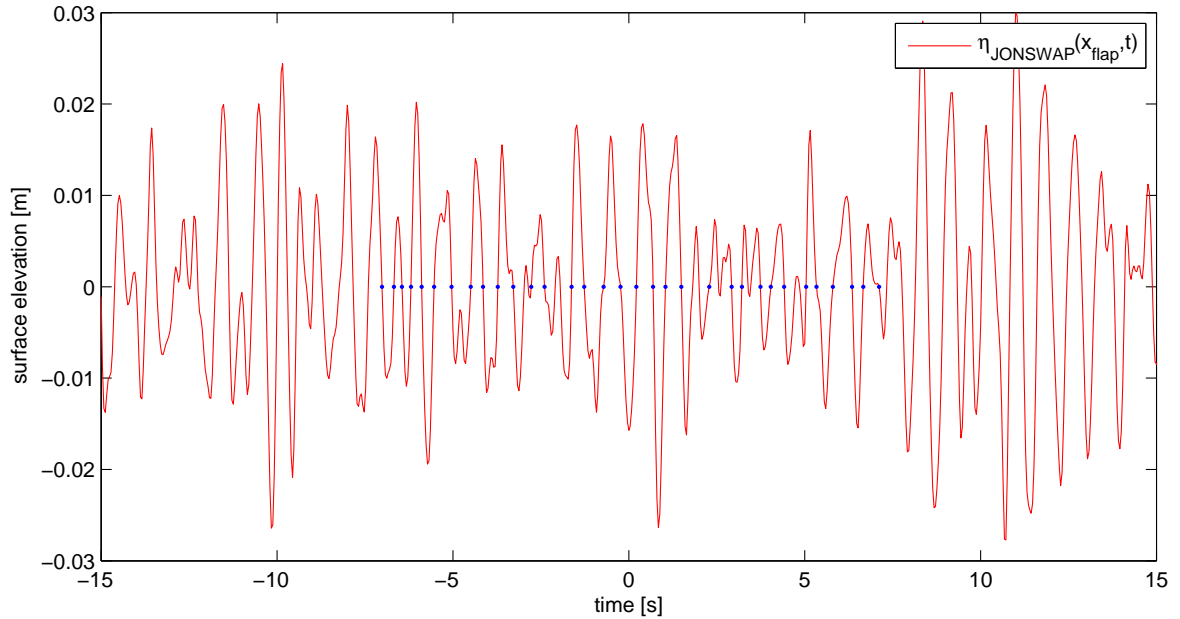


**Figure 6.9:** Main Roots (blue dots) of JONSWAP Wave (red solid line) of Addressed Area; Shifted in Time to have Targeted Rogue Wave Area at  $t = 0s$

After that, we calculate the averaged wave period  $T_{aver}$  and stretch/condense the time axis of the chosen waves locally to get waves with equal wave periods (see figure 6.10). By this, we will get a wave area which has equalized phases (time periods). Therefore, a multiplication of the Peregrine phase distortion keeps the necessary phase modulation to initiate a Breather dynamic. The amplitudes are not the key feature of the perturbation and even amplitude shifts

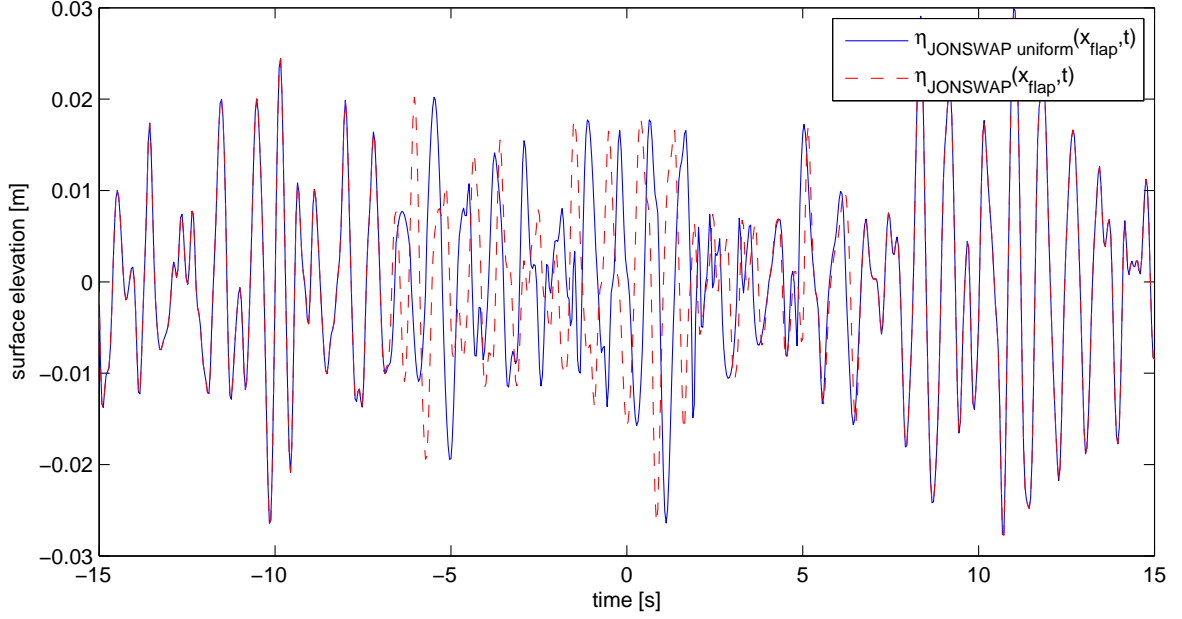


**Figure 6.10:** JONSWAP with temporally Uniform Wave Area (blue solid line) and related JONSWAP Wave (red dashed line)

in time do not destroy the growing instability according to section 6.2. Though in this case, the amplitude changes in the periodic uniform wave area are severe, the run HOS-NWT simulations showed that even these heavily amplitude changes do not suppress the Breather dynamic (but can cause formative modification of the steep wave event shape, of course).

In concrete terms, we multiply the Peregrine distortion term to the uniformed wave area, i.e.

$$\eta_{\text{uni-dist}}(x_{\text{flap}}, t) = \text{Re} \left\{ \hat{\eta}_{\text{JONSWAP uniform}}(x_{\text{flap}}, t) * \left( 1 - \frac{4(1 - ik_d^2 a_d^2 \omega_d t)}{1 + [2\sqrt{2}k_d^2 a_d (x - \frac{\omega_d}{2k_d} t)]^2 + k_d^4 a_d^4 \omega_d^2 t^2} \right) \right\} \quad (6.10)$$

, with  $\hat{\eta}_{\text{JONSWAP uniform}}$  is the complex version of the JONSWAP wave  $\eta_{\text{JONSWAP uniform}}$  phase-uniformed in the chosen temporal area. Furthermore,  $\omega_d = \frac{2\pi}{T_{\text{aver}}}$ ,  $k_d = \frac{\omega_d^2}{g}$ , and  $a_d = \frac{H_s}{2}$  or if this leads to a too steep breaking wave  $a_d = \frac{\varepsilon_{\text{aimed}}}{k_d}$ .

Figure 6.11 compares the initial JONSWAP wave field to the distorted one for a Peregrine modulation with  $x = -40.865$ . Also the pure phase modulation according to section 5.4 is applicable (and will lead to the qualitatively same wave evolution).

In the end, this whole process of injecting a distortion to the JONSWAP wave field is just a phase modulation (with an associated amplitude modulation if the pure phase modulation according to section 5.4 is not taken) of an existing localized wave group. This modulated

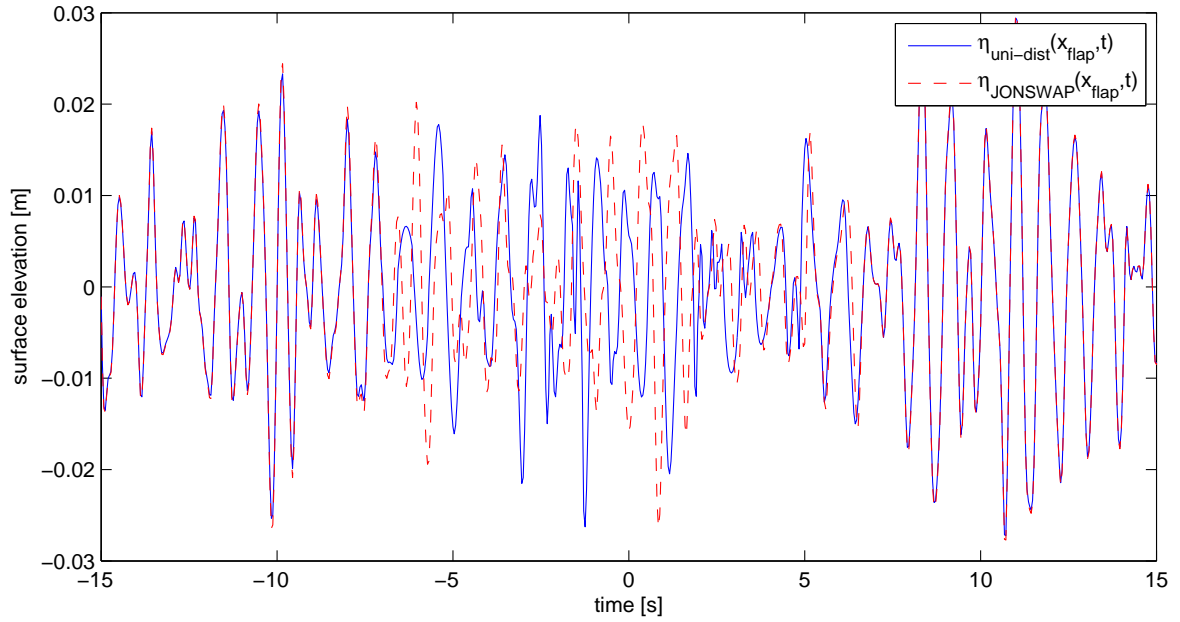


**Figure 6.11:** JONSWAP with Distortion (blue solid line) and related JONSWAP Wave (red dashed line)

JONSWAP wave will evolve a rogue wave in the targeted wave area. Figure 6.12 shows a HOS-NWT simulation of the JONSWAP with distortion in its uniformed wave area (blue solid line) in its maximal peak and the related, original JONSWAP wave (red dashed line) at the same spatial position.

$\eta_{\text{uni-dist}}$  has a maximal freak index of  $AI_{\text{max}} = 2.23$ . Before and after the distortion area the waves of  $\eta_{\text{uni-dist}}$  and  $\eta_{\text{JONSWAP}}$  are very similar. If we compare figure 6.9 with figure 6.12 we realize that the distortion area width has almost not changed until the spatial position of the maximal peak. Its width is nearly constant: An indicator for a nonlinear, non-dispersive effect.

Figure 6.13 presents the HOS-NWT simulation of the distorted JONSWAP  $\eta_{\text{uni-dist}}$  (blue solid line) and the related JONSWAP  $\eta_{\text{JONSWAP}}$  (red dashed line) in different spatial positions  $x^*$ . We see that the temporal distortion width (indicated by the two vertical blue lines) stays almost constant until the maximal peak in  $x^* = 18.42m$ . This is in agreement with studies of [AT14] who showed a local reduction of the dispersive effects for nonlinear rogue waves in irregular, directed sea states. They simulated rogue waves with linear, weakly and fully nonlinear potential solvers and concluded that 'the difference in the shape of the wave group under nonlinear evolution is dramatic' leading to more localized and less spread rogue waves with longer spatial durability. Though the steep wave event has already a freak index of  $AI > 2$  two meters before and behind the maximal peak, the increasing and decreasing is

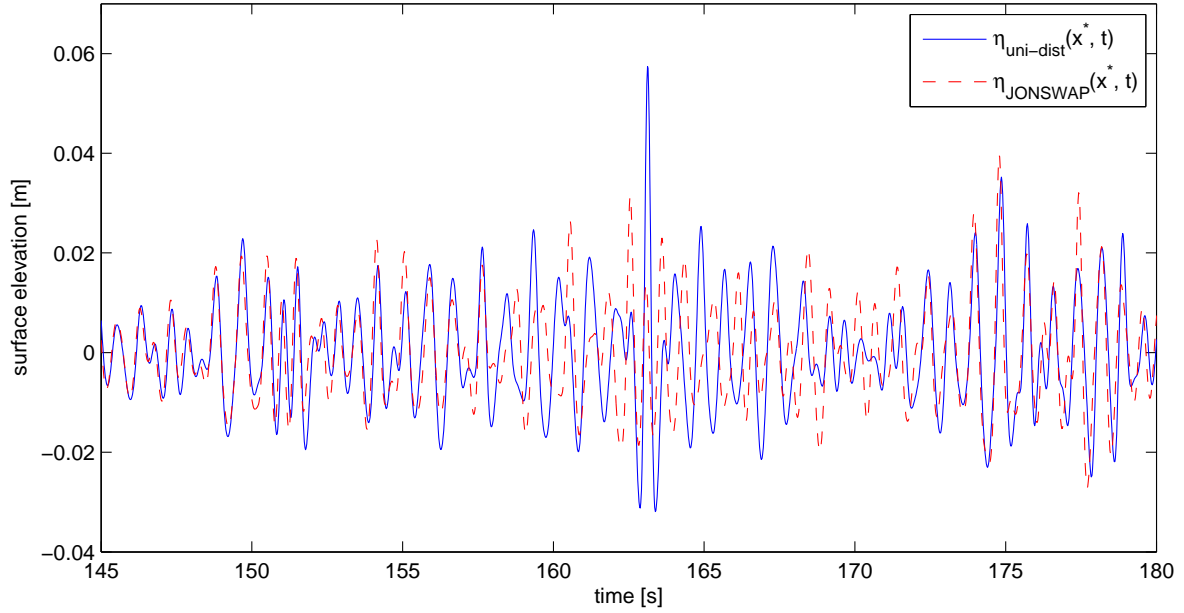


**Figure 6.12:** JONSWAP with Distortion (blue solid line) in its Maximal Peak  $x^* = 18.42m$  and related JONSWAP Wave (red dashed line) at the Same Spatial Position

faster than for the standard Peregrine Breather and in the experiments of the previous sections and chapters (see section 5.4). Again, this is in agreement with [AT14] who proves a much faster development of the maximal peak and shorter durability of rogue waves in the presence of irregular sea states comparing to uniform, unidirectional carrier waves. Nevertheless, the durability is higher than in weakly nonlinear simulations. However, this dynamic change has to be quantified still, especially in real wave tank experiments.

As expected, the distortion area grows after the maximal peak due to predominant dispersive effects until the distortion 'get lost' in the irregular JONSWAP wave leading to isolated phase shifts (blue circles and blue box) which will disperse more and more from each other. This may refer to the 'wave pumping' for a Breather with a uniform carrier wave (see section 5.4).

As already mentioned also the pure phase distortion will lead to a Breather dynamic as well as the use of the modification parameters of chapter 5. Nevertheless, further studies should be performed to

- quantify the change of the Breather dynamic for changes of the distortion term according to the parameters of chapter 5 and the pure phase modulated growing instability/ies.

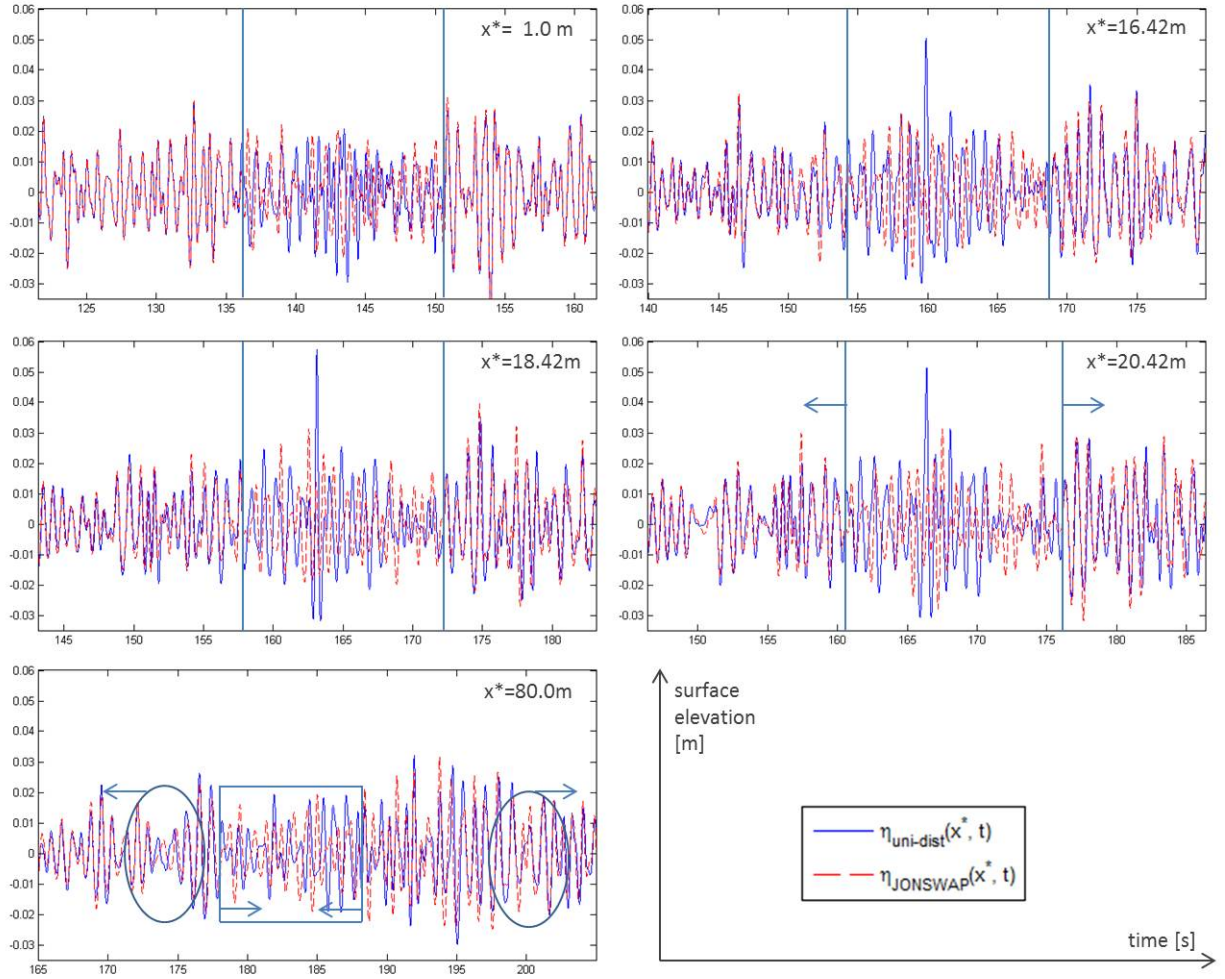


**Figure 6.13:** JONSWAP with Distortion (blue solid line) and related JONSWAP Wave (red dashed line) in Different Locations (HOS-NWT Simulation)

- measure the impact of the irregular carrier wave to the steep wave event shape and qualitative behavior. Does the Breather dynamic occur on every irregular carrier wave by the described injection? What about JONSWAP spectra with different parameters?
- analyze whether the perturbation according to section 6.3 may enable (more) form stable Breather dynamics and maybe even deal with not uniformed irregular carrier waves. A time-varying of  $\omega(t)$  and  $k(t)$  in the distortion term could be needed, too.
- check whether the Breather dynamic occurs for all  $k_d > k_p$ ,  $k_d < k_p$ , and  $k_d = k_p$ . Simulations for all three cases of  $k_d$  have been performed and delivered a Breather dynamic always. However, there will be limits to  $k_d$  as it defines the steepness (wave breaking) and the 'energy' of the modulation. So [Dui99] argued that a 'Benjamin Feir instability

is depressed when the local wave group velocity [ of the instability ] increases and is intensified when the group velocity [ of the carrier wave ] becomes smaller.'

However, this injection of a growing modulation instability is promising and - as shown in the next subsection - may provide an explanation of the many real ocean rogue waves which are not explainable (see section 1.1) by linear theory.

### 6.4.3 Reference to Real Extreme Waves

The injection of a Breather dynamic by the process described in subsection 6.4.2 is a phase modulation (with an associated amplitude modulation if the pure phase modulation according to section 5.4 is not taken) of an existing localized wave group, in the end. This specific phase property may occur by external wind forces, currents, or just by statistical coincidence. [Alb78, AS78, FBL<sup>+</sup>16] argue that typical, measured sea wave parameters result in stable (and due to dispersed waves in the swell area outside of the fetch slightly regular) wave trains which are the base of the here presented Breather distortion. Even crossing seas are known to build such localized stable wave packets (see [AT14]). By all means, it does not seem unrealistic that these phase property may be formed in an oceanic wave field now and then. This may answer some of the hundreds of times more arising rogue waves in the world oceans than forecasted by the linear theory and its statistics ([Mor04, Sta04, For03]). Therefore, we will compare the created Breather wave of subsection 6.4.2 to the Draupner wave ([Hav04]) and try to analyze whether this steep wave event is explainable by the nonlinear injection according to equation (6.10), now.

#### Comparing the Time Series and Spectra of the Draupner Wave

[WTT04] realized that the Draupner rogue wave (see figure 1.1) is unusually steep and its wavelengths in the peak, as well as the troughs, are short followed and preceded by longer waves. Furthermore, the whole extreme wave looks lifted. A linear rogue wave would rather either have a 'set-down' of the extreme wave or at least direct troughs with low frequency, i.e. with long wavelengths. [ATY<sup>+</sup>11] analyzed the Draupner extreme wave further. They realized that the spectra with and without the Draupner wave area have a prominent difference: The spectrum including the steep wave event has a second peak at frequency  $f_{p2}$  next to the main peak at  $f_p$ . [WTT04] and [ATY<sup>+</sup>11] conclude that this is the result of 'two wave-groups crossing, whose mean wave directions were separated by about 90° or more' so that 'the nonlinear interactions between the two systems becomes negligible.'

Another explanation delivers us subsection 6.4.2. The typical Breather shape (see e.g. figure 3.5) is steep, has troughs and a peak of short wavelengths compared with the longer preceding and following waves due to the frequency down-shifting effect. Furthermore, the absolute peak amplitude is much higher than the troughs ones. This may explain the observed unusual properties of the Draupner Wave by [WTT04].

For explaining the spectral characteristics found by [ATY+11], we compare the spectrum of the HOS-NWT simulation of  $\eta_{\text{uni-dist}}$  (blue solid line) and  $\eta_{\text{JONSWAP}}$  (red dashed line) from figure 6.13 one meter behind the flap ( $x^* = 1.0m$ ) in figure 6.14. The spectra are realized by taking the times series and adding the Hilbert transform of the time series as the imaginary part of the signal. This constructed analytical signal has no negative frequencies in its spectrum. Then a Fourier transformation and a transformation according to formula (3.1) is processed and averaged over ten consecutively wave frequencies.

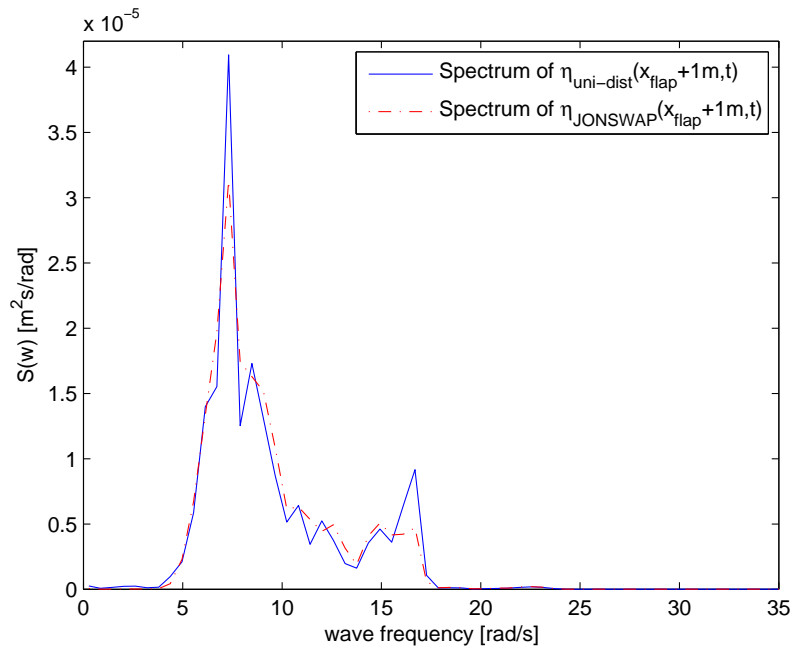


**Figure 6.14:** Spectra of  $\eta_{\text{uni-dist}}$  (blue solid line) and  $\eta_{\text{JONSWAP}}$  (red dashed line) One Meter Behind the Flap

We see that the surface below the curves is almost the same ('energy' of the wave field), but the disturbed JONSWAP spectrum is increased in the main wave frequency and has a close second peak. These enhancements are explainable due to the described injection process: The uniformed wave group has - in this case - a slightly shorter wavelength  $L_{\text{aver}}$  than the main frequency one. In addition, the phase perturbation of the Peregrine distortion term leads to a wavelength change of  $L_{\text{aver}}$  as we can see in figure 5.12 and even more evident in figure 5.13.

The uniformed, shorter waves and the modulated decreased wavelength waves reason the second peak and the modulated increased wavelength waves reason the emphasized main spectral peak. Furthermore, a third high-frequency peak is visible. This peak may be explained by the sever amplitude differences in the uniformed wave area. The spectral decomposition needs high-frequency waves to project this.

Exactly these three peaks are spotted by [SA13] for the standard Peregrine Breather (which has also sever amplitude changes in the waves around the maximal peak) and by [ATY<sup>+</sup>11] for the Draupner wave which is presented in figure 6.15.

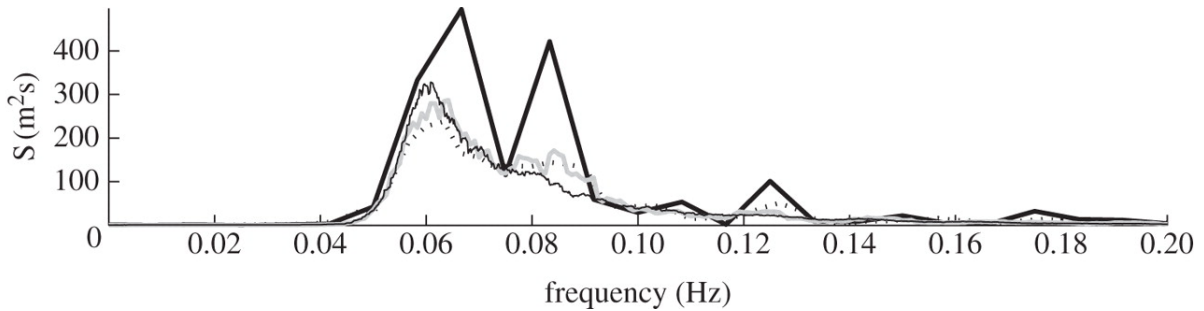


**Figure 6.15:** Spectra of time records containing the Draupner wave. Data are windowed using a Hann window. The data are smoothed by taking an average over 0.001 Hz to improve the clarity of the longer datasets. Black solid line, 2min dataset; black dashed line, 5min; grey solid line, 20min dataset; black thin line, 120min dataset. All Copyrights belong to [ATY<sup>+</sup>11].

The spectrum of the HOS-NWT simulation of  $\eta_{\text{uni-dist}}$  and  $\eta_{\text{JONSWAP}}$  of figure 6.13 in the spatial position of the maximal peak of  $\eta_{\text{uni-dist}}$  ( $x^* = 18.42m$ ) is presented in figure 6.16. We see again that the surfaces below the curves are almost the same, though reduced as a whole due to dissipation. The two main peaks separated from each other and the second peak is relatively increased, i.e. some energy is focused in this shorter wavelength. This is the typical dynamic of a Breather directly visible in the evolution of the wavelengths pictured in figure 5.14 (maximal peak in  $x = 26m$ ). (Hint: The increase of the wavelengths in figure 5.14 is not visible in the spectrum of figure 6.16 as this increase is due to the frequency down-shifting of the uniform carrier wave. The waves belonging to the wavelengths of the frequency down-shift have small amplitudes shifting the main spectral peak just a bit to a smaller frequency.) Furthermore, we do not have the - against the related JONSWAP - emphasized third peak anymore. [Os10b] interprets this dissolving of the third peak as a focusing of a second instability in the first instability while developing the main wave peak. This third peak is still existing in the Draupner spectra: an indicator that the Draupner wave peak at the measured position was not yet fully

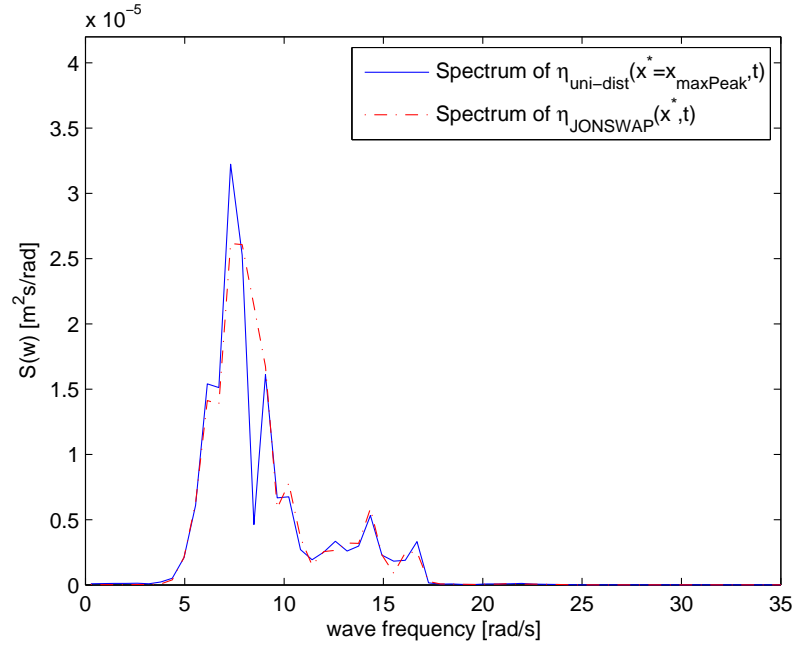


**Figure 6.16:** Spectra of  $\eta_{\text{uni-dist}}$  (blue solid line) and  $\eta_{\text{JONSWAP}}$  (red dashed line) in Spatial Position of Maximal Peak of  $\eta_{\text{uni-dist}}$

developed, as also determined by the 'best fit Peregrine model' analysis tool in section 2.2. Tracking the wave spectra of the HOS simulation of the Draupner Wave ascertains a further growing of the peak for about one more wavelength.

In addition, if we have a deeper look at the wave periods of figure 2.1, we see that the 'best fit Peregrine model' and the Draupner wave have similar wavelengths until the peak and also after the peak reminding that the constant phase shift is due to the NLS neglected - in irregular wave fields persistent - frequency down-shift. This disproportionate number of waves with similar wave periods may - as explained - cause the additionally second peak of the Draupner spectrum and be the base for the Breather distortion according to subsection 6.4.2.

In the end, the alignment of real rogue waves with the theories (see section 1.2) of linear effects, crossing seas, and nonlinear effects like the Breather injection due to subsection 6.4.2 can be performed only, if we get the measured time series of a steep wave event like the Draupner wave in more spatial positions in and perpendicular to the wave propagation direction added by local ocean conditions, current strengths, and angular and spectral spread of the sea state. This has not been available yet.

### Reverse Engineering of Steep Wave Events

The Breather injection process of subsection 6.4.2 also allows us to reverse engineer a real occurred steep wave event with surrounding waves of nearly equal wavelengths like the Draupner wave. To this end, we have to determine the theoretical spatial position of the extreme wave by the 'best fit Peregrine model' analysis tool as described in section 4.1, first. Then, the wave frequency of the modulation has to be detected by the above described spectral analysis and matched to the wavelengths of the surrounding waves of the maximal peak. With this information we can take out the Breather distortion term according to equation (6.10) (or the parametrized versions according to chapters 5, 6.2, 6.3) and reverse engineer the real freak wave.

### A new Forecast Model for Nonlinear Rogue Waves

If we compare the Benjamin-Feir index  $I_{BF}$  (see section 5.1) for the irregular wave field  $\eta_{\text{JONSWAP}}(x_{\text{falp}} + 1m)$  created by a JONSWAP spectrum and the distorted JONSWAP wave  $\eta_{\text{uni-dist}}(x_{\text{falp}} + 1m)$ , we will recognize a slightly increased index. In all run simulations this increase was between 4% and maximal 10%. However, the Benjamin-Feir indexes have always been around 0.5 and thereby smaller than one. Hence, this indicator index has never forecasted an unstable wave train or better to say a high probability of a freak wave. And even if, the Benjamin-Feir index would just predict a freak wave but does not determine the spatial or temporal localization of the steep wave event anyway.

Hint: The Benjamin-Feir index  $I_{BF}$  according to equation (5.2) needs the spectral bandwidth to be calculated. The width at the half spectral maximum was taken as an estimate of this value according to [OOS<sup>+</sup>06]. Furthermore, we counter-checked the values of spectral bandwidth and  $I_{BF}$  with a different way of determination using the spectral moments of the spectra presented in [KPS09c] and [Del08].

[Cha13] has already mentioned a triangular spectrum as an indicator for an upcoming freak wave. He even mentioned that the determination of phase-shifts might be used to forecast rogue waves. This is to underline as the Breather dynamic injected by the process of subsection 6.4.2 is clearly visible in a wavelength plot over time. If we detect a nearly non-dispersive wave group which can be matched to a uniform wave group distorted according to equation (6.10) (or its 'shaped' versions according to chapters 5, 6.2, 6.3), we can not only predict a rogue wave in the short-term but also forecast the temporal and spatial position of the upcoming nonlinear Breather freak wave. If we even measure the local wavelengths of that wave group in two spatial positions, we could determine whether the wavelengths evolve like predicted by the Peregrine distortion term and the experiments of section 5.4 and therefore will most likely lead

to an extreme wave. Alternatively, a spectral transportation equation according to the theories of [GCV56, GCV57, GC53] may forecast the spectral changes of the sea waves. In addition, the 'best fit (shaped) Peregrine model' and (GPU computing real-time) HOS simulations with integrated spectral analysis may support this forecast process as shown in this section.

Since chapter 5 and this chapter prove that the Breather is shapeable, a database of all possible local wavelength evolutions in time and space leading to Breather freak waves would have to be built. Then a measured wave could be counter-checked against the database by a cross-correlation just-in-time leading to a prediction of freak waves and their temporal and spatial emerge. Buoy data of real rogue waves would help to build up this database and analyze the reliability of this process. Unfortunately, there are just a few existing time series of such steep wave events and none of them have a spatial resolution. But the more and more improved satellites may deliver these data sets soon.



## 7 Further Possibilities of Injecting Breather Dynamics in an Irregular Wave Field

After having presented a way to inject a localized steep wave event and compared it to a real occurred rogue wave in chapter 6, we will now discuss further possibilities of causing a Breather dynamic in an irregular wave field briefly.

In section 7.1 we will recap and classify some ways of causing extreme waves in an irregular wave field of different researchers. In addition, we will present a further way to inject a Breather dynamic to a directed irregular wave field by the Peregrine distortion term in sections 7.2 and 7.3 which does not require a uniformed wavelength / phase area in the initial carrier wave like in section 6.4. We will discuss the dynamics and relating spectra of the wave fields.

### 7.1 Current State of Research

#### Perturbation to regular carrier wave of Breather wave train

[ADA09], [CHB+13], and [DT99] analyzed the robustness of the Peregrine model driven Breather wave field  $\eta(x, t) = \text{Re} \left\{ q_p(x, t) e^{i(k_0 x - \omega_0 t)} \right\}$  (with  $q_p(x, t)$  according to equation (2.9)) to initial small perturbations and forcing wind. The results show the persistence of the Breather evolution dynamics. Of course, by this, the initial uniform carrier wave changes to a slightly irregular wave field. Especially, the wind perturbed Peregrine wave looks like a Breather dynamic on an arbitrary directed wave field. [CHB+13] even proved the persistence of the characteristic Peregrine spectrum.

#### Modifying the JONSWAP spectrum to cause rogue waves most likely

In addition, [OOS02] and [OOSB01] showed that by increasing the enhancement factor  $\gamma$  and Phillips constant  $\alpha$  in the JONSWAP spectrum increases the probability of a freak wave evolution in a related directed wave field. The enhancement factor  $\gamma$  reduces the bandwidth of the JONSWAP spectrum and by that 'regularizes' the directed wave field and increases the mean steepness and Benjamin-Feir index  $I_{BF}$ . The Phillips constant  $\alpha$  controls the overall energy in the spectrum and is related to wind speed and fetch length. It is not surprising that a narrow spectrum with an almost uniformed wave field with some sideband modulations and

much overall energy may lead to a rogue wave. This is the inherent idea of the Benjamin-Feir index (5.2) and Benjamin-Feir side-band modulations (see section 2.1). However, this extreme wave evolution is not locally or temporally predictable and the high values for enhancement factor ( $\gamma > 3.3$ ) and Phillips constant are exceptions to the default values of an oceanic wave field.

#### Replacing a part of a JONSWAP generated wave field with a Peregrine Breather wave

[Cha16] replaced a main peak of a JONSWAP generated wave field by a standard Peregrine Breather  $\eta(x, t) = \text{Re} \left\{ q_p(x, t) e^{i(k_0 x - \omega_0 t)} \right\}$  ( $q_p(x, t)$  according to (2.9)) ten wavelengths before its maximal peak. Peregrine Breather and JONSWAP had the same frequency and peak frequency, respectively. Therefore, the wave groups move in the same averaged group velocity. Hence, the JONSWAP wave field will not propagate into the Peregrine distortion area in the first instance. But even if, the Breather dynamic is robust against small changes of propagating waves of the JONSWAP wave field as shown in [ADA09], especially if the Breather instability has been highly developed already, i.e. has much energy.

Figure 7.1 presents a wave tank experiment of cutting in a Peregrine Breather into a JONSWAP wave field run in the Hamburg Ship Model Basin. We see that the Breather dynamic occurs and that the Peregrine driven extreme wave is almost not disturbed. The freak index in the maximal peak is  $AI = 2.85$ . Of course, if we take different group velocities or if we reduce the time width which belongs to the 'pure Peregrine model', i.e. taking less uniform waves in front and behind the maximal distortion of the cut in Peregrine Breather wave, the evolution of the Peregrine Breather will be more disturbed. In this case, we would need a higher developed Peregrine in the sense of  $\eta(x_{\text{flap}} = -\text{some wavelengths}, t)$  as cut in driving time series so that the Breather is able to 'survive'. For further analysis, we refer to [Cha16].

## 7.2 Multiplying the Breather Phase Distortion to each Superposed Wave of the JONSWAP Wave Field

As the JONSWAP wave field (see section 6.4.1, here in order 1)

$$\eta_{\text{JONSWAP}}(x, t) = \text{Re} \left\{ \sum_l \left( A_l e^{i(k_l x - \omega_l t - \theta_l)} \right) \right\}, \text{ with } A_l = \sqrt{S_l * 2d\omega} \quad (7.1)$$

is a wave field created by superposing uniform waves, we question whether it is possible to provoke a Breather dynamic by disturbing every single wave by the Peregrine distortion term.

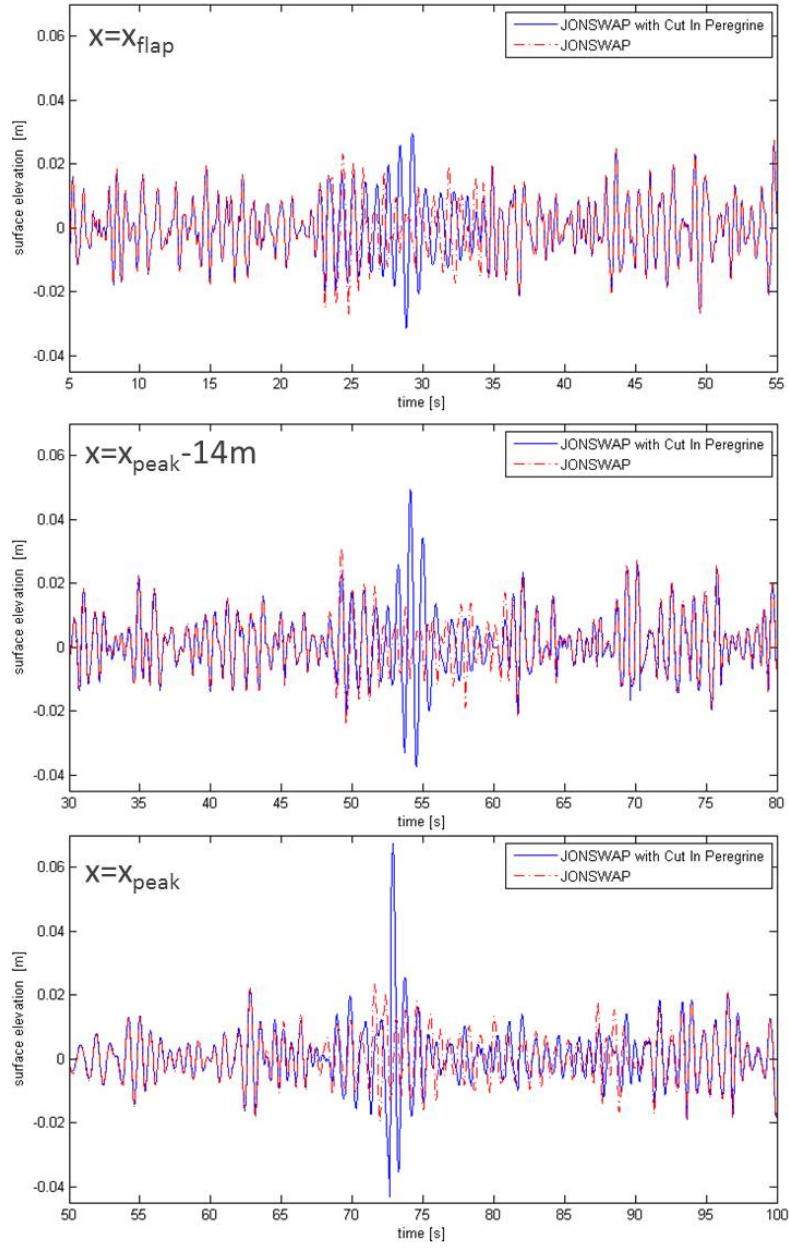


**Figure 7.1:** JONSWAP wave with Cut In Peregrine Breather (blue solid line) and related JONSWAP Wave (red dashed line) in Different Locations

To keep the modification small we decide to disturb by the pure phase modification according to section 5.4 first:

$$\eta_{\text{phasedist}}(x, t) = \text{Re} \left\{ \sum_l \left( A_l e^{i(k_l x - \omega_l t - \theta_l)} \left( \frac{\text{dist}(k_l, \omega_l, A_l, x, t)}{|\text{dist}(k_l, \omega_l, A_l, x, t)|} \right) \right) \right\} \quad (7.2)$$

$$, \text{ with } \text{dist}(k_l, \omega_l, A_l, x, t) = 1 - \frac{4(1 - ik_l^2 A_l^2 \omega_l t)}{1 + [2\sqrt{2}k_l^2 A_l(x - \frac{\omega_l}{2k_l}t)]^2 + k_l^4 A_l^4 \omega_l^2 t^2}$$

With this formula we form a Breather wave according to section 5.4 for every considered spectrum frequency and superpose these single waves to one wave field (here: 256 waves). Furthermore, we do not have to uniform the wavelengths in the distortion area as done in section 6.4 but we can use an arbitrary irregular directed wave field right away for injecting a growing instability modulation. We just need the decomposed wave field into its uniform spectral waves.

Hint: [KPS09b] shows that the case of interacting breathers which may be called 'multi-breathers' 'is sensitive with respect to any kind of perturbation' and will 'result in chaotic behavior of the wave modulations' within the Nonlinear Schroedinger equation. So high order simulations or wave experiments have to be performed to analyze the dynamics of these disturbed wave fields.

Figure 7.2 presents the driving time series and the measurements of the phase disturbed JONSWAP  $\eta_{\text{phasedist}}(x, t)$  and the related JONSWAP wave  $\eta_{\text{JONSWAP}}(x, t)$  in different spatial positions. The Benjamin-Feir index (calculated according to subsection 6.4.3) of the driving time series is increased from  $I_{BF} = 0.4211$  to  $I_{BF} = 0.5310$  by the perturbation. However, both values do not forecast a freak wave.

Already after  $5m$  a focusing in the distortion area (marked by the two vertical red lines) is seen. Nevertheless, this focusing is different to the Breather dynamics in the previous chapters. We do not see one dominating wave, but an amplitude increased wave group. This wave group splits into two at  $x = 13.645m$  where we measure the maximal peak of the wave field. The first amplitude increased wave group stays moderate while the second wave group develops two high waves with a freak index of  $AI = 2.83$  for its maximal wave. After the maximal peak, the two wave groups diverge more and more. They will dissolve in the background JONSWAP wave field, later.

However, we see that the distortion area does not stay localized until the maximal peak of the Breather dynamic. Dispersive effects extend the distortion area from the start. Interpreting the wave field as linear superposed phase distorted Breathers of 256 different wavelengths, this

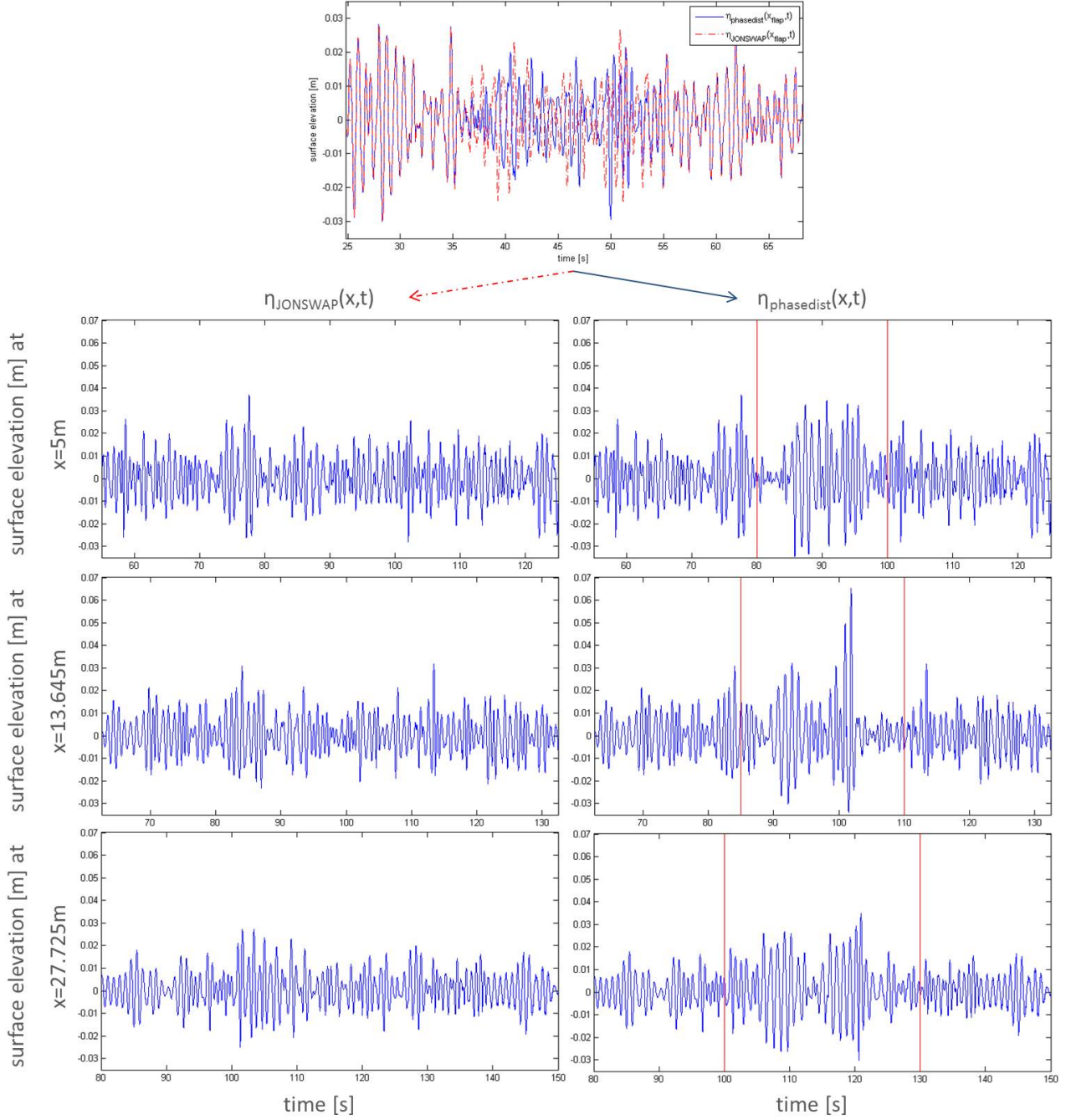


**Figure 7.2:**  $\eta_{\text{phasedist}}$  (right pictures) and related JONSWAP Wave  $\eta_{\text{JONSWAP}}$  (left pictures) in Different Locations. Red Vertical Lines Indicate Distortion Area.

may not be surprising and explain why the 256 phase distorted Breathers do not superpose to a giant super freak wave. However, nonlinear effects do not only take place in the 256 superposed Breathers, but also between the waves as the dynamic evolves two amplitude increased wave groups. It looks like the injected Breathers focus in two instabilities over time (which is in agreement with the studies of [Osb10b]).

These two amplitude increased wave groups may be interpreted as a higher-order Breather according to [LYLG<sup>+</sup>15], though a second order rational Breather would also develop a third wave group behind the maximal peak similar to the first wave group. Therefore, in figure 7.3 we picture the wave spectra for the same spatial positions as in figure 7.2 to understand the dynamics better (determination of the wave spectra: see subsection 6.4.3).

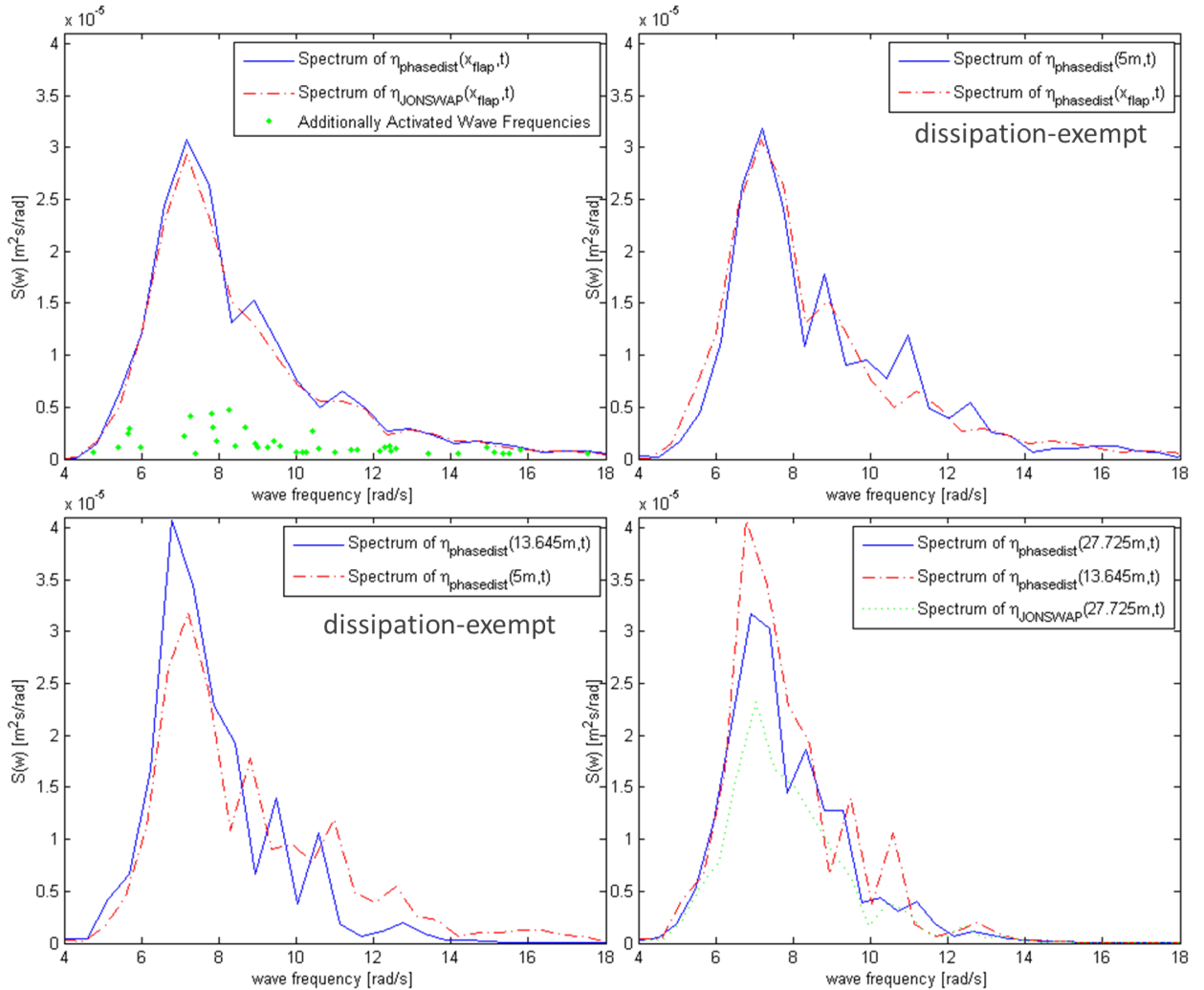


**Figure 7.3:** Spectra of Driving Time Series of  $\eta_{\text{phasedist}}$  and  $\eta_{\text{JONSWAP}}$  (left upper picture) and Evolution of Spectra of  $\eta_{\text{phasedist}}$  in Different Locations

Already in the spectrum of the driving time series we can see two extra spectral peaks if we compare it to the spectrum of the not perturbed JONSWAP wave field. The 256 superposed Breathers add up in a way that two wave frequencies are emphasized. The number of extra spectral peaks depends on the spectrum of the driving time series of the not perturbed JONSWAP wave field  $\eta_{\text{JONSWAP}}(x_{\text{flap}}, t)$ : The small already existing spectral 'hooks' are increased by the distortion according to equation (7.2). This depends on the randomly chosen phase offsets  $\theta_l$  in equation (7.1). First experiments showed that these 'hooks' also control the number of amplified wave groups. However, this has to be further analyzed in proceeding studies. Yet, two additional spectral peaks seem to be the most frequent case.

5m further, the two additional spectral peaks 'gained' energy due to nonlinear effects. Furthermore, a third spectral peak occurs. In the maximal peak of the  $\eta_{\text{phasedist}}$  spatial evolution the main spectral peak is increased and has 'absorbed' (focused energy) the first extra spectral peak. The two still existing additional spectral peaks get closer to the main spectral frequency and to each other starting to coalesce. [Osb10b] interprets this coalescing as a focusing and merging of instabilities, while the lowest instability frequency is always able to focus the most of the energy on itself. 14.08m behind the location of the maximal peak the additional spectral peaks have coalesced and moved closer to the main peak. The amplitude amplified wave groups start to dissolve in the background JONSWAP wave field.

Hence, we may interpret the spectrum evolution as competing growing modulation instabilities if we compare it to the spectrum evolution of section 6.4.3. This would explain the two amplitude increased wave groups and the big changes of the frequency positions of the two smaller spectral peaks. This is also investigated in the following section 7.3.

It should be mentioned that the spectra of  $\eta_{\text{phasedist}}(x^* = 5m, t)$  and  $\eta_{\text{phasedist}}(x^* = 13.645m, t)$  are artificially dissipation-exempt by multiplying  $\frac{\text{surface below Spectrum of } \eta_{\text{phasedist}}(x_{\text{flap}}, t)}{\text{surface below Spectrum of } \eta_{\text{phasedist}}(x^*, t)}$ . Actually, the spectrum 'loses' energy by dissipation which is also seen by the spatial evolution in figure 7.2. Nevertheless, the perturbation seems to stabilize the wave field in the distortion area. Therefore, in the lower right picture the spectrum of the related not disturbed JONSWAP  $\eta_{\text{JONSWAP}}$  at  $x = 27.725$  is presented as well as the not dissipation-exempt spectrum of  $\eta_{\text{phasedist}}(27.725m, t)$ . We see that the overall dissipation had been damped in the breathing JONSWAP.

In the left upper picture of figure 7.3 we also compare the additionally activated wave frequencies in the driving times series due to the phase distortion: The plotted spectrum is averaged over ten consecutively wave frequencies. Some of these wave frequencies have a spectral density of  $S(w) = 0$  or  $S(w) \approx 0$ . These wave frequencies are not activated in the sense that their related Fourier decomposed amplitude is (almost) zero. The phase distortion leads to additionally

activated wave frequencies, i.e. wave frequencies whose related amplitudes are not zero anymore. Some of these additionally activated wave frequencies may act like sideband perturbations according to Benjamin and Feir (see [BF67, BF72]). This is also discussed in [Osb10b] and may explain the growing Breathers dynamic and also the segregation of the wave groups into a series of pulsating wave groups. However, this has to be analyzed further still.

### 7.3 Multiplying the Breather Distortion to each Superposed Wave of the JONSWAP Wave Field

We question whether the Breather dynamic changes, if we - in contrast to equation (7.2) - multiply the full Peregrine distortion to each superposed wave of the JONSWAP wave field, i.e.

$$\eta_{\text{dist}}(x, t) = \text{Re} \left\{ \sum_l \left( A_l e^{i(k_l x - \omega_l t - \theta_l)} \left( 1 - \frac{4(1 - ik_l^2 A_l^2 \omega_l t)}{1 + [2\sqrt{2}k_l^2 A_l (x - \frac{\omega_l}{2k_l} t)]^2 + k_l^4 A_l^4 \omega_l^2 t^2} \right) \right) \right\} \quad (7.3)$$

Like this, we superpose phase offset Peregrine Breather waves according to equation (2.9) and their resulting surface elevation of order one  $\eta(x, t) = \text{Re} \left\{ q_p(x, t) e^{i(k_0 x - \omega_0 t)} \right\}$  of different wave numbers, wave frequencies, and amplitudes.

Figure 7.4 presents the driving time series compared to the related not disturbed JONSWAP wave as well as their spectra in the upper pictures. We see that the distortion with included amplitude amplification increased the energy of the spectrum in contrast to the perturbation (7.2). Furthermore, not the already existing slight hooks of the pure JONSWAP spectrum are emphasized, but the main peak is increased and split into two peaks. By this, the distortion increases the wave amplitudes beside the phase changes in the perturbation area. Furthermore, the Benjamin-Feir index (calculated according to subsection 6.4.3) of the driving time series is increased from  $I_{BF} = 0.4211$  to  $I_{BF} = 0.5397$  by the perturbation which is slightly higher than the index of the pure phase disturbed wave field. However, as bandwidth and mean wave steepness (due to the amplitude amplification) are increased, the values do not differ that much. Either way, none of the values does forecast a freak wave. Moreover, the additionally activated wave frequencies as explained in section 7.2 are presented, i.e. wave frequencies whose related Fourier decomposed wave amplitudes are not zero anymore.

### 7.3 Multiplying the Breather Distortion to each Superposed Wave of the JONSWAP Wave Field

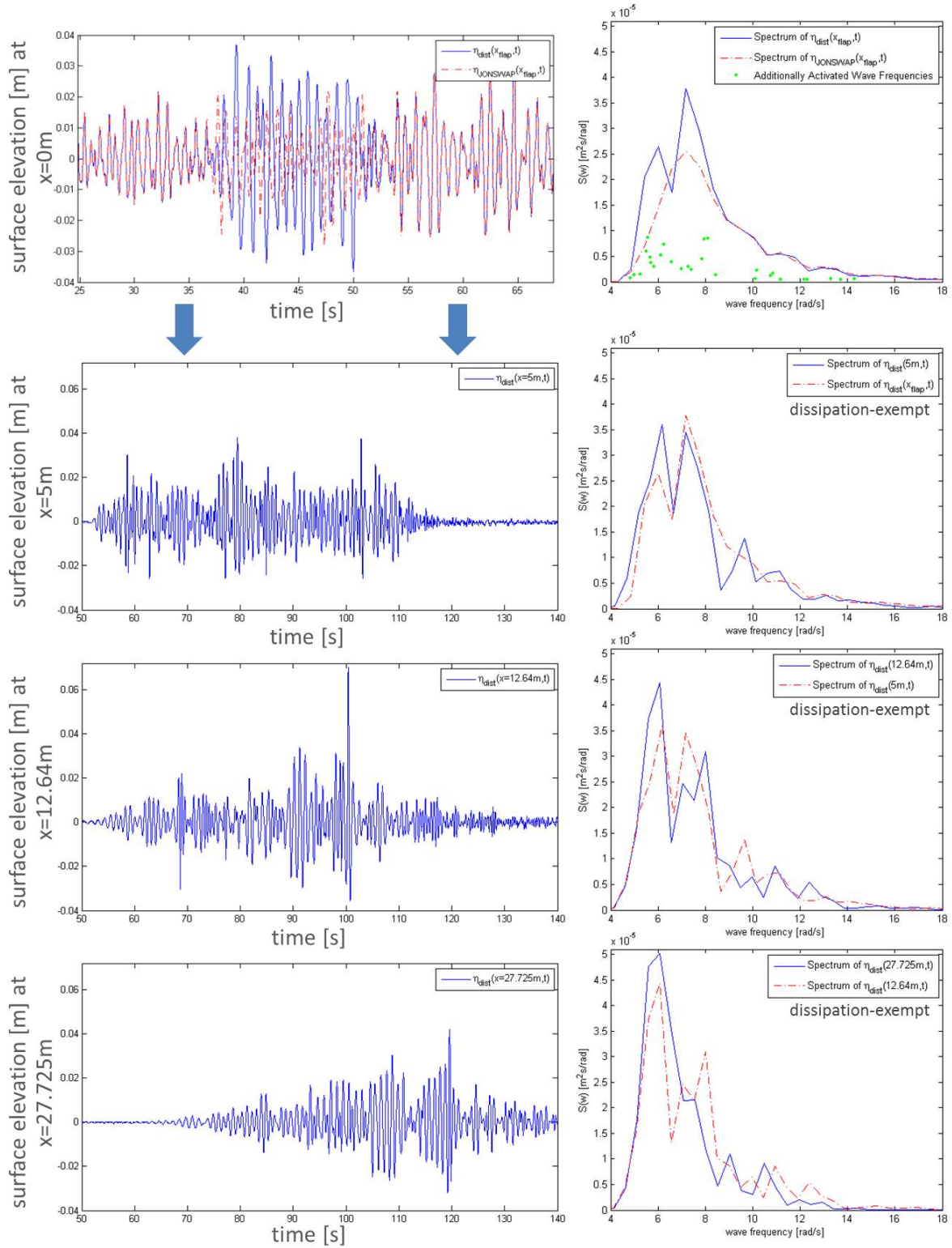


**Figure 7.4:** Surface Elevation and Spectra of Driving Time Series of  $\eta_{\text{dist}}$  and  $\eta_{\text{JONSWAP}}$  (upper pictures) and Evolution of Surface Elevation and Spectra of  $\eta_{\text{dist}}$  in Different Locations

Below the upper pictures of figure 7.4 the evolution of the surface elevation as well as the wave spectra is shown. These spectra are artificially dissipation-exempt by multiplying  $\frac{\text{surface below Spectrum of } \eta_{\text{flap}}(x_{\text{flap}}, t)}{\text{surface below Spectrum of } \eta_{\text{dist}}(x^*, t)}$ . The surface elevations are measured in separately experiments so that the time line of the pictures do not correlate to each other.

After 5m we conjecture two focusing wave groups around 80s already. The related spectrum has two main peaks with almost the same spectral density. A third peak arises which will move more and more to the second main peak wave frequency and is almost coalesced with it at  $x = 12.65m$  in agreement with [Osb10b] who describes the focusing of instabilities in few remaining ones during the evolution of freak waves. In this spatial location, the wave field has its highest peak with a freak index of  $AI = 3.0229$ . Compared to the pure phase distortion of section 7.2 the maximal peak occurs one meter earlier and is higher due to the extra amplitude amplifying perturbation. The second amplitude increased wave group is clearly separated now and stays moderate in its elevation.

At  $x = 27.725m$  the two coalesced spectral peaks are almost gone and the remaining spectrum evolves to an almost standard JONSWAP spectrum beside some small high-frequency peaks. This is also seen in the surface elevation plot. The two amplitude increased wave groups diverge more and more and will dissolve in the background wave later.

As in the pure phase modulated version, this may be interpreted as two competing growing modulation instabilities, of which the one with the lowest frequency will be able to focus the most energy leading to a extreme wave in the wave field. This 'winning' low-frequency instability is in agreement with [Osb10b] who describes the focusing of competing instabilities by inverse scattering transform analysis. The shift of the energy to the low-frequency spectral peak which has initially a smaller spectral density than the second peak is striking.

The evolution of the related JONSWAP wave field is not presented here. However, it can be mentioned that the dispersive effects start right from the beginning as also seen with the pure phase distortion in section 7.2.

We see that the qualitative behavior of the surface evolution of pure phase distorted JONSWAP wave field and the full distortion according to the Peregrine Breather wave is similar. Both wave fields evolve two amplitude amplified wave groups of which one develops a high rogue wave peak, though none of them has a Benjamin-Feir index forecasting this behavior. Furthermore, both wave fields raise two persisting additional spectral peaks (again similar to the Draupner wave spectrum of section 6.4). The low-frequency spectral peak (longer wavelength) focuses the most energy on itself - even if it has not the highest spectral density initially - causing an extreme wave and the two other spectral peaks coalesce right behind the maximal peak of

the wave field. After that, an almost standard JONSWAP spectrum with some small high-frequency spectral hooks develops. Dissipation and dispersive effects take place right from the start.

These methods deliver a possibility to inject a Breather dynamic into an arbitrary directed (JONSWAP) wave field (gained by the decomposition of the wave field into its uniform spectral waves). Nevertheless, the two amplitude increased wave groups look unusual for naturally occurring rogue waves. However, beside the more realistic appearing freak wave of section [6.4.2](#) another Breather dynamic causing perturbation is found showing the importance of nonlinear effects in explaining the many extreme waves on the world oceans.



## 8 Summary, Conclusion, and Future Work

### 8.1 Summary and Conclusion

This thesis is dedicated to analyzing nonlinear, analytical Breather solutions of the Nonlinear Schroedinger equation (NLS) to be used to induce spatially and temporally predetermined rogue waves with realistic properties like shape, height, and steepness occurring in regular and irregular sea states. To this end, we like to modify the distortion term as well as the carrier wave of a promising analytical NLS solution to force the targeted rogue wave in an arbitrary directed sea state. Furthermore, we question if the injection of a Breather dynamic can be performed 'undiscoverable' and 'energy conservatively'. This knowledge should even provide a way to reverse engineer known, real occurred extreme waves and depict a forecast model for nonlinear steep wave events.

We identified the Peregrine Breather solution to be a promising prototype for nonlinear rogue waves. After presenting various wave equations and their (graphics processing unit) simulations we analyzed the limits and by that the use cases of each wave evolution model. These numerical tools in combination with some depicted analyzing software as well as the reviewed wave tank facilities at the Hamburg Ship Model Basin provided all needed means to study our objectives.

We modified the Peregrine Breather distortion term to get predefined rogue wave shapes. The parameter  $\Gamma$  defining the theoretical maximal absolute distortion value delivered an option to modify the freak index and the maximal steepness of the extreme wave. In addition, we recapped that the steepness  $\varepsilon_0$  of the Peregrine Breather model will change the number of waves in the steep wave event. Therefore, several reported freak wave shapes can be achieved. Furthermore, we identified the wave number of the perturbation term for relocating the maximal wave peak of an extreme wave in the times series. By this, we were able to relocate the maximal peak and to reduce or even cancel the amplitude reduced waves in front or behind the freak wave peak. All these parameter studies have been quantified and its limits determined for several carrier waves.

Also, we experimentally showed and reasoned by the higher order dispersion relation and the NLS summands that the phase modulation of the Peregrine Breather model is the crucial modulation to cause a nonlinear growing modulation instability. We excluded dispersive effects as

the reason for the growing Breather dynamic by analyzing the evolution of the local wavelengths and by comparing nonlinear with linear wave simulations. We saw that the nonlinear effects of the Peregrine model phase modulation do not only suppress the dispersive effects but also raise the 'dispersive potential' until the maximal peak of the growing modulation instability. Just after the maximal peak the dispersive effects start and may even prolong the extreme wave event durability. Hence, the rogue wave caused due to pure phase distortion may be more persevering than the standard Peregrine distortion with amplitude modulation, and it provides a way to induce a Breather dynamic 'energy conservatively' and 'undiscoverable'.

After this experimental study on the distortion term of the Peregrine Breather model, we analyzed the robustness of the extreme wave event evolution to changes in the carrier wave. In agreement with the identification and reasoning of the Peregrine phase modulation as the crucial perturbation to cause growing Breather instabilities, a temporal phase shift in the distortion area will lead directly to dispersive effects which destroy the Breather dynamics. However, a temporal amplitude shift in the distortion will preserve the non-dispersive perturbation area and will lead to a Breather dynamic. Whereas, a combination of a temporal phase and amplitude shift straight according to the Peregrine distortion term will preserve the non-dispersive perturbation area and will not destroy the rogue dynamics. The phase shift is balanced by the amplitude shift. In this case, we recognized a shape and frequency persistence accordingly to the inherently combined standard Peregrine models.

This gathered knowledge enabled us to inject a Breather dynamic by the Peregrine distortion term into an arbitrary, directed sea state built by a JONSWAP ocean spectrum. The procedure is explained and a high order simulation has been presented to show the dynamics of this induced rogue wave. Again, we saw that the temporal distortion area width was constant until the maximal peak of the freak wave. After that, the dispersive effects started and the Breather dissolved in the background irregular wave field.

This new way of inducing a Breather dynamic in an irregular sea state was then compared to a real occurred rogue wave: the Draupner wave. It was shown that this new Breather injection could explain the recognized surface elevation properties and spectra evolution. This led us to a depiction of the reverse engineering of real nonlinear rogue waves in simulations and wave tank experiments to enable scientists to perform targeted nonlinear wave-structure-experiments and studies on the extreme wave dynamics. Furthermore, we deduced a possible forecast model for these nonlinear freak waves and sketched the implementation of such a tool.

As the above described Breather injection needs an area of artificially or randomly gained regular wavelengths (which is not so unusual due to dispersion and according to some presented

references), we also presented further possibilities of inducing Breather dynamics to irregular wave fields. Beside the current state of research, we found the Breather causing distortion due to multiplying the Peregrine distortion term to every single uniform wave of the spectral decomposition. This will lead to breathing wave groups of which one develops a freak wave peak. We compared the Breather evolution to the related not modified irregular wave field and identified nonlinear as well as linear dispersive effects during the whole wave group evolution.

Therefore, we analyzed the spectral evolution of the disturbed breathing wave field and identified additional focusing and coalescing spectral peaks as well as an amplification of the main wave frequency peak. However, in the rogue wave evolution the most energy is focused in the spectral peak with the lowest frequency even if it has not the highest spectral density initially. As an explanation of the dynamics, competing growing modulation instabilities as well as Breathers of higher order and additionally activated wave frequencies behaving like Benjamin-Feir sideband modulations have been discussed. This Breather injection has been performed for the pure phase modulation as well as the 'full' perturbation according to the Peregrine distortion term. Both modifications have been compared and resulted in qualitatively similar behaviors in the surface elevation as well as the spectral evolution.

By all this, we were able to achieve our objectives. This improves the analytical, physical understanding of the nonlinear dynamics of rogue waves and proves that nonlinear effects have to be taken into account to understand the appearance of rogue waves in the world oceans and seas, especially to explain the high frequency of extreme surface waves. But most of all it provides scientists with a box of bricks to reverse engineer known, real steep wave events and their nonlinear impacts as well as to cause targeted space- and time-located nonlinear breathing freak wave events in any predefined or random directed sea state. The inducing of a rogue wave can be done 'undiscoverable' and 'energy conservatively' by the pure phase modulation and has never delivered a wave field with a Benjamin-Feir index bigger than 1, i.e. has never revealed its rogue wave modulation by the standard freak wave probability index. All these results will help to investigate the dynamics and potential impacts in experimental, simulative, and analytical studies and will hopefully lead to improved marine structure designs and a forecast model for rogue waves.

## 8.2 Directions for Future Work

### Directly Connected Proceeding Studies

Beside the already in the chapters mentioned limit and quantification studies, also the combination of Breather shaping (chapter 5) with the injection in irregular wave fields according to section 6.4 and chapter 7 should be further investigated. Exemplary, we present a JONSWAP wave field distorted in every single superposed wave according to section 7.3 with an amplified distortion term according to section 5.1. The resulting measured rogue wave in its maximal peak is presented in figure 8.1. It has a freak index of  $AI = 5.76$  and breathes in several wave groups like a high order Breather.

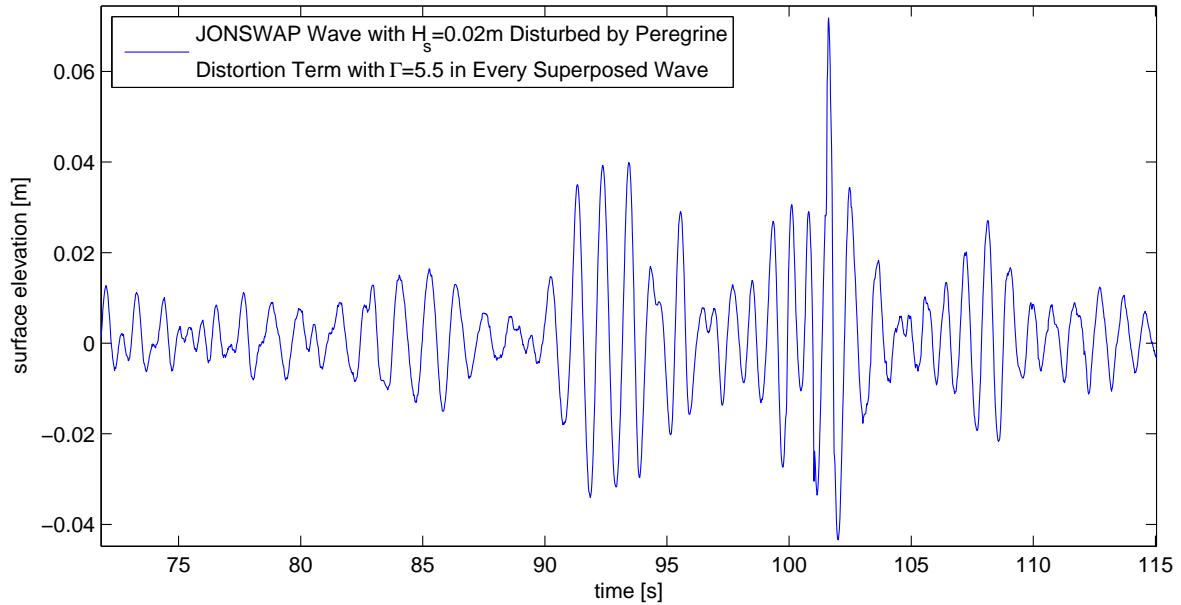


**Figure 8.1:** JONSWAP Wave Field with  $H_s = 0.02m$  Disturbed by Peregrine Distortion Term with  $\Gamma = 5.5$  in Every Superposed Wave; Freak Index  $AI = 5.76$

Additionally, it should be checked whether it is possible to use the wave number of the distortion term to enable the propagation of the Breather on smooth water as the relating 'group velocity of the modulation' is increased. Furthermore, the additional activated frequencies presented in chapter 7 should be tracked and analyzed whether they explain the occurring Breather dynamics. Also to be studied is if all uniform waves of the spectral decomposition of the wave field have to be disturbed or if less superposed Peregrine waves or even just the spectral harmonics would be sufficient to cause Breather dynamics. The reverse engineering of a real rogue wave according to section 6.4 as well as the forecast model should be performed and

confirmed. Then, with a minimal invasive change of the phases, we even may be able to suppress evolving rogue waves.

Moreover, a longer durability of the extreme wave event has been noticed for white walls with white-capping. Furthermore, recursive behavior of the growing modulation instability has been noticed if the rogue wave broke before reaching its maximal peak. The wave seems to go back to an earlier state of the growing modulation and raise a high peak again and again. In numerical simulations, this behavior was even noticed for not breaking waves as if it would be a time-periodic Kuznetsov-Ma-Breather (see [Ma79, Kuz77]). This should be investigated further.

All rogue wave injections should also be checked for (highly) directional spread and not directed sea states as well as for crossing seas known to allow higher wave steepnesses than usually possible due to wave breaking, and which form localized wave packets due to energy exchange that are more likely to be unstable to modulations (see [AT14]).

Of course, further analyzing tools like the Hilbert spectrum, auto- and cross-correlation, kurtosis value, inverse scattering transform analysis, etcetera may provide an improved comprehension of the underlying dynamics.

But in the end, the alignment of real rogue waves and the theories (see section 1.2) of linear effects, crossing seas, and nonlinear effects like the Breather injection due to subsection 6.4.2 can be performed only, if we get the measured time series of a steep wave event like the Draupner wave in more spatial positions in and perpendicular to the wave propagation direction added by local ocean conditions, current strengths, and angular and spectral spread of the sea state. This has not been available yet, though the improved satellites with their Synthetic Aperture Radar (SAR) systems may deliver more data as good as in situ measurements soon, hopefully.

#### Transfer to Other Use Cases

Beside the obvious use cases of the results of this thesis, it should also be checked whether the studies can be used to reduce white signal noise by amplifying the information signal peaks and reducing the preceding and following signal waves. In this sense, the inducing of Breathers in an arbitrary directed wave signal could also be used to encode signals as the high peaks are temporally and spatially localized. Furthermore, the energy focusing of the Breather dynamic could be used in an energy harvesting setup.

As the NLS is not only limited to gravity deep water waves only but is also a governing equation in nonlinear optics, quantum mechanics, electrostatic, and electromagnetic physics, it should

be analyzed whether the improved understanding of nonlinear extreme water waves can be transferred to other (dispersive and non-dispersive) physical domains, too.

### Outlook: Propagation of Modulation Instabilities into Neighboring Wave Domains

Some first studies of wave domains with induced Breather dynamic next to wave domains without growing modulation instabilities showed the possibility of transferring the Breather dynamics into the neighboring wave fields. To this end, some wave flaps drove the wave field with modulation instability, and some drove the related standard wave field or totally different sea states like smooth water, uniform waves, or different JONSWAP wave fields.

It was determined that the phase difference of the two wave domains defines if and how the modulation instability can 'infiltrate' the neighboring wave field. If the wave domain with Breather dynamic is in phase with the neighboring, not breathing waves, the Breather dynamic will induce a growing modulation instability and a time-delayed rogue wave occurs. The delay is proportional to the distance to the wave field with modulation instability. Furthermore, the maximal peak reduces to the modulation instability with pure phase modulation. This time delayed Breathers with diagonal arranged maximal peaks leads visually to a 'Kaventsmann': a fast, bulky, individual wave which does not follow the mean propagation direction. The higher the phase difference of the two neighboring wave domains the more peak height reduction and increased time delays are recognized.

These phenomena could directly relate to the crossing seas theories which may be explained by the directional propagation of the modulation instability perpendicular to the main wave propagation. Also colliding Breathers building a Multibreather similar to section 7.2 and 7.3 and in [KPS09b] may occur. In addition, it explains how a 'wall of water' could occur without being induced in the wave field along the whole wave crest. So far, this dynamic perpendicular to the mean wave propagation is rather interpreted as crossing seas with (more than) 90° angle difference.

On the other hand, a phase difference of  $\pi$  will block the propagation of the modulation instability into neighboring wave domains and result in domain walls as described in [TGCH17]. Therefore, we can support or prevent the directional transfer (of the nonlinear modulation instability), i.e. wedge the (Breather) wave group in or even direct it. Nevertheless, all this has to be analyzed and studied in future works still.

## References

- [AAT09] AKHMEDIEV, N. ; ANKIEWICZ, A. ; TAKI, M.: Waves that appear from nowhere and disappear without a trace. In: *Physics Letters A* 373 (2009), Februar, S. 675–678. <http://dx.doi.org/10.1016/j.physleta.2008.12.036>. – DOI 10.1016/j.physleta.2008.12.036
- [ADA09] ANKIEWICZ, Adrian ; DEVINE, Natasha ; AKHMEDIEV, Nail: Are rogue waves robust against perturbations? 373 (2009), 10, S. 3997–4000
- [AEK85] AKHMEDIEVA, N. N. ; ELEONSKII, V. M. ; KULAGIN, N. E.: Generation of a periodic sequence of picosecond pulses in an optical fiber - Exact solutions. In: *Zhurnal Eksperimentalnoi i Teoreticheskoi Fiziki* 89 (1985), November, S. 1542–1551
- [AK86] AKHMEDIEV, N. N. ; KORNEEV, V. I.: Modulation instability and periodic solutions of the nonlinear Schrödinger equation. In: *Theoretical and Mathematical Physics* 69 (1986), November, S. 1089–1093. <http://dx.doi.org/10.1007/BF01037866>. – DOI 10.1007/BF01037866
- [Alb78] ALBERT, I.E.: EFFECTS OF RANDOMNESS ON THE STABILITY OF TWO-DIMENSIONAL SURFACE WAVETRAINS. 363 (1978), 01, S. 525–546
- [AS78] ALBER, I.E. ; SAFFMAN, P.G.: *Stability of Random Nonlinear Deep Water Waves with Finite Bandwidth Spectra*. TRW, Defense and Space Systems Group, 1978 <https://books.google.de/books?id=5McDHQAACAAJ>
- [AT14] ADCOCK, Thomas A A. ; TAYLOR, Paul H.: The physics of anomalous (rogue) ocean waves. In: *Reports on Progress in Physics* 77 (2014), Nr. 10, 105901. <http://stacks.iop.org/0034-4885/77/i=10/a=105901>
- [ATY<sup>+</sup>11] ADCOCK, T A A. ; TAYLOR, P H. ; YAN, S ; MA, Q W. ; JANSSEN, P A E M.: Did the Draupner wave occur in a crossing sea? In: *Proceedings of the Royal Society* (2011)
- [BDTF11] *Kapitel 4*. In: BONNEFOY, Félicien ; DUCROZET, Guillaume ; TOUZÉ, David L. ; FERRANT, Pierre: *TIME DOMAIN SIMULATION OF NONLINEAR WATER WAVES USING SPECTRAL METHODS*. WORLD SCIENTIFIC, 2011, 129-164

- [BF67] BENJAMIN, T. B. ; FEIR, J. E.: The disintegration of wave trains on deep water Part 1. Theory. In: *Journal of Fluid Mechanics* 27 (1967), Nr. 3, S. 417–430. <http://dx.doi.org/10.1017/S002211206700045X>. – DOI 10.1017/S002211206700045X
- [BF72] BENJAMIN, T. B. ; F.R.S.: The stability of solitary waves. In: *Proceedings of the Royal Society of London A: Mathematical, Physical and Engineering Sciences* 328 (1972), Nr. 1573, 153–183. <http://dx.doi.org/10.1098/rspa.1972.0074>. – DOI 10.1098/rspa.1972.0074. – ISSN 0080–4630
- [Boy00] BOYD, J.P.: *Chebyshev and Fourier Spectral Methods*. DOVER Publications, Inc., 2000
- [CHA11] CHABCHOUB, Amin ; HOFFMANN, Norbert ; AKHMEDIEV, N: Rogue Wave Observation in a Water Wave Tank. 106 (2011), 05, S. 204502
- [CHA12] CHABCHOUB, Amin ; HOFFMANN, Norbert ; AKHMEDIEV, N: Observation of rogue wave holes in a water wave tank. 117 (2012), 11
- [Cha13] CHABSCHOUB, Amin: *An Experimental Study on Breathers in Water Waves*, Technical University Hamburg, Diss., 2013
- [Cha16] CHABCHOUB, Amin: Tracking Breather Dynamics in Irregular Sea State Conditions. 117 (2016), 04
- [CHB<sup>+</sup>13] CHABCHOUB, A. ; HOFFMANN, N. ; BRANGER, H. ; KHARIF, C. ; AKHMEDIEV, N.: Experiments on wind-perturbed rogue wave hydrodynamics using the Peregrine breather model. In: *Physics of Fluids* 25 (2013), Nr. 10, S. 101704. <http://dx.doi.org/10.1063/1.4824706>. – DOI 10.1063/1.4824706
- [CLSY81] CRAWFORD, Donald R. ; LAKE, Bruce M. ; SAFFMAN, Philip G. ; YUEN, Henry C.: Stability of weakly nonlinear deep-water waves in two and three dimensions. In: *Journal of Fluid Mechanics* 105 (1981), S. 177–191. <http://dx.doi.org/10.1017/S0022112081003169>. – DOI 10.1017/S0022112081003169
- [CSS92] CRAIG, W ; SULEM, C ; SULEM, P L.: Nonlinear modulation of gravity waves: a rigorous approach. In: *Nonlinearity* 5 (1992), Nr. 2, 497. <http://stacks.iop.org/0951-7715/5/i=2/a=009>

- [DBLTF07] DUCROZET, G. ; BONNEFOY, F. ; LE TOUZÉ, D. ; FERRANT, P.: 3-D HOS simulations of extreme waves in open seas. In: *Natural Hazards and Earth System Sciences* 7 (2007), Nr. 1, 109–122. <http://dx.doi.org/10.5194/nhess-7-109-2007>. – DOI 10.5194/nhess-7-109-2007
- [DBTF12] DUCROZET, Guillaume ; BONNEFOY, Félicien ; TOUZÉ, David L. ; FERRANT, Pierre: A modified High-Order Spectral method for wavemaker modeling in a numerical wave tank. In: *European Journal of Mechanics - B/Fluids* 34 (2012), 19 - 34. <http://dx.doi.org/https://doi.org/10.1016/j.euromechflu.2012.01.017>. – DOI <https://doi.org/10.1016/j.euromechflu.2012.01.017>. – ISSN 0997–7546
- [DBTF16] DUCROZET, Guillaume ; BONNEFOY, Félicien ; TOUZÉ, David L. ; FERRANT, Pierre: HOS-ocean: Open-source solver for nonlinear waves in open ocean based on High-Order Spectral method. In: *Computer Physics Communications* 203 (2016), 245 - 254. <http://dx.doi.org/https://doi.org/10.1016/j.cpc.2016.02.017>. – DOI <https://doi.org/10.1016/j.cpc.2016.02.017>. – ISSN 0010–4655
- [Deb94] DEBNATH, L.: The Theory of Nonlinear Dispersive Waves. In: *Nonlinear Water Waves*. Academic Press, 1994, Kapitel 7, S. 303–395
- [Del08] DELFT, TU: *Overview of Ocean Wave Statistics - Chapter 4 Spectral Analysis*. <https://upcommons.upc.edu/bitstream/handle/2099.1/6034/06.pdf?sequence=7>. Version: 2008. – [Online; accessed 08-June-2018]
- [Del12] DELTARES: *AukePC - Wave software for experimental facilities - User & Technical Reference - Manual*, 2012
- [DKM08] DYSTHE, Kristian ; KROGSTAD, Harald E. ; MÜLLER, Peter: Oceanic Rogue Waves. In: *Annual Review of Fluid Mechanics* 40 (2008), Nr. 1, 287–310. <http://dx.doi.org/10.1146/annurev.fluid.40.111406.102203>. – DOI 10.1146/annurev.fluid.40.111406.102203
- [DMEG82] DODD, R. K. ; MORRIS, H. C. ; EILBECK, J. C. ; GIBBON, J. D.: *Soliton and nonlinear wave equations*. 1982
- [DT99] DYSTHE, Kristian B. ; TRULSEN, Karsten: Note on Breather Type Solutions of the NLS as Models for Freak-Waves. In: *Physica Scripta* 1999 (1999), Nr. T82, 48. <http://stacks.iop.org/1402-4896/1999/i=T82/a=012>

- [Dui99] DUIN, Cornelis A. v.: The effect of non-uniformity of modulated wavepackets on the mechanism of Benjamin Feir instability. 399 (1999), 11, S. 237–249
- [Dys79] DYSTHE, K B.: Note on a Modification to the Nonlinear Schrodinger Equation for Application to Deep Water Waves. In: *Proceedings of the Royal Society of London A: Mathematical, Physical and Engineering Sciences* 369 (1979), Nr. 1736, 105–114. <http://dx.doi.org/10.1098/rspa.1979.0154>. – DOI 10.1098/rspa.1979.0154. – ISSN 0080–4630
- [FBL<sup>+</sup>16] FEDELE, F ; BRENNAN, J ; LEON, S P. ; DUDLEY, J ; DIAS, F: Real world ocean rogue waves explained without the modulational instability. In: *Scientific Reports* 6 (2016), June. <http://dx.doi.org/10.1038/srep27715>
- [FCKDO12] F. CLAUSS, Günther ; KLEIN, Marco ; DUDEK, Matthias ; ONORATO, Miguel: Application of Breather Solutions for the Investigation of Wave/Structure Interaction in High Steep Waves. In: *Proceedings of the International Conference on Offshore Mechanics and Arctic Engineering - OMAE* Bd. 2, 2012
- [For03] FORRISTALL, G. Z.: *Understanding rogue waves: Are new physics really necessary? 14th Aha Huliko'a Hawaiian Winter Workshop*. 2003
- [GC53] GELCI, R ; CAZALÉ, H: Une theorie energetique de la houle appliquee au Maroc. (1953), 01, S. 64–66
- [GCV56] GELCI, R ; CAZALÉ, H ; VASSAL, J: Utilization des diagrammes de propagation à la prévision énergétique de la houle. 8 (1956), 01, S. 169–197
- [GCV57] GELCI, R ; CAZALÉ, H ; VASSAL, J: Prévision de la houle. La méthode des densités spectroangulaires. 9 (1957), 01, S. 416–435
- [GT07] GRAMSTAD, ODIN ; TRULSEN, KARSTEN: Influence of crest and group length on the occurrence of freak waves. In: *Journal of Fluid Mechanics* 582 (2007), S. 463–472. <http://dx.doi.org/10.1017/S0022112007006507>. – DOI 10.1017/S0022112007006507
- [Hav04] HAVER, S.: A possible freak wave event measured at the Draupner Jacket January 1 1995. In: *Proceedings Rogue Waves* (2004)
- [HKS<sup>+</sup>10] HÖHMANN, R ; KUHL, Ulrich ; STÖCKMANN, H-J ; KAPLAN, Lev ; HELLER, Eric: Freak Waves in the Linear Regime: A Microwave Study. 104 (2010), 03, S. 093901

- [HPBB<sup>+</sup>73] HASSELMANN, Klaus ; P. BARNETT, T ; BOUWS, E ; CARLSON, H ; E. CARTWRIGHT, D ; ENKE, K ; A EWING, J ; GIENAPP, H ; E. HASSELMANN, D ; KRUSEMAN, P ; MEERBURG, A ; MÜLLER, P ; OLBERS, Dirk ; RICHTER, K ; SELL, W ; WALDEN, H: Measurements of wind-wave growth and swell decay during the Joint North Sea Wave Project (JONSWAP). 8 (1973), 01, S. 1–95
- [HPD99] HENDERSON, K. L. ; PEREGRINE, D. H. ; DOLD, J. W.: Unsteady water wave modulations: Fully nonlinear solutions and comparison with the nonlinear Schrödinger equation. In: *Wave Motion* 29 (1999), 5, Nr. 4, S. 341–361. – ISSN 0165–2125
- [Joh97a] JOHNSON, R S.: A modern introduction to the mathematical theory of water waves. In: *Cambridge Univ Press* (1997)
- [Joh97b] JOHNSON, R.S.: On the modulation of water waves in the neighbourhood of  $kh \approx 1.363$ . In: *Proceedings Royal Society London A* 357:131–141 (1997)
- [KM83] KAKUTANI, T. ; MICHIIRO, K.: Marginal state of modulation instability - Note on Benjamin-Feir instability. In: *Journal Physic Society Japan* 52:4129–4137 (1983)
- [KP01] KATZ, Joseph ; PLOTKIN, Allen: *Low-Speed Aerodynamics*. 2. Cambridge University Press, 2001 (Cambridge Aerospace Series). <http://dx.doi.org/10.1017/CB09780511810329>. <http://dx.doi.org/10.1017/CB09780511810329>
- [KP03] KHARIF, Christian ; PELINOVSKY, Efim: Physical mechanisms of the rogue wave phenomenon. In: *European Journal of Mechanics - B/Fluids* 22 (2003), Nr. 6, 603 – 634. <http://dx.doi.org/https://doi.org/10.1016/j.euromechflu.2003.09.002>. – DOI <https://doi.org/10.1016/j.euromechflu.2003.09.002>. – ISSN 0997–7546
- [KPS09a] KHARIF, C ; PELINOVSKI, E ; SLUNYAEV, A: *Rogue Waves in the Ocean*. Springer, 2009
- [KPS09b] *Kapitel 4*. In: KHARIF, C ; PELINOVSKI, E ; SLUNYAEV, A: *Rogue Waves in the Ocean*. Springer, 2009, S. 111–117
- [KPS09c] *Kapitel 2*. In: KHARIF, C ; PELINOVSKI, E ; SLUNYAEV, A: *Rogue Waves in the Ocean*. Springer, 2009, S. 48–53

- [Kuz77] KUZNETSOV, E. A.: Solitons in a parametrically unstable plasma. In: *Akademiia Nauk SSSR Doklady* 236 (1977), September, S. 575–577
- [Lee12] LEE, N C.: Derivation of nonlinear Schrödinger equation for electrostatic and electromagnetic waves in fully relativistic two-fluid plasmas by the reductive perturbation method. In: *Physics of Plasmas* 19 (2012)
- [Liu07] LIU: *Freaque Waves*, [http://freaquewaves.blogspot.com/2006\\_07\\_01\\_archive.html](http://freaquewaves.blogspot.com/2006_07_01_archive.html). Website, 2007. – Accessed September 2017
- [LM85] LO, Edmond ; MEI, Chiang: A numerical study of water-wave modulation based on a higher-order nonlinear Schrödinger equation. In: *J. Fluid Mech.* Bd. 150, 1985, S. 395–416
- [LYLG<sup>+</sup>15] LIU, Changfu ; YAN LI, YAN ; GAO, MEIPING ; WANG, ZEPING ; DAI, Zhengde ; WANG, Chuanjian: Rogue wave solutions of the nonlinear Schrödinger equation with variable coefficients. 85 (2015), 07
- [Ma79] MA, Yan-Chow: The Perturbed Plane-Wave Solutions of the Cubic Schrödinger Equation. In: *Studies in Applied Mathematics* 60 (1979), Nr. 1, 43–58. <http://dx.doi.org/10.1002/sapm197960143>. – DOI 10.1002/sapm197960143. – ISSN 1467–9590
- [Mor04] MORI, Nobuhito: Occurrence probability of a freak wave in a nonlinear wave field. In: *Ocean Engineering* 31 (2004), Nr. 2, 165 - 175. [http://dx.doi.org/https://doi.org/10.1016/S0029-8018\(03\)00119-7](http://dx.doi.org/https://doi.org/10.1016/S0029-8018(03)00119-7). – DOI [https://doi.org/10.1016/S0029-8018\(03\)00119-7](https://doi.org/10.1016/S0029-8018(03)00119-7). – ISSN 0029–8018
- [Nan18] NANTES, Ecole C.: *Hydrodynamics, Energetics and Atmospheric Environment Laboratory*. <https://github.com/LHEEA>. Version: 2018. – [Online; accessed 12-May-2018]
- [New81] NEWELL, A C.: Solitons in the mathematics and physics. In: *Soc Ind Appl Math Univ Arizona* (1981)
- [NVI18a] NVIDIA: *CUDA Zone of NVIDIA*. <https://developer.nvidia.com/cuda-zone>. Version: 2018. – [Online; accessed 12-May-2018]
- [NVI18b] NVIDIA: *GPU Accelerated Applications*. <https://developer.nvidia.com/computeworks>. Version: 2018. – [Online; accessed 12-May-2018]

- 
- [Oka84] OKAMURA, Makoto: Instabilities of Weakly Nonlinear Standing Gravity Waves. In: *Journal of the Physical Society of Japan* 53 (1984), Nr. 11, 3788–3796. <http://dx.doi.org/10.1143/JPSJ.53.3788>. – DOI 10.1143/JPSJ.53.3788
- [OO06] ONORATO, M ; OSBORNE, A R.: Modulational instability in crossing sea states: a possible mechanism for the formation of freak waves. In: *Physical Review Letters* 96 (2006), Nr. 1
- [OOS02] ONORATO, M. ; OSBORNE, A. R. ; SERIO, M.: Extreme wave events in directional, random oceanic sea states. In: *Physics of Fluids* 14 (2002), April, S. L25–L28. <http://dx.doi.org/10.1063/1.1453466>. – DOI 10.1063/1.1453466
- [OOS<sup>+</sup>06] ONORATO, M. ; OSBORNE, A.R. ; SERIO, M. ; CAVALERI, L. ; BRANDINI, C. ; STANSBERG, C.T.: Extreme waves, modulational instability and second order theory: wave flume experiments on irregular waves. In: *European Journal of Mechanics - B/Fluids* 25 (2006), Nr. 5, 586 – 601. <http://dx.doi.org/https://doi.org/10.1016/j.euromechflu.2006.01.002>. – DOI <https://doi.org/10.1016/j.euromechflu.2006.01.002>. – ISSN 0997–7546. – Rogue waves
- [OOSB01] ONORATO, Miguel ; OSBORNE, Alfred R. ; SERIO, Marina ; BERTONE, Serena: Freak Waves in Random Oceanic Sea States. In: *Phys. Rev. Lett.* 86 (2001), Jun, 5831–5834. <http://dx.doi.org/10.1103/PhysRevLett.86.5831>. – DOI 10.1103/PhysRevLett.86.5831
- [OPCK13] ONORATO, M ; PROMENT, D ; CLAUSS, G ; KLEIN, M: Rogue Waves: From Nonlinear Schrödinger Breather Solutions to Sea-Keeping Test. In: *PLoS ONE* 8 (2013), February, Nr. 2. <https://ueaeprints.uea.ac.uk/41940/>. – © 2013 Onorato et al. This is an open-access article distributed under the terms of the Creative Commons Attribution License, which permits unrestricted use, distribution, and reproduction in any medium, provided the original author and source are credited.
- [Osb10a] OSBORNE, A: *Nonlinear Ocean Waves and the Inverse Scattering Transform, Volume 97*. Academic Press, 2010
- [Osb10b] *Kapitel Laboratory Experiments of Rogue Waves*. In: OSBORNE, A: *Nonlinear Ocean Waves and the Inverse Scattering Transform, Volume 97*. Academic Press, 2010, S. 745–779

- [Per83] PEREGRINE, D. H.: Water waves, nonlinear Schrödinger equations and their solutions. In: *The Journal of the Australian Mathematical Society. Series B. Applied Mathematics* 25 (1983), Nr. 1. <http://dx.doi.org/10.1017/S0334270000003891>. – DOI 10.1017/S0334270000003891
- [SA13] SHEMER, L. ; ALPEROVICH, L.: Peregrine Breather Revisited. In: *Physics of Fluids* 25 (2013), S. 051701
- [SD08] SHEMER, Lev ; DORFMAN, Boris: Spatial vs. Temporal Evolution of Nonlinear Wave Groups: Experiments and Modeling Based on the Dysthe Equation. In: *Proceedings of the International Conference on Offshore Mechanics and Arctic Engineering - OMAE* Bd. 2, 2008
- [SG10] SHRIRA, V. I. ; GEOGJAEV, V. V.: What makes the Peregrine soliton so special as a prototype of freak waves? In: *Journal of Engineering Mathematics* 67 (2010), Juni, S. 11–22. <http://dx.doi.org/10.1007/s10665-009-9347-2>. – DOI 10.1007/s10665-009-9347-2
- [Slu05] SLUNYAEV, A V.: A high-order nonlinear envelope equation for gravity waves in finite-depth water. In: *Journal of Experimental and Theoretical Physics* 101 (2005), Nov, Nr. 5, 926–941. <http://dx.doi.org/10.1134/1.2149072>. – DOI 10.1134/1.2149072. – ISSN 1090–6509
- [SPS<sup>+</sup>13] SLUNYAEV, A. ; PELINOVSKY, E. ; SERGEEVA, A. ; CHABCHOUB, A. ; HOFFMANN, N. ; ONORATO, M. ; AKHMEDIEV, N.: Super-rogue waves in simulations based on weakly nonlinear and fully nonlinear hydrodynamic equations. In: *Phys. Rev. E* 88 (2013), Jul, 012909. <http://dx.doi.org/10.1103/PhysRevE.88.012909>. – DOI 10.1103/PhysRevE.88.012909
- [SRKJ07] SOLLI, D R. ; ROPERS, C ; KOONATH, P ; JALALI, B: Optical rogue waves. In: *Nature* 450 (2007), S. 1054–1057
- [Sta04] STANSELL, Paul: Distributions of freak wave heights measured in the North Sea. In: *Applied Ocean Research* 26 (2004), Nr. 1, 35 - 48. <http://dx.doi.org/https://doi.org/10.1016/j.apor.2004.01.004>. – DOI <https://doi.org/10.1016/j.apor.2004.01.004>. – ISSN 0141–1187
- [Su82] SU, M. Y.: Evolution of groups of gravity waves with moderate to high steepness. In: *Physics of Fluids* 25 (1982), S. 2167–2174

- 
- [Sua15] SUAREZ, Pablo: *An introduction to the Split Step Fourier Method using MATLAB*. [https://www.researchgate.net/publication/281441538\\_An\\_introduction\\_to\\_the\\_Split\\_Step\\_Fourier\\_Method\\_using\\_MATLAB](https://www.researchgate.net/publication/281441538_An_introduction_to_the_Split_Step_Fourier_Method_using_MATLAB). Version: 2015. – [Online; accessed 12-May-2018]
- [TBOW10] TOFFOLI, A. ; BABANIN, A. ; ONORATO, M. ; WASEDA, T.: Maximum steepness of oceanic waves: Field and laboratory experiments. In: *Geophysical Research Letters* 37 (2010). <http://dx.doi.org/10.1029/2009GL041771>. – DOI 10.1029/2009GL041771
- [TFH<sup>+</sup>84] TORSETHAUGEN, K. ; FAANES, T. ; HAVER, S. ; HAVNELABORATORIET, Norges hydrodynamiske laboratorier. Divisjon vassdrags-og ; SKIPSFORSKNINGSINSTITUTT, Norges ; HØGSKOLE, Selskapet for industriell og teknisk forskning ved Norges t.: *Characteristica for Extreme Sea States on the Norwegian Continental Shelf*. Norwegian Hydrodynamics Laboratories, Division River and Harbour Laboratory, 1984 (Report (Norges hydrodynamiske laboratorier)). <https://books.google.de/books?id=U5pBmAEACAAJ>
- [TGCH17] TSITOURA, Fotini ; GIETZ, U ; CHABCHOUB, Amin ; HOFFMANN, Norbert: Observation of domain walls in deep water surface gravity waves. (2017), 06
- [Tul96] *Kapitel Breaking of ocean waves and downshifting*. In: TULIN, M.P.: *Waves and Nonlinear Processes in Hydrodynamics*. Kluwer, 1996, S. 177–190
- [WAF09] WAFO: *WAFO*, <https://code.google.com/archive/p/wafo/>. Website, 2009. – Accessed March 2018
- [WH86] WEIDEMAN, J. A. C. ; HERBST, B. M.: Split-Step Methods for the Solution of the Nonlinear Schrodinger Equation. In: *SIAM Journal on Numerical Analysis* 23 (1986), Nr. 3, 485–507. <http://www.jstor.org/stable/2157521>. – ISSN 00361429
- [Wik17] WIKIPEDIA: *Stokes wave* — *Wikipedia, The Free Encyclopedia*. [https://en.wikipedia.org/w/index.php?title=Stokes\\_wave&oldid=811553595](https://en.wikipedia.org/w/index.php?title=Stokes_wave&oldid=811553595). Version: 2017. – [Online; accessed 10-December-2017]
- [Wik18] WIKIPEDIA: *Monsterwaves* — *Wikipedia, The Free Encyclopedia*. <https://de.wikipedia.org/wiki/Monsterwelle>. Version: 2018. – [Online; accessed 14-June-2018]

- [WTT04] WALKER, D.A.G. ; TAYLOR, P.H. ; TAYLOR, R. E.: The shape of large surface waves on the open sea and the Draupner New Year wave. In: *Applied Ocean Research* 26 (2004), Nr. 3, 73 - 83. <http://dx.doi.org/https://doi.org/10.1016/j.apor.2005.02.001>. – DOI <https://doi.org/10.1016/j.apor.2005.02.001>. – ISSN 0141–1187
  
- [YL82] YUEN, Henry C. ; LAKE, Bruce M.: Nonlinear Dynamics of Deep-Water Gravity Waves. Version: 1982. [http://dx.doi.org/https://doi.org/10.1016/S0065-2156\(08\)70066-8](http://dx.doi.org/https://doi.org/10.1016/S0065-2156(08)70066-8). Elsevier, 1982. – DOI [https://doi.org/10.1016/S0065-2156\(08\)70066-8](https://doi.org/10.1016/S0065-2156(08)70066-8). – ISSN 0065–2156, 67 - 229
  
- [Yue91] *Kapitel* Recent Advances in Nonlinear Water Waves. An Overview. In: YUEN, H.C.: *Proceedings of the International School of Physics - Nonlinear Topics in Ocean Physics*. Societa Italiana di Fisica, 1991, S. 461–498
  
- [YZHK11] YING, L H. ; ZHUANG, Z ; HELLER, E J. ; KAPLAN, L: Linear and nonlinear rogue wave statistics in the presence of random currents. In: *Nonlinearity* 24 (2011), Nr. 11, R67. <http://stacks.iop.org/0951-7715/24/i=11/a=R01>
  
- [Zak68] ZAKHAROV, V. E.: Stability of periodic waves of finite amplitude on a surface of deep fluid. In: *Appl. Mech. Tech. Phys.* 9 (1968), S. 190–194
  
- [ZS72] ZAKHAROV, V. E. ; SHABAT, A. B.: Exact Theory of Two-dimensional Self-focusing and One-dimensional Self-modulation of Waves in Nonlinear Media. In: *Soviet Journal of Experimental and Theoretical Physics* 34 (1972), S. 62

# Curriculum Vitae

## Personal Information

---

Name	Andy Witt
Date of Birth	March 01 <sup>st</sup> , 1983 in Brunsbüttel
Nationality	German
Contact	mail@andy-witt.com



## Education and Professional Experience

---

08/2017 - today	Founder & Business Executive of CALC4XL GmbH
04/2013 - 08/2017	Research Associate of the Technical University Hamburg Analytical, Numerical, and Experimental Studies on Wave Dynamics Besides: Giving Lectures, Supervising Exams
03/2013	Engineering Diploma Graduation (Title: 'Diplom-Ingenieur') Thesis: 'Fast Multipole and Graphics Processing Unit Computation Accelerated High Order Boundary Element Method'
04/2007 - 02/2012	Product Manager at Software Company FACTON GmbH
04/2004 - 04/2007	Customer Service at Biotech Company QIAGEN N.V.
02/2004	Granted Study Scholarship of German National Academic Foundation
10/2003	Start of Studies at the Technical University Hamburg IT-Engineering Majoring in Technical Dynamics (Applied Physics) and Scientific Arithmetics (Applied Mathematics)
04/2003 - 04/2004	Choreograph and Fitness & Group Instructor at TUI AG
07/2002 - 04/2003	Military Service at 1 <sup>st</sup> NBC Defence Battalion 610
08/1993 - 06/2002	Academic High School
08/1989 - 07/1993	Primary School